SUPERCONDUCTIVITY, INCLUDING HIGH-TEMPERATURE SUPERCONDUCTIVITY

Temperature-dependent resistance of a finite one-dimensional Josephson junction array

K. Engström* and J. M. Kinaret

Department of Applied Physics, Chalmers University of Technology and Göteborg University SE-412 96 Göteborg, Sweden

(Submitted August 27, 2001)
Fiz. Nizk. Temp. **28**, 3–9 (January 2002)

We study theoretically the temperature and array-length dependences of the resistance of a finite one-dimensional array of Josephson junctions. We use both analytic approximations and numerical simulations, and conclude that within the self-charging model, all finite arrays are resistive in the low-temperature limit. A heuristic analysis shows qualitative agreement with the resistance obtained from Monte Carlo simulations, establishing a connection between resistance and the occurrence of vortices in the corresponding 1+1D *XY* model. We compare our results with recent experiments and conclude that while the self-charging model reproduces some of the experimental observations, it underestimates the superconducting tendencies in the experimental structures. © *2002 American Institute of Physics.*
[DOI: 10.1063/1.1449177]

1. INTRODUCTION

The one-dimensional Josephson junction array is a prime example of a system exhibiting a zero-temperature superconductor–insulator quantum phase transition (QPT). Various investigations of the system, using different approximations for the capacitance matrix and dissipation,[1–5] have revealed a rich phase diagram. Most theoretical studies so far have focused on the limit of infinite system size and zero temperature. This sequence of limits by definition excludes finite size effects and is therefore mathematically simple, lending itself to standard quantum statistical mechanics treatments. Recent experiments[6] on chains consisting of 63 to 255 junctions show results suggestive of the predicted infinite-system QPT. However, the measured array resistances were found to depend both on the number of junctions and the temperature in a non-obvious fashion. In particular, the resistance of a given array varied nonmonotonically as a function of temperature and exhibited regions of pronounced quasi-reentrant insulating and superconducting behaviors. In this paper we investigate this as yet unexplained nonmonotonicity in terms of a familiar path integral treatment of the problem. We also discuss the effects of finite chain length on both sides of the nominal superconductor–insulator transition point.

Finite one-dimensional arrays of Josephson junctions have previously been analyzed by Inoue *et al.*,[3] who discussed the zero-temperature behavior in terms of real-time phase slips. They calculated the length dependence of the crossover between low- and high-resistance regimes, and found qualitative agreement with the measurements of Chow *et al.* Explicit resistance values were calculated only in the $N\to\infty$ limit, though. Our results agree with those of Inoue *et al.* in that we also find a resistive low-temperature behavior, but in contrast to the earlier work we also analyze the finite-temperature behavior of the array.

The paper is organized as follows: Sec. 2 presents the model. In Sec. 3 we present a qualitative analysis of the dependence of the linear-response resistance on parameters such as system length, temperature, and Josephson coupling. The qualitative results are put on a firmer footing in Sec. 4, in which we present Monte Carlo data in support of the preceding arguments and make a comparison with existing experimental data. Conclusions and discussion follow in Sec. 5.

2. MODEL

Among the simplest models incorporating both charging and Josephson effects is the self-charging model[1] in which only the self-capacitance C_0 of the individual islands is taken into account (Fig. 1). The Hamiltonian in this case takes the simple form

$$H=\sum_i \left[E_C\hat{n}_i^2-2E_J\cos(\hat{\varphi}_{i+1}-\hat{\varphi}_i)\right],$$

where $E_C=(2e)^2/(2C_0)$ is the charging energy; E_J is the Josephson energy, and $\hat{\varphi}_i$ is the phase conjugate to the number of Cooper pairs $\hat{n}_i$ on grain i.

Quite generally, the behavior of a quantum D-dimensional system can be understood in terms of a D

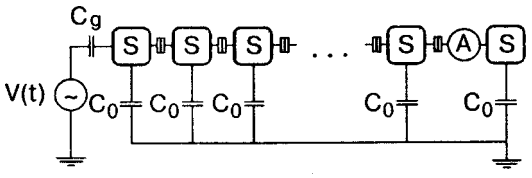

FIG. 1. Regions marked with *S* denote superconducting grains, separated by tunnel junctions. Each grain is capacitively coupled to a ground plane through a capacitance C_0. The response to the externally applied voltage $V(t)$ is measured by a fictitious ideal current-meter *A* between any two grains. The total number of Cooper pairs on the array is conserved.

+1-dimensional classical system, where the extra dimension is imaginary time.[7] As was shown by Bradley and Doniach,[1] the self-charging model maps onto a 2D *XY*-model on a cylindrical[8] lattice of length N and circumference $N_\tau \propto T^{-1}$ in the imaginary-time (τ) direction. The equivalent coupling constant of the *XY* model is given by $K \equiv \sqrt{E_J/E_C}$. Hence, the QPT is of the Kosterlitz–Thouless–Berezinskii (KTB) type,[9] corresponding to the unbinding of vortices in the 2D spin field $\varphi(x,\tau)$—in real-time formalism the vortices correspond to phase slips.[3] Note that the vortices that appear in the analysis of 2D Josephson arrays are real vortices of the field $\varphi(x,y)$ and hence are quite different from the structures that we focus on, which are vortices of $\varphi(x,\tau)$ or phase slips of $\varphi(x,t)$.

The step size $\Delta\tau$ in the imaginary time direction is so chosen that the resulting *XY* model is isotropic. This approximation is valid provided that the characteristic time scale for variations of $\varphi(x,\tau)$ is slower than $\Delta\tau$, i.e., provided that K is not too small.

The current $I(x,t)$ arising in response to an applied voltage $V(t)$ can be obtained by standard linear response formalism.[10] In the 2D *XY* model this requires a knowledge of spin–spin correlations.

3. QUALITATIVE ANALYSIS

3.1. Introduction

It is well known[1,7] that the appearance of resistance in Josephson junction arrays can be associated with isolated vortices in the two-dimensional *XY* model. However, the quantitative connection between the number of isolated vortices and resistance R is not clear, but the resistance is believed to be a monotonic function of the number of independent vortices.[7] In this Sec. we use this connection to determine the qualitative temperature and system size dependences of R for finite one-dimensional arrays of Josephson junctions.

Since the vortex excitations and spin waves decouple in the 2D *XY* model, we can write the partition function as $Z = Z_{sw}\Sigma_{n=0}^{\infty} Z_n$, where Z_{sw} is the spin-wave contribution and Z_n is the contribution from a spin configuration with n vortices ($Z_0 = 1$). In general it is unclear which of the vortices should be classified as isolated (and hence contribute significantly to the resistance) and which of them belong to closely bound vortex–antivortex pairs. However, we know that in the limit of large K the free energy cost of creating an isolated vortex is very high, and most vortices occur in vorticity-neutral pairs, and we can therefore approximate $Z_{2n+1} \approx Z_1 Z_{2n}$. Hence, for large K, the number of unbound vortices is approximately $\langle N_V \rangle \approx (\Sigma_{n=1}^{\infty} Z_1 Z_{2n})/(\Sigma_{n=0}^{\infty} Z_n) = Z_1/(1+Z_1) \approx Z_1$. In the opposite limit of small K all vortices are nearly independent, and $\langle N_V \rangle \approx (\Sigma_{n=0}^{\infty} n Z_n)/(\Sigma_{n=0}^{\infty} Z_n)$. In this limit the vortex gas can be described as a collection of indistinguishable particles, so that $Z_n = (1/n!) Z_1^n$, and we again find $\langle N_V \rangle \approx Z_1$. Consequently, we use Z_1 as an estimate for the number of free vortices in the system.

The partition function $Z_1 = \int \mathcal{D}\varphi(x,t) \mathrm{e}^{-H[\varphi]}$ (where the integration extends over single-vortex configurations $\varphi(x,t)$ only) is estimated by calculating the typical energy E_{typ} of a single vortex and multiplying $\mathrm{e}^{-E_{\mathrm{typ}}}$ by an entropic factor which gives the number of possible places where a vortex may appear. This argument by Kosterlitz and Thouless[9,11] demonstrates the existence of a phase transition in an infinite 2D *XY* model, and for the present purposes we extend it to a cylindrical geometry. A typical vortex configuration, centered at (x_0, τ_0), that satisfies periodic boundary conditions in the imaginary time direction is ($|\tau| < N_\tau/2$)

$$\varphi(x,\tau) = \arctan\left[\coth\left(\frac{\pi}{N_\tau}(x = x_0) \right) \tan\left(\frac{\pi}{N_\tau} \right) \right] + \frac{\pi}{N_\tau}\tau + \pi\,\mathrm{sgn}(\tau)[1 - \theta(x - x_0)],$$

where we choose the principal branch of arctan and where the last two terms were added to guarantee that the spin directions end up in the proper quadrant.[12] Using a continuum approximation for the energy E_{typ} and taking the entropy S_{typ} to be $\sim \ln NN_\tau$, we find, apart from uninteresting constants, a typical free energy

$$F = E_{\mathrm{typ}} - S_{\mathrm{typ}} \approx K\pi \left\{ \ln\left[\frac{\sinh(\pi(N/N_\tau))}{\sinh(\pi(2/N_\tau))} \right] - \frac{\pi}{2}\frac{N}{N_\tau} \right\} - \ln(NN_\tau). \quad (1)$$

In the following two Sections we investigate the dependence of F on the chain length N and temperature N_τ^{-1}.

In order to facilitate a direct comparison with experiments,[6] we fix the charging energy to $E_C = 500\ \mu\mathrm{eV}$ and vary K by varying E_J. Experimentally, E_J can be tuned by means of an external magnetic field. For simplicity, we ignore the temperature dependence of E_J.

3.2. Results

Keeping the aspect ratio $A \equiv N_\tau/N \propto (NT)^{-1}$ fixed in Eq. (1) and sending N to infinity, we get

$$F \approx (\pi K - 2)\ln N + O(N^{-1}) + \mathrm{const},$$

and we recover the familiar infinite-system result for a continuum: a phase transition occurs at $K = K_{KTB} \equiv 2/\pi$. Note, however, that the limits $N \to \infty$ and $T \to 0$ do not commute. The experimentally relevant limit where N is kept fixed as T is lowered is

$$F \approx (K\pi - 1)\ln N - \ln N_\tau - K\frac{\pi^2}{2}\frac{N}{N_\tau} + \mathrm{const} \overset{T\to 0}{\to} -\infty. \quad (2)$$

Hence, in the limit of low temperatures, free vortices are always present in a finite array, suggesting that the low-temperature behavior of finite arrays is insulating rather than superconducting. This is an immediate consequence of the periodic boundary conditions in the imaginary-time direction, which remove the customary logarithmic divergence of E_{typ}.

While the limit $F \to -\infty$ as $T \to 0$ is independent of both the coupling constant K and the array length N, the number of free vortices at a particular temperature, and hence the resistance $R(N,T,K)$, depends on N and K as shown in Fig. 2. However, in the limit $N_\tau \gg N$, the value of F is roughly independent of the chain length N at a special value of K

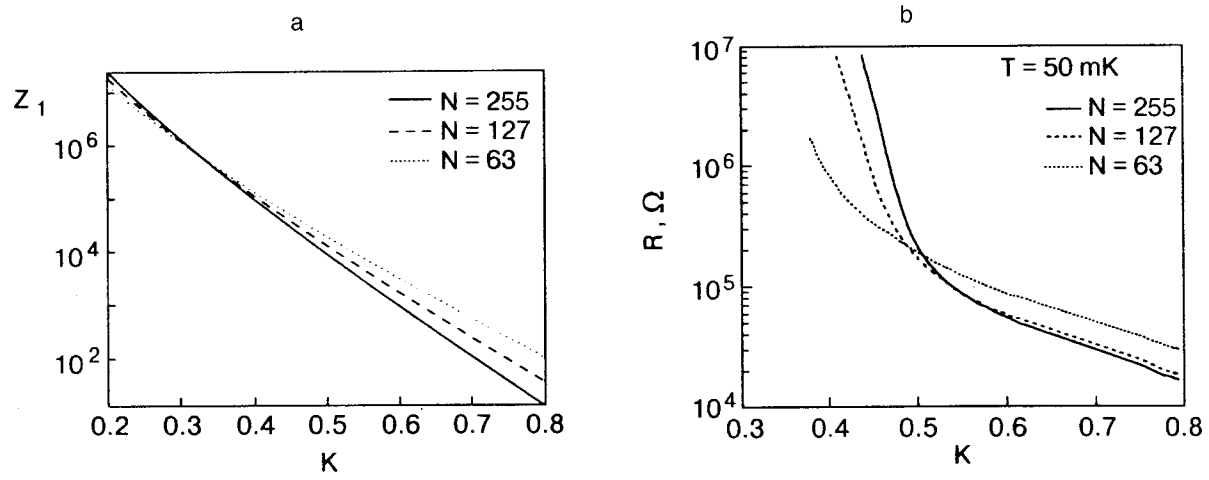

FIG. 2. Variation of Z_1 with K for different chain lengths N at a very low temperature. Note that the quantity on the vertical axis is not the actual resistance, but the number of free vortices in the system, a quantity that is related to the resistance. For $K>K^*=1/\pi$ the number of free vortices decreases with chain length, while for $K<K^*$, Z_1 decreases with increasing N (a). Corresponding measured resistances. (Reproduced from Ref. 6 with permission.) (b).

$=K^*\equiv 1/\pi$, which is different from the critical coupling of the infinite system, $K_{KTB}=2/\pi$.[1)] This suggests the possibility of a *length-independent resistance* at this special value of K. Furthermore, in the insulating regime ($K<K^*$), $Z_1=e^{-F}(\sim R)$ increases with increasing array length, while in the superconducting limit Z_1 seems to decrease with chain length (Fig. 2a). This is indeed what experimentalists report.[6] The observed value of the special coupling $K^*_{\rm exp}\approx 0.5$ lies in between these two values K_{KTB} and K^*.

The preceding analysis disregards the effect of vortex–antivortex pairs on the free energy of isolated vortices. These pairs partially screen out the spin–spin interactions, hence lowering the energy of vortex configurations, or equivalently, renormalizing the coupling constant to an effective value $K_{\rm eff}(K)<K$. This effect is more pronounced below K^*, when vortex–antivortex pairs are abundant, effectively bending the curves in Fig. 2a upwards for small K. However, this argument does not explain why $K_{\rm eff}(K)$ should reproduce the experimentally observed similar slopes of the different curves in the two regimes separately (Fig. 2b).

4. NUMERICAL ANALYSIS

4.1. Methods

The $\omega\to 0$ limit of the intrinsic linear-response conductance of the array can be compactly expressed as

$$\sigma_0=-\frac{1}{i\hbar}\frac{\partial}{\partial\omega}\chi^{\rm ret}_{jj}(q=0,\omega)\big|_{\omega=0}. \tag{3}$$

As usual,[10] the retarded response function is obtained from the analytic continuation

$$\chi^{\rm ret}_{jj}(q=0,\omega)=\lim_{i\omega_n\to\omega+i\delta}\int_0^{\hbar\beta}d\tau e^{i\omega_n\tau}\sum_x \chi_{jj}(x,\tau)$$

of the corresponding temperature Green's function, $\chi_{jj}(x,\tau)=\langle j_{N-x}(\tau)j_N(0)\rangle$. Here $\omega_n\equiv n2\pi/\beta$ denotes the nth bosonic Matsubara frequency, and $j_x(\tau)=(2e/\hbar)E_J\sin[\varphi(x,\tau)-\varphi(x-1,\tau)]$ is the local current at (x,τ).

Using the Wolff algorithm,[13] a sequence of equilibrium configurations was generated, from which the desired correlation function could be evaluated. The number of update steps taken was typically of the order of 10^7.

The problem of analytically continuing imaginary-time Monte Carlo data to real frequencies is notoriously difficult, and sophisticated statistical methods have been developed to deal with it.[14] However, in accordance with earlier work on two-dimensional Josephson junction arrays,[15] we have found it sufficient to fit the MC data to a functional Padé-type form that can easily be analytically continued,

$$\chi_{jj}(q=0,i\omega_n)=\frac{A}{B\omega_n^2+C|\omega_n|+1}.$$

This functional form is motivated by analytic calculations on the superconducting[1] and insulating[16] sides of the superconductor–insulator transition in infinite arrays at zero temperature. It has the required symmetry and accurately fits the low-frequency part of the MC data.

4.2. Results

The conductance is now obtained straightforwardly. Conditions for the fitting parameters are imposed by the requirements that the resulting real-time Green's function be causal, and that the conductance be positive. A typical fit is shown in Fig. 3.

The simulations suffer from noise problems and therefore become quite time-consuming, particularly at low temperatures. This problem becomes rather pronounced, since the dependences we wish to examine typically vary only logarithmically. We were therefore forced to consider only small systems (typically, $N=10$ and values to N_τ ranging from $N/2$ to $8N$) and to focus on the temperature dependence only. A plot of the resulting resistance, together with the corresponding heuristic result, is shown in Fig. 4. Comparison between the MC data and the heuristic argument (Fig. 4) suggests that the connection between R and Z_1 is roughly $R(K,T)=R_0(K)[Z_1(K,T)]^\alpha$ and $\alpha\approx 2$, where $R_0(K)$ is a coupling-constant-dependent resistance scale.

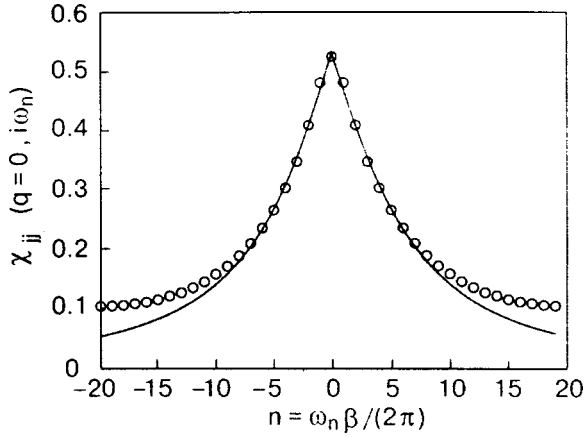

FIG. 3. Example of a Padé-type rational polynomial fit to $\chi_{jj}(q=0,i\omega_n)$ for small Matsubara frequencies. In this particular case, $N=10$, $N_\tau=40$ and $K=1.2$. (The correlation function is given in units of the critical current squared, I_c^2).

4.3. Comparison with experiments

In the experiment by Chow *et al.*[6] the mutual capacitance C_m between grains was much larger than the ground capacitance C_g, and therefore the experiment does not exactly correspond to the self-charging model we have investigated. The $C_m \gg C_g$ case was analyzed by Bradley and Doniach,[1] who concluded that C_m-dominated arrays are always insulating in the $T\to 0$, $N\to\infty$ limit, as opposed to G_g-dominated arrays, which become superconducting for large values of E_J/E_C. Consequently, we expect that including nonzero mutual capacitances would result in an increase of the resistance at finite N and T.

The large values of N used in experiments render a direct MC analysis unfeasible; we therefore compare the experiments with the simple analytic estimates in Sec. 3. Figure 5a shows the estimated number of isolated vortices Z_1 plotted as a function of T for several different values of the coupling constant K. For low values of K, which are consistent with the charging and Josephson energies in the experiments, we find that Z_1 increases monotonically with decreasing temperature, suggesting a monotonically increasing $R(T)$. For large values of K,[2)] the number of isolated vortices varies nonmonotonically with temperature, reaching a minimum at a low temperature $T_{\min}$ that is roughly independent of K, and exhibiting a local maximum at a higher, K-dependent temperature $T_{\max}$. This is indicated in the inset of Fig. 5a, where the shaded area corresponds to regions with $\partial Z_1/\partial T>0$. This is in qualitative agreement with the experimental results by Chow *et al.*[6] shown in Fig. 5b. However, since this structure appears for very large K and is rather weak, it is not clear that it can be identified with the experimentally observed re-entrant behavior.

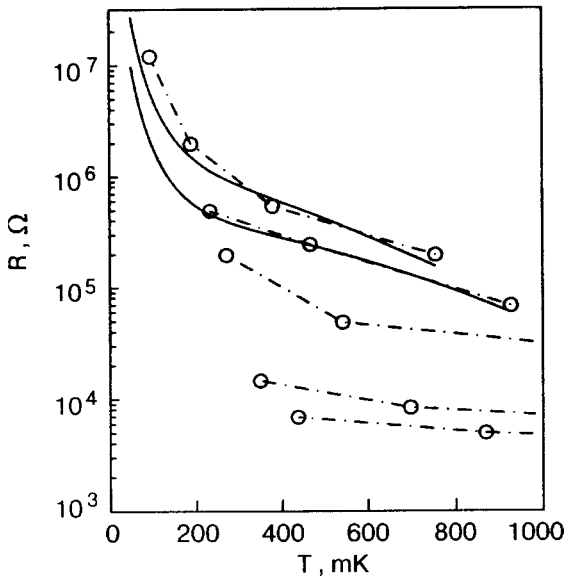

FIG. 4. The resistance obtained from Monte Carlo calculations for a chain of length $N=10$ (dashed-dotted lines are included as a guide to the eye). From top to bottom, the data correspond to $K=0.65$, 0.8, 0.93, 1.2, and 1.5, respectively. The solid lines plot the quantity $R_0(K)[Z_1(K)]^2$ of Sec. 4.2. for the two lowest values of K. For larger values of K, both the MC data and the analytic expression display few features, and a comparison becomes less meaningful.

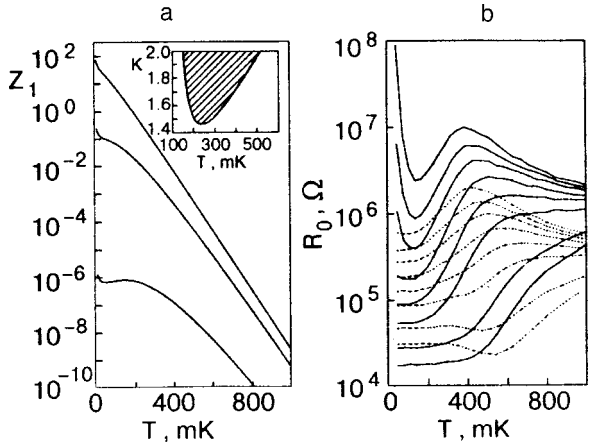

FIG. 5. The quantity Z_1 (~number of isolated vortices) for a $N=63$ chain. The different curves correspond, from top to bottom, to increasing values of the coupling constant $K=\sqrt{E_J/E_C}$ (0.5, 1, and 2, respectively). Inset: "phase diagram" showing regions where $\partial Z_1/\partial T>0$ (shaded area) for a $N=20$ array. The location and width of the shaded region both scale as N^{-1} (a). Experimentally measured linear-response resistance versus temperature, $R(T)$, for two chains of respectively 63 (dashed line) and 255 (solid line) Josephson junctions. From top to bottom in each set of curves, the ratio E_J/E_C increases. (From Ref. 6) (b).

5. CONCLUSIONS AND DISCUSSION

We have studied the linear-response resistance of a finite one-dimensional array of Josephson junctions as a function of the array length N and the energy scales E_C, E_J, and k_BT. The model we have used is the simplest one that incorporates both charging phenomena and phase coupling between adjacent superconductors. Using a standard mapping onto a two-dimensional XY model on a cylinder, we can relate the resistance to phase fluctuations or vortices in the XY model. We have analyzed the model both using analytic approximations and by means of numerical Monte Carlo calculations.

We find that the low-temperature resistance is independent of the array length for $E_J/E_C \approx 1/\pi^2 \approx 0.1$, which can be compared with the experimental value of approximately 0.2. We also conclude, based on analytical and numerical results, that the array becomes highly resistive in the low-

temperature limit for all values of E_J/E_C. This is in apparent contradiction with the experiments that indicate a saturation of resistance at low temperatures. However, since the temperature dependence that we find is quite weak (logarithmic), one has to be careful in identifying the measurements at a low but finite temperature as the zero-temperature limit.

The experimentally observed resistance saturation at low temperatures is puzzling and may be due to processes that are not included in our model. A possible explanation is that random background charges result in frustration, hence reducing the charge order and, consequently, the resistance of the array.[17] Resistance saturation may also arise with the self-charging model as a result of an external coupling such as charge transfer between the array and external electrodes. Since the internal dynamics of the model only leads to logarithmic dependences $F\sim\log(N,1/T)$, the system is very sensitive to any perturbation that leads to free energy contributions that are linear in $1/T$ and possibly even in N. Such a term arises, e.g., from the coupling between the array and the external electrodes and is expected to affect the behavior of the array in the limit $T\to 0$. Specifically, if the free energy acquires a form $F\approx -\ln N_\tau+\gamma/T$ [cf. Eq. (3)], the free energy acquires a minimum at $T=\gamma$, and for temperatures $T<\gamma$ the number of free vortices (and hence the resistance) is reduced. It should be possible to determine experimentally if the saturation of the resistance at low temperatures is due to such coupling to the external leads—if this is the case, the saturation temperature should vary with the strength of the coupling.

We wish to acknowledge fruitful discussions with, and insightful contributions from, Robert Shekhter, Sebastian Eggert, David Haviland, and Steven Girvin. Financial support was provided by the Swedish Foundation for Strategic Research (SSF) program ''Quantum Devices and Nano-Science'' and by the Swedish Natural Science Research Council.

*E-mail: klase@fy.chalmers.se

[1)]A standard finite-size scaling argument would imply size-independent behavior at $K=2/\pi$. However, such an argument applies to *isotropic* rescaling, where both N and N_τ are changed.

[2)]Non-monotonicity appears for $K\gtrsim 1.63-3.4N^{-1}+O(N^{-2})$.

[1] R. M. Bradley and S. Doniach, Phys. Rev. B **30**, 1138 (1984).
[2] S. G. Chung, J. Phys.: Condens. Matter **9**, L619 (1997).
[3] T. Inoue, M. Nishida, and S. Kurihara, cond mat/9903349 (unpublished).
[4] A. I. Larkin and L. I. Glazman, Phys. Rev. Lett. **79**, 3736 (1997).
[5] M.-S. Choi, J. Yi, M. Y. Choi, J. Choi, and S.-I. Lee, Phys. Rev. B **57**, R716 (1998).
[6] E. Chow, P. Delsing, and D. B. Haviland, Phys. Rev. Lett. **81**, 204 (1998).
[7] S. L. Sondhi, S. M. Girvin, J. P. Carini, and D. Shahar, Rev. Mod. Phys. **69**, 315 (1997).
[8] G. Schön and A. D. Zaikin, Phys. Rep. **198**, 239 (1990).
[9] J. M. Kosterlitz and D. J. Thouless, J. Phys. C **6**, 1181 (1973).
[10] G. D. Mahan, *Many-Particle Physics*, Plenum, New York (1993).
[11] P. M. Chaikin and T. C. Lubensky, *Principles of Condensed Matter Physics*, Cambridge University Press, Cambridge (1995).
[12] Similar instanton configurations have been studied by I. V. Krive, P. Sandstrom, R. I. Shekhter, S. M. Girvin, and M. Jonson, Phys. Rev. B **52**, 16451 (1995).
[13] U. Wolff, Phys. Rev. Lett. **62**, 361 (1989).
[14] M. Jarrell and J. E. Gubernatis, Phys. Rep. **269**, 133 (1996).
[15] M. Wallin, E. S. Sorensen, S. M. Girvin, and A. P. Young, Phys. Rev. B **49**, 12115 (1994).
[16] K. B. Efetov, Sov. Phys. JETP **51**, 1015 (1980).
[17] C. Bruder, R. Fazio, A. Kampf, A. van Otterlo, and G. Schon, Phys. Scr. **42**, 159 (1992).

This article was published in English in the original Russian journal. Reproduced here with stylistic changes by AIP.

Pinning of Abrikosov vortices on dislocations and the critical current in high-temperature superconductors

É. A. Pashitskiĭ* and V. I. Vakaryuk

Institute of Physics of the National Academy of Sciences of Ukraine, pr. Nauki 46, 03022 Kiev, Ukraine
(Submitted September 6, 2001)
Fiz. Nizk. Temp. **28**, 16–23 (January 2002)

The microscopic mechanisms for single-particle core pinning of quantum vortices on the insulating cores of isolated dislocations are investigated for both parallel and mutually tilted orientations of the vortex and dislocation and also for pinning on an infinite periodic chain of edge dislocations. The theoretical results are consistent with experiment in regard to the temperature and orientation dependences of the depinning critical current in low magnetic fields, when the interaction between vortices is exponentially small, and they also predict strong anisotropy of the pinning force along and transverse to the chains of edge dislocations.
 [DOI: 10.1063/1.1449179]

INTRODUCTION

In an external magnetic field the critical current in type-II superconductors is determined by the pinning force on the vortex lattice at defects and inhomogeneities of the crystal lattice.[1,2] The elementary pinning forces of individual vortices can be due to various causes: interaction of the normal core of the vortex with microscopic cavities (pores) in the superconductor,[3,4] magnetic interaction of the vortex currents with their mirror images near the surface of the superconductor[5] and with small ferromagnetic particles,[6] local variation of the Ginzburg–Landau parameter κ or the upper critical field H_{c2} due to nonuniformities of the electron mean free path[2,7] for scattering on point defects (so-called δl pinning), paraelastic and dielastic interactions of vortices with dislocations and with other defects of the crystal lattice due to the change of the specific volume and elastic moduli at the phase transition from the normal N to the superconducting S state,[8–11] and the change of the electrostatic energy of interaction of the normal core of the vortex with charged cores of dislocations in the ionic lattice of a metal as a result of the change of the screening properties of the conduction electrons at the $N–S$ transition.[12]

The question of the value of the critical current has become particularly topical since the discovery of high-temperature superconductors (HTSCs).[13] The problem of increasing the critical current density j_c in HTSC materials based on layered cuprate metal-oxide compounds (MOCs) and the study of the specific physical mechanisms that limit the superconducting currents in various HTSC samples have been the subject of a colossal number of papers (see, e.g., the reviews[14,15]). In particular, it is necessary to understand why the critical current density j_c in thin films of cuprate MOCs, as a rule, is much higher than in rather perfect crystals.[16–18] The key to this puzzle may be the fact that the systems and types of structural defects of the crystal lattice in thin films and bulk samples are different, as can be observed by electron and scanning tunneling microscopy.[15]

In the growth of layered *crystals* of cuprate MOCs a large-scale block structure can arise, with rather larger angles of mutual misorientation of the blocks ($\theta \geqslant 5°$) both in the plane of the layers (ab) and with respect to the direction of the **c** axis. Here Josephson weak links can be formed at the boundaries between blocks, substantially suppressing the superconducting current and leading to a dependence of j_c on magnetic field.

Epitaxial *films* of cuprate MOCs deposited by various methods on single-crystal substrates with close values of the lattice constant, as a rule, contain a certain number of growth screw dislocations (SDs) and a much larger number of edge dislocations (EDs) oriented both along the **c** axis and in the ab plane, parallel to the two-dimensional CuO_2 layers. In the process of polygonization or thermal annealing of the films it is energetically favorable for pileups of linear EDs parallel to the axis $\mathbf{c} \| z$ and perpendicular to the substrate to align into quasiperiodic chains (dislocation walls) with Burgers vectors **B** perpendicular to the plane of the wall, since in that case the energy of the elastic deformations of the crystal lattice is minimum because of the mutual compensation (annihilation) of the elastic strains (dilatations) of different sign from the neighboring EDs.[19] As a result of this, an epitaxial film separates along its entire thickness into a system of single-crystal blocks slightly misoriented in the ab plane, separated by low-angle boundaries with misorientation angles of adjacent blocks $\theta \leqslant 5°$ and accordingly with average distances between EDs of $d \approx |\mathbf{B}|/\theta \geqslant 45$ Å for $|\mathbf{B}| \approx a \approx 4$ Å. At the same time, the characteristic dimensions of the blocks, i.e., the length L of the low-angle boundaries, can vary in different films from several hundred to several thousand angstroms ($L \approx 300–3000$ Å), depending on the structure of the substrate, the method of deposition, and the thickness of the film.

Upon the passage of a transport supercurrent through the epitaxial films the low-angle boundaries can play a dual role. On the one hand, they lead to a limiting of j_c due an effect considered in Ref. 20, viz., a local suppression of the superconducting order parameter ψ along the boundaries in a layer with a thickness of the order of several coherence lengths ξ, and, accordingly, to suppression of the local depairing current density $j_0 \sim \psi^3$ flowing through the superconducting

channels between nonsuperconducting (insulating) cores of the EDs in the low-angle boundaries. The theoretical results[20,21] as to the dependence of j_c on the misorientation angle θ of the blocks and on the parameter $\tau=1-T/T_c$ (where T_c is the temperature of the superconducting transition) are in good agreement with the experimental dependences $j_c(\theta)$ and $j_c(\tau)$ in the absence of external magnetic field.[21,22]

On the other hand, the plastically deformed insulating cores of the linear EDs oriented along the low-angle boundaries can serve as effective pinning centers for Abrikosov quantum vortices and thereby make for an increase of the critical supercurrents in external magnetic fields and in the self-field of the supercurrent, especially in the case of a parallel orientation of the vortices and dislocations. This is confirmed by the experimental data on the orientational dependence of j_c on the angle θ between the direction of the magnetic field **H** and the **c** axis.[23,24] The empirical $j_c(\theta)$ curves for films are, as a rule, characterized by the presence of two maxima (peaks) at angles $\theta=0°$ and $\theta=90°$, which corresponds to the maximum pinning of the vortices on EDs oriented along the **c** axis in the ab plane. The presence of a maximum in $j_c(\theta)$ at $\theta=90°$ can also be explained by the pinning of vortices on insulating interlayers between the superconducting CuO_2 layers (intrinsic pinning).[25] However, for the HTSC compound YBaCuO, where the coherence length ξ is larger than the distance between adjacent CuO_2 layers, this effect is apparently not dominant.

In this paper we consider the microscopic mechanisms for single-particle core pinning of vortices on insulating cores of isolated EDs and SDs for both parallel and tilted mutual orientations of the vortex and dislocation and also on an infinite periodic chain of EDs. We discuss the possibility of an interaction of vortices with elastic dilatational fields produced by the dislocations. The theoretical results are consistent with experiment in regard to the temperature and orientation dependences of j_c in low fields, when the interaction between vortices is exponentially small, and predict a strong anisotropy of the pinning force along and transverse to the chains of EDs.

SINGLE-PARTICLE PINNING OF VORTICES ON EDGE DISLOCATIONS

The core of a dislocation in an ionic crystal of a cuprate MOC of the YBaCuO type in the general case has a rather complex structure, but in the simplest approximation it can be represented as a nonsuperconducting metallic or insulating channel of radius r_0. The problem of the electromagnetic interaction of a vortex with a cylindrical insulating (or empty) cavity was considered by Mkrtchyan and Shmidt[4] under the condition $r_0 \gg \xi$. However, for a dislocation core this inequality does not hold, and it is therefore necessary to do a more detailed analysis of the core pinning of vortices on dislocations.

According to Ref. 14, in the framework of the Ginzburg–Landau (GL) theory the energy of pinning of an isolated vortex is determined by the local suppression of the bulk superconducting order parameter near the defect. The pinning energy (per unit length) of a vortex on an extended structural defect of the crystal lattice characterized by cylindrical symmetry, e.g., a cylindrical channel (radiation track) created by a fast ion or the insulating core of an ED (or SD), in the case of a parallel mutual orientation of the vortex and axis of the defect is given by the expression

$$\varepsilon_{\rm pin}(\mathbf{u})=-\int d^2r\,U_{\rm pin}(\mathbf{r})\,p_V(\mathbf{r}-\mathbf{u}). \tag{1}$$

Here $p_V(r)=1-|\psi_V(r)|^2$ is the structure factor of the vortex, $\psi_V(r)$ is the radial distribution, normalized to the bulk value ψ_0, of the dimensionless superconducting order parameter inside the vortex core, and $U_{\rm pin}(\mathbf{r})$ is the effective pinning potential, which for a hollow channel or an insulating dislocation core of radius $r_0>\xi$ can be written in the form

$$U_{\rm pin}(r)=\begin{cases} U_0, & r\leqslant r_0; \\ 0, & r>r_0 \end{cases} \quad U_0=\varepsilon_0/2\pi\xi^2, \tag{2}$$

where $\varepsilon_0=(\varphi_0/4\pi\lambda)^2$, φ_0 is the magnetic flux quantum, $\lambda=\lambda_0/\sqrt{\tau}$ is the London penetration depth for the magnetic field, and $\xi=\xi_0/\sqrt{\tau}$ is the coherence length. We will make use of the following approximating relations obtained by variational and numerical methods:[26]

$$|\Psi_V(r)|=\frac{r}{\sqrt{r^2+2\xi^2}}; \quad p_V(r)=2\frac{\xi^2}{r^2+2\xi^2}. \tag{3}$$

Substituting expressions (2) for $U_{\rm pin}(r)$ and (3) for $p_V(r)$ in (1) and doing the integration, we obtain

$$\varepsilon_{\rm pin}(\tilde{u})=-\varepsilon_0\ln\left[W(\tilde{u},\tilde{r}_0)-\tilde{u}^2+\tilde{r}_0^2+\frac{1}{2}\right], \tag{4}$$

where

$$W(\tilde{u},\tilde{r}_0)=\left[\tilde{r}_0^4+(1-2\tilde{u}^2)\tilde{r}_0^2+\left(\frac{1}{2}+\tilde{u}^2\right)\right]^{1/2}; \quad \tilde{u}=u/2\xi;\ \ \tilde{r}_0=r_0/2\xi. \tag{5}$$

For a coaxial arrangement of the vortex and channel or dislocation core (i.e., for $u=0$) expression (4) reduces to the minimum value of the pinning potential given in Ref. 14:

$$\varepsilon_{\rm pin}(0)=-\varepsilon_0\ln(1+r_0^2/2\xi^2), \tag{6}$$

and in the case of a parallel displacement of the vortex to the edge of the channel or dislocation core ($u=r_0$) we find, according to (4) and (5),

$$\varepsilon_{\rm pin}(r_0)=-\varepsilon_0\ln\left(\frac{1}{2}\sqrt{1/4+2(r_0/2\xi)^2}\right). \tag{7}$$

Figure 1a shows the $\varepsilon_{\rm pin}(u)$ curves calculated according to formulas (4) and (5) for different values of the ratio $r_0/2\xi$, and Fig. 1b shows the corresponding pinning forces $f_{\rm pin}(u)=-d\varepsilon_{\rm pin}(u)/du$. We see that the maximum value of the core pinning force for $r_0>\xi$ is reached for displacements $u=r_0$.

For a cylindrical channel (pore) of larger radius ($r_0 \gg \xi$) the pinning energy both at the center of the channel (6) and at its boundary (7) increases with increasing r_0, diverging logarithmically for $r_0\to\infty$. Formally this means that for a vortex localized near a plane boundary of a superconductor, an infinitely high potential barrier for its entry into the volume of the superconductor arises. At the same time, how-

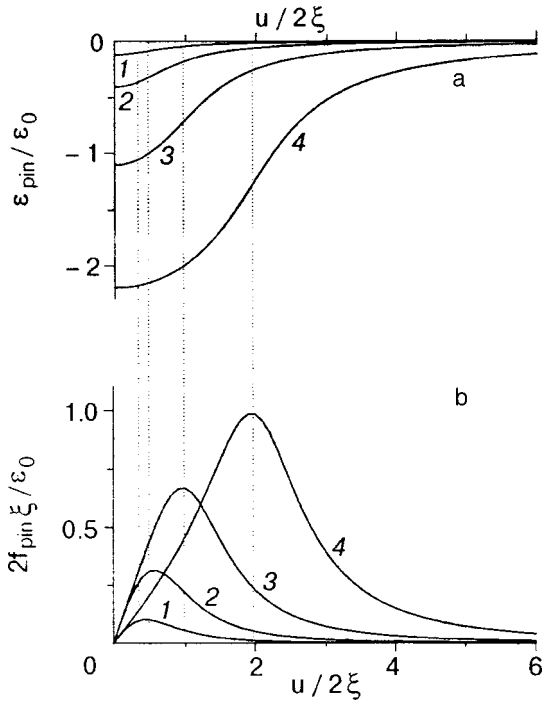

FIG. 1. Energy (a) and the corresponding pinning force (b) as functions of the displacement u for an isolated vortex at a parallel insulating channel for different values of the dimensionless parameter $\alpha = r_0/2\xi$: 0.25 (*1*), 0.5 (*2*), 1 (*3*), 2 (*4*).

ever, the maximum pinning force at the boundary of a channel with $u = r_0 \to \infty$ tends toward a constant limit of $\sqrt{2}\varepsilon_0/\xi$.

The logarithmic divergence of potentials (6) and (7) for $r_0 \to \infty$ is due to the power-law (quadratic) decay of the form factor $p_V \propto r^{-2}$ as $r \to \infty$, according to Eq. (3). However, if expression (3) for $|\psi_V(r)|$ is cut off at a distance $r = \lambda$ and is formally complemented in the region $r > \lambda$ by an exponential asymptotic expression of the form

$$|\psi_V(r)| = 1 - \frac{\pi\lambda}{2\kappa^2 r}\exp(-r/\lambda), \tag{8}$$

corresponding to the exponential decay of the vortex supercurrent (here $\kappa = \lambda/\xi$ is the Ginzburg–Landau parameter), the value of the pinning potential (1) for $r_0 \to \infty$ remains finite and is practically equal to the value obtained in Ref. 4 for the electromagnetic pinning energy of a vortex (a Bean–Livingston barrier) at the boundary of a semi-infinite superconductor:

$$\varepsilon_{\rm pin}^{\rm el-m}(u) = -\varepsilon_0 \begin{cases} \ln(\lambda/u), & \xi < u < \lambda \\ \sqrt{\pi\lambda/2u}\exp(-u/\lambda), & u \gg \lambda \end{cases}. \tag{9}$$

On the other hand, under the condition $r_0 < \xi$, which holds for the cores of EDs and SDs, Eqs. (4) and (5) imply the simple expressions for the potential and pinning force:

$$\varepsilon_{\rm pin}(u) = -\varepsilon_0 \frac{r_0^2}{u^2 + 2\xi^2}; \quad f_{\rm pin}(u) = -\varepsilon_0 \frac{2ur_0^2}{(u^2+2\xi^2)^2}. \tag{10}$$

The result (10) can also be obtained directly from (1) together with (3) with the use of a 2D δ-function potential for the insulating core of a dislocation of small radius $r_0 \to 0$:

$$U_{\rm pin}(r) = U_0 \pi r_0^2 \delta^2(r). \tag{11}$$

It should be noted, however, that for $r_0 \leqslant \xi$ it is necessary to take the proximity effect into account, so that the minimum effective radius of the dislocation core is equal in order of magnitude to ξ (see Ref. 14).

According to Eq. (10), the maximum pinning force on a vortex at the core of an ED (or SD) is reached at a vortex displacement $u = \sqrt{2/3}\xi$ and has the value

$$f_{\rm pin}^{\max} = \frac{9}{32}\left(\frac{2}{3}\right)^{1/2}\frac{\varepsilon_0 r_0^2}{\xi^3}. \tag{12}$$

Assuming that in thin films in low magnetic fields the main role is played by the pinning of vortices on the cores of dislocations and not on point defects of the lattice (see Ref. 15), we can use relation (12) to obtain an estimate of the maximum depinning critical current at $r_0 > \xi$ for YBaCuO: $j_c = c f_{\rm pin}^{\max}/\varphi_0 \approx 2\times 10^7 r_0^2/\xi_0^2\tau^{5/2}$ A/cm+2 for $\xi_0 \approx 12$ Å, $\lambda \approx 1000$ Å. If the radius of the insulating core of the dislocation is of the order of or smaller than ξ, then we should substitute ξ for r_0 in (12) in view of the proximity effect; consequently, the temperature dependence becomes $j_c \propto \tau^{3/2}$ (cf. Ref. 21).

In concluding this Section we note that in HTSC materials as a result of the strong anisotropic dependence of the critical temperature T_c on pressure, which is manifested upon uniaxial compression or extension of the crystals,[27,28] the elastic stress field produced by the dislocations can lead to a local variation of T_c and of the superconducting order parameter. For example, the elastic strain field around an isolated ED parallel to the axis $\mathbf{c} \| z$ is determined by the dilatation:

$$\epsilon(r) = \frac{|B|(1-2\sigma)}{2\pi(1-\sigma)}\frac{\sin\varphi}{r}, \tag{13}$$

where σ is Poisson's ratio, φ is the azimuthal angle in the ab plane, measured from the direction $\mathbf{B} \| y$, and $r = \sqrt{x^2+y^2}$. When the characteristic anisotropy of the pressure dependence of T_c in YBaCuO crystals is taken into account, the local variation of T_c as a function of r and φ in the field of dilatation (13) has the form[20]

$$\delta T_c(r,\varphi) = -\frac{|\mathbf{B}|C\sin\varphi}{2\pi(1-\sigma)r}[(1-2\sigma) + 2\beta\cos^2\varphi], \tag{14}$$

where

$$C = (C_a + C_b)/2; \quad \beta = (C_a - C_b)/(C_a + C_b); \\ C_a = -\partial T_c/\partial\epsilon_a; \quad C_b = -\partial T_c/\partial\epsilon_b, \tag{15}$$

and ϵ_a and ϵ_b are the diagonal components of the strain tensor along the **a** and **b** axes (for $\mathbf{B} \| \mathbf{a}$). From Eq. (14) we can find the region within which the local value $T_c(r,\varphi) = T_{c0} + \delta T_c(r,\varphi)$ (where T_{c0} is the critical temperature of the undeformed crystal) is below the sample temperature T:

$$r_n(\varphi,T) = R_0(T)|\sin\varphi(1+\beta_0\cos^2\varphi)|, \tag{16}$$

where

$$R_0(T) = \frac{C|\mathbf{b}|(1-2\sigma)}{2\pi T_{c0}(1-\sigma)\tau}; \quad \beta_0 = \frac{\beta}{1-2\sigma}; \tag{17}$$

$\tau = 1 - T/T_{c0}$.

For parameter values typical for the optimally doped $YBa_2Cu_3O_{7-\delta}$ crystal, which is anisotropic in the ab plane ($C_\alpha \approx -220$ K; $C_b \approx 320$ K; $\sigma \approx 0.28$; $T_{c0} \sim 92$ K), we obtain estimates for the effective radius of a normal metallic domain $R_0(T) \approx 0.43/\tau$ Å and anisotropy parameter $\beta \approx -25$. For $T \approx 77$ K ($\tau \approx 0.16$) the maximum value of the radius (16) in the direction $\varphi = -\pi/4$ is $r_n^{\max} \approx 25$ Å. For the BiSrCaCuO crystal with $T_c \approx 110$ K, which is nearly isotropic in the plane of the layers ab ($C_a \approx C_b \approx 300$ K, $\beta \approx 0$, and $\sigma \approx 0.25$), we obtain the estimate $R_0(T) \approx 1.33/\tau$ Å.

The local variations of the superconducting order parameter ψ in the vicinity of the boundary (16) of the normal region arising near an ED in the field of the elastic dilatation can be found only with allowance for the proximity effect through a solution of the GL equation with inhomogeneous coefficients. Here the region of suppressed values of ψ near r_n is smeared on a scale of the order of ξ, so that the corresponding derivative of the potential $U_{\rm pin}$ with respect to r, which ultimately determines the pinning force, is substantially decreased in absolute value. This means that the pinning of vortices at metallic domains in the fields of elastic dilatations of EDs and SDs, as a rule, is much less efficient than at dislocation cores found in the insulating state.

PINNING OF VORTICES AT CHAINS OF DISLOCATIONS

As we have said, the low-angle boundaries between slightly misoriented single-crystal blocks in epitaxial films of cuprate MOCs are quasiperiodic chains of EDs with a distance between adjacent dislocations $d(\theta) \approx |\mathbf{B}|/\theta \geqslant 45$ Å, if the misorientation angles of the blocks $\theta \leqslant 5°$. Such features of the crystal structure can play the role of pinning centers for vortices in an external magnetic field of practically any value $H \neq 0$, since the demagnetizing factor of a thin film is close to unity, and the magnetic induction $B \approx H$.

With allowance for (10), the pinning potential created by an infinite chain of insulating cores of EDs periodically distributed along the x axis takes the form

$$\varepsilon_{\rm pin}(x,y) = -\varepsilon_0 r_0^2 \sum_{n=-\infty}^{\infty} [(nd+x)^2 + y^2 + 2\xi^2]^{-1}, \quad (18)$$

where x and y characterize the position of the vortex relative to the central ED at the point $x = y = 0$. We note that elastic dilatations of adjacent EDs in the chain have opposite signs and compensate each other, so that the pinning of the vortices on a collective dilatation of the chain of EDs is suppressed to an even greater degree than for an isolated ED.

Doing the summation in (18) with the use of the well-known formula

$$\sum_{n=-\infty}^{\infty} (n+z)^{-1} = \pi \cot(\pi z), \quad (19)$$

we obtain an expression for the pinning potential of a vortex on a periodic chain of EDs:

$$\varepsilon_{\rm pin}(x,y) = -\varepsilon_0 \frac{2\pi^2 r_0^2}{d^2\sqrt{\tilde{\xi}^2 + y^2}} \frac{\sinh\sqrt{\tilde{\xi}^2 + \tilde{y}^2}}{\cosh\sqrt{\tilde{\xi}^2 + \tilde{y}^2} - \cos\tilde{x}}, \quad (20)$$

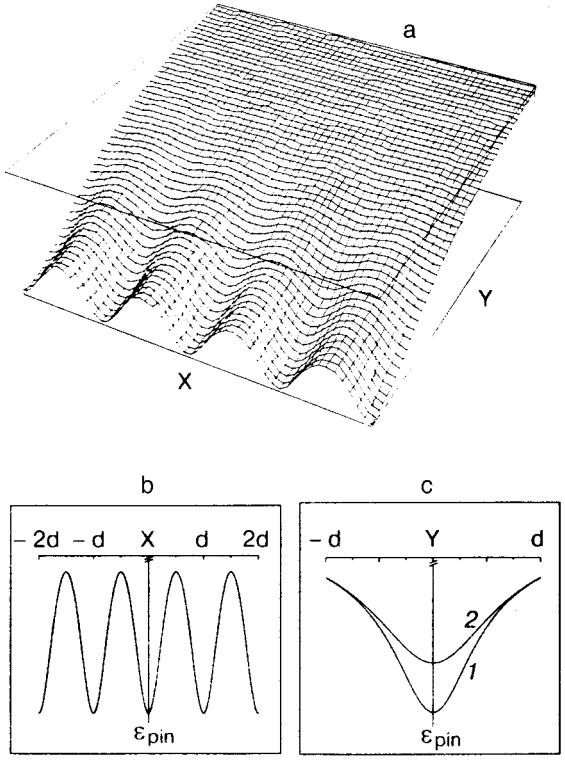

FIG. 2. Shape of the pinning potential of an isolated vortex on a periodic infinite chain of edge dislocations (a); the cross section of the potential along the "gully" (the $\tilde{y} = 0$ plane) (b); transverse cross sections of the potential in the planes corresponding to the minimum and maximum of the longitudinal periodic potential (the planes $\tilde{x} = 0$ (curve *1*) and $\tilde{x} = 3/2$ (curve *2*) (c).

where

$$\tilde{\xi} = 2\pi\sqrt{2}\xi/d, \quad \tilde{x} = 2\pi\sqrt{2}x/d, \quad \tilde{y} = 2\pi\sqrt{2}y/d. \quad (21)$$

Figure 2a shows the shape of this potential in the xy plane. As we see from the figure, the potential has the shape of a deep "gully" with a periodic spatial modulation of the "bottom" along the $\tilde{x}$ axis. Shown are the cross sections of the potential in different planes corresponding to the periodic behavior of the potential along the "gully" (Fig. 2b) and the minimum and maximum of the modulation in the transverse cross section (Fig. 2c).

Figure 3a shows the behavior of the maximum pinning forces $f_{\rm pin\parallel}^{\max}$ and $f_{\rm pin\perp}^{\max}$ along and transverse to the chain of EDs as a function of the distance d between dislocations at a fixed value of the coherence length ξ, and Fig. 3b shows the ratio of these forces as a function of the parameter ξ/d. We see that for $d \leqslant 2\xi$ there exists a strong anisotropy of the pinning force acting on a vortex along and transverse to the chain of EDs, and for $d \leqslant \xi$ the longitudinal pinning force is exponentially small, i.e., the bottom of the "gully" becomes almost flat, which makes for a free "slipping" of the vortices along the chain of EDs. In the transverse direction the potential barrier and the pinning force fall off as $T \to T_c$ by a power law, which determines the temperature dependence of the critical current. In particular, for $\tau \ll 1$ and $\xi \gg d$ it follows from (20) that $j_c \propto \tau^{1/2}$ for $\xi > r_0$ (cf. Ref. 21).

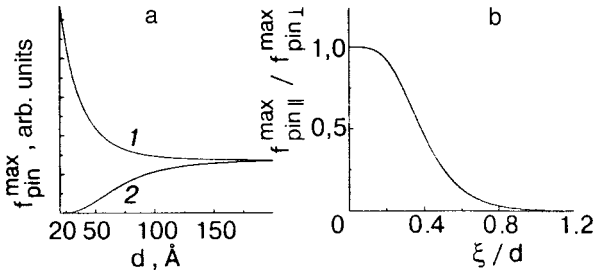

FIG. 3. Pinning forces for an isolated vortex on a periodic infinite chain of edge dislocations, calculated according to formula (20): a — pinning force transverse to (curve *1*) and along (curve *2*) the chain as functions of the distance d between adjacent dislocations (for $\xi=30$ Å); b — the ratio of the longitudinal and transverse pinning forces as a function of the parameter ξ/d.

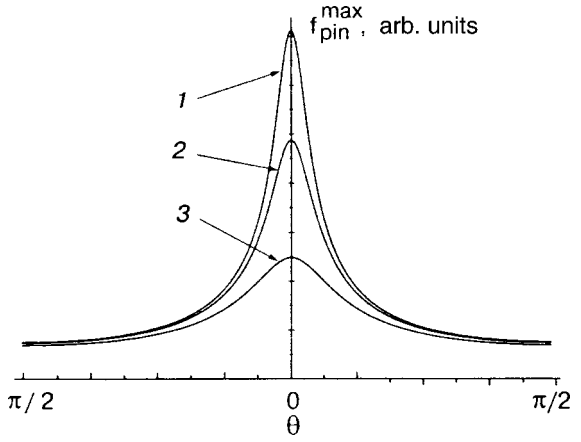

FIG. 4. Pinning force of a rectilinear isolated vortex at a dislocation core as a function of the tilt angle θ of the vortex with respect to the dislocation, for various values of the parameter $\beta=L/\xi$: 20 (*1*), 15 (*2*), 7 (*3*).

PINNING OF VORTICES ON DISLOCATIONS IN A TILTED MAGNETIC FIELD

As we mentioned in the Introduction, the critical current j_c in epitaxial films of cuprate MOCs with the **c** axis oriented perpendicular to the substrate in an external magnetic field **H** exhibits a highly anisotropic dependence on the angle θ between the directions of **H** and **c**. As a rule, in such films one observes two maxima (peaks) on $j_c(\theta)$ at angles $\theta=0°$ (**H**$\|$**c**) and $\theta=90°$ (**H**$\perp$**c**), which is apparently indicative of the existence of two pronounced systems of extended defects (dislocations) oriented along the **c** axis and in the ab plane, and of the efficiency of the mechanism for the pinning of Abrikosov vortices on such defects.

We shall show that the simplest model of a single-particle core pinning of vortices at δ-function dislocation core with a potential of the form (11) in a tilted magnetic field allows one to describe correctly the experimental orientation dependence of $j_c(\theta)$ in cuprate epitaxial films.[15,23,24]

The total volume energy of pinning of a vortex inclined at an angle θ to the dislocation line, which is parallel to the z axis, is given in Cartesian coordinates by the expression

$$\tilde{\varepsilon}_{\rm pin}(\mathbf{u}')=\int dx\int dy\int dz U_{\rm pin}(x,y)p_V(\mathbf{r}'+\mathbf{u}'), \qquad (22)$$

where the form factor p_V is written in a coordinate system rotated by an angle θ about the y axis. Here the displacements of the vortices along the x and z (or x' and z') axes can be neglected, since they correspond to parallel transport of an infinitely long vortex relative to a rectilinear dislocation, and the displacement $u_{y'}\equiv u_y\equiv u$.

Introducing a δ-function pinning potential of the type (11), with $\delta^2(r)\equiv\delta(x)\delta(y)$, at a dislocation core of small radius and taking into account the obvious relation $x'=z\sin\theta$, we obtain for the form factor (3) as a result of the integration in (22) (for $\theta\neq 0$);

$$\tilde{\varepsilon}_{\rm pin}(u,\theta)=-2\pi r_0^2U_0\xi^2\int_{-\infty}^{\infty}\frac{dz}{z^2\sin^2\theta+u^2+2\xi^2}$$

$$=-\frac{\pi\varepsilon_0 r_0^2}{|\sin\theta|\sqrt{u^2+2\xi^2}}. \qquad (23)$$

Expression (23) diverges at the point $\theta=0$, i.e., for a parallel orientation of an infinitely long vortex and infinitely long dislocation. To eliminate this divergence it is necessary to cut off the integration over z in (23) at some finite length of the rectilinear part of the dislocation and/or vortex. In particular, for symmetric limits $L/2$ and $-L/2$ we obtain the expression

$$\tilde{\varepsilon}_{\rm pin}(u,\theta)=-\frac{2\varepsilon_0 r_0^2}{|\sin\theta|\sqrt{u^2+2\xi^2}}\,\mathrm{arctg}\frac{L|\sin\theta|}{2\sqrt{u^2+2\xi^2}}, \qquad (24)$$

which remains finite at $\theta=0$, where it takes the value (cf. Eq. (10)

$$\tilde{\varepsilon}_{\rm pin}(u,0)=-\varepsilon_0\frac{r_0^2L}{u^2+2\xi^2}. \qquad (25)$$

Figure 4 shows the theoretical angle dependence of the maximum pinning force $f_{\rm pin}^{\rm max}(\theta)$ calculated on the basis of expression (24) for different values of the dimensionless parameter L/ξ in the angle interval $-\pi/2\leqslant\theta\leqslant\pi/2$. We see that the theoretical dependence $f_{\rm pin}^{\rm max}(\theta)$ agrees quite satisfactorily with the experimentally measured dependence $j_c(\theta)$ in YBaCuO epitaxial films (Fig. 5). The difference of the experimental angle dependences for different systems of dislocations (parallel and perpendicular to the **c** axis) and in different films may be due to both a different length of the linear parts of the dislocation (or vortex) lines and to different values of the core radius r_0.

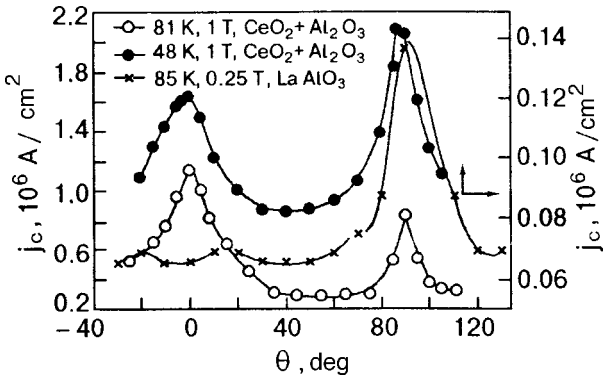

FIG. 5. Experimentally measured $j_c(\theta)$ curves for YBaCuO films.[15]

CONCLUSIONS

In summary, the simplest models of a single-particle core pinning of Abrikosov vortices at the cores of dislocations in low magnetic fields permit a qualitatively correct description of the main characteristics of the temperature and angle (orientation) dependences of the pinning force and critical currents. Of particular interest is the single-particle pinning of vortices at low-angle boundaries between single-crystal blocks which are slightly misoriented in the ab plane in HTSC epitaxial films. Such boundaries are periodic chains of edge dislocations and have a strong anisotropy of the pinning force along and transverse to the chains at distances between adjacent edge dislocations $d \leqslant 2\xi$. As a result of this, the depinning critical current density flowing through a low-angle boundary can be much smaller than the value j_c associated with volume pinning of vortices at individual dislocations.

In closing, we thank V. M. Pan, S. M. Ryabchenko, and A. V. Semenov for helpful discussions of the results.

*E-mail: pashitsk@iop.kiev.ua

[1] A. M. Campbell and J. E. Evetts, *Critical Currents in Superconductors* [Taylor and Francis, London (1972), Mir, Moscow (1975)].
[2] A. I. Larkin and Yu. N. Ovchinnikov, Zh. Éksp. Teor. Fiz. **65**, 1704 (1973) [Sov. Phys. JETP **38**, 854 (1975)]; JETP Lett. **27**, 280 (1978).
[3] P. W. Anderson, Phys. Rev. Lett. **9**, 309 (1962).
[4] G. S. Mkrtchyan and V. V. Shmidt, Zh. Éksp. Teor. Fiz. **61**, 367 (1971) [Sov. Phys. JETP **34**, 195 (1972)]; Usp. Fiz. Nauk **112**, 353 (1974) [Sov. Phys. Usp. **17**, 459 (1974)].
[5] C. P. Bean and J. D. Livingston, Phys. Rev. Lett. **12**, 14 (1964).
[6] T. H. Alden and J. D. Livingston, J. Appl. Phys. **37**, 3551 (1966).
[7] A. I. Larkin, Zh. Éksp. Teor. Fiz. **58**, 1466 (1970) [Sov. Phys. JETP **31**, 784 (1970)].
[8] W. W. Webb, Phys. Rev. Lett. **11**, 191 (1963).
[9] K. Miyahara, F. Irie, and K. Yamafuji, J. Phys. Soc. Jpn. **27**, 290 (1969).
[10] B. Kronmuller and R. Schmucher, Phys. Status Solidi B **57**, 667 (1973).
[11] E. J. Kramer, J. Appl. Phys. **49**, 742 (1978).
[12] É. A. Pashitskiĭ, Fiz. Tverd. Tela (Leningrad) **22**, 608 (1980) [Sov. Phys. Solid State **22**, 356 (1980)].
[13] J. G. Bednorz and K. A. Muller, Z. Phys. B **64**, 189 (1986).
[14] G. Blatter, M. V. Feigelman, V. G. Geshkenbein, A. I. Larkin, and V. M. Vinokur, Rev. Mod. Phys. **66**, 1125 (1994).
[15] V. M. Pan, Usp. Fiz. Met. **1**, 49 (2000).
[16] G. W. Crabtree, J. Z. Liu, A. Umezawa, W. K. Kwok, C. H. Sowers, S. K. Malik, B. W. Veal, D. J. Lam, M. B. Brodsky, and J. W. Downey, Phys. Rev. B **36**, 4021 (1987).
[17] M. Daenmling, J. M. Seuntjens, and D. C. Larbalestier, Nature (London) **346**, 332 (1989).
[18] V. F. Solovjov, V. M. Pan, and H. C. Freyhardt, Phys. Rev. B **50**, 13724 (1994).
[19] J. B. Hirth and J. Lothe, *Theory of Dislocations*, McGraw–Hill, New York (1968).
[20] A. Gurevich and É. A. Pashitskiĭ, Phys. Rev. B **57**, 13878 (1998).
[21] É. A. Pashitskiĭ, V. I. Vakaryuk, S. M. Ryabchenko, and Yu. V. Fedotov, Fiz. Nizk. Temp. **27**, 131 (2001) [Low Temp. Phys. **27**, 96 (2001)].
[22] D. Dimos, P. Chaudhari, and J. Manhart, Phys. Rev. B **41**, 4038 (1990).
[23] A. Diaz, L. Mechin, P. Berghuis, and J. E. Evetts, Phys. Rev. Lett. **80**, 3855 (1998).
[24] V. A. Komashko, A. G. Popov, V. L. Svechnikov, A. V. Pronin, V. S. Melnikov, A. Yu. Galkin, V. M. Pan, C. L. Snead, and M. Suenaga, Supercond. Sci. Technol. **13**, 209 (2000).
[25] M. Tachiki and S. Takahashi, Solid State Commun. **70**, 291 (1989).
[26] J. R. Clem, J. Low Temp. Phys. **18**, 427 (1975).
[27] C. Meingast, O. Kraut, T. Wolf, H. Wuhl, A. Erb, and G. Muller-Vogt, Phys. Rev. Lett. **67**, 1634 (1991).
[28] C. Meingast, A. Junod, and E. Walker, Physica C **272**, 106 (1996).

Translated by Steve Torstveit

Fluctuation conductivity in $YBa_2Cu_3O_{7-y}$ films with different oxygen content. I. Optimally and lightly doped YBCO films

A. L. Solovjov*

B. Verkin Institute for Low Temperature Physics and Engineering, National Academy of Sciences of Ukraine, pr. Lenina 47, 61103 Kharkov, Ukraine

H.-U. Habermeier and T. Haage

Max-Planck-Institute für Festkorperforschung, Heisenbergstr. 1, 70569 Stuttgart, Germany
(Submitted June 6, 2001; revised September 18, 2001)
Fiz. Nizk. Temp. **28**, 24–35 (January 2002)

Fluctuation conductivity in $YBa_2Cu_3O_{7-y}$ (YBCO) films with different oxygen concentrations is investigated. All of the samples exhibit a clear transition from the Maki–Thompson mechanism of scattering of fluctuational pairs to the Aslamazov–Larkin mechanism as the temperature approaches T_c. The values of the transition temperature are used to determine the coherence length $\xi_c(0)$ along the c axis and the phase relaxation time $\tau_\varphi(100\text{K})$ of the fluctuational pairs. Despite the decrease of T_c from 87.4 to 54.2 K with decreasing oxygen content in the samples studied, a value $\tau_\varphi(100\text{K})=(3.35\pm0.01)\times10^{-13}$ s is obtained for all the samples. It is shown that the dependence of $\xi_c(0)$ on T_c conforms to the standard theory of superconductivity. The mechanisms for the scattering of charge carriers and for superconducting pairing in high-T_c superconductors are analyzed. © *2002 American Institute of Physics.* [DOI: 10.1063/1.1449180]

INTRODUCTION

It is now thought that the property of superconductivity in high-T_c superconductors (HTSCs) can be basically understood by studying their normal-state properties, which are extremely specific.[1–4] However, in spite of the significant efforts of investigators, the physics of superconducting pairing and the mechanisms for the scattering of charge carriers in the normal state are not yet completely clear. Even the results of such classic experiments as resistivity measurements and the Hall effect are extremely contradictory. Their temperature dependence, especially for the optimally doped YBCO systems, is known to be directly opposite. For example, the Hall coefficient $R_H \propto 1/T$ and exhibits a pronounced maximum at T_{on}, corresponding to the onset of the resistive transition to the superconducting state.[5] At the same time, the longitudinal resistivity ρ_{xx} is a linear function of T over an anomalously wide temperature interval. Thus, in order to explain the experiment, it is necessary to assume that the scattering mechanism can have appreciable anisotropy or to consider at least two different scattering mechanisms, operating in the absence and in the presence of a magnetic field.[6] Moreover, the electron–phonon interaction constant $\lambda_{e\text{ph}}$ in HTSCs is too small to account for the high critical temperatures T_c observed in experiment in terms of the ordinary electron–phonon interaction,[1,7–9] and this also points to the necessity of considering an alternative scattering mechanism for explaining the linear temperature dependence of the resistivity. This problem has been the subject of a great many papers, a detailed analysis of which is given in Ref. 6. These papers can be roughly divided into two groups.

The first group consists of papers based on the assumption that the scattering in cuprates is due to the interaction with two different types of excitations.[10–12] In the best-known and most widely discussed (but extremely exotic) model of resonant valence bands,[13] these excitations are spinons and holons, which contribute to the resistivity. However, the holon contribution is assumed to be the governing one, whereas the spinons, which are efficiently coupled to the magnetic field **H**, should determine the temperature dependence of the Hall effect.

The second group of papers use models based on the concept of anisotropy of the carrier scattering, the cause of which may be the complex band structure of the cuprates[14,15] or the influence of spin fluctuations.[16–18] However, in spite of considerable efforts the goal of explaining all of the experimentally observed anomalies, primarily the different temperature dependence of ρ_{xx} and R_H, in terms of a unified theory has long remained elusive. The situation was clarified considerably with the advent of the ''nearly antiferromagnetic Fermi liquid'' (NAFL) model.[6]

According to the NAFL model, the scattering of carriers in HTSCs is governed by an extremely nonuniform antiferromagnetic interaction V_{eff}. The main scattering centers are those points of the Fermi surface that intersect the magnetic Brillouin zone — so-called hot spots. This naturally leads to appreciable anisotropy in the behavior of the charge carriers, since the temperature dependence of the intensity of their scattering at the hot spots is different from that on the rest of the Fermi surface. It is assumed that the intensity of V_{eff} is temperature dependent. As a result, three regions with different temperature dependence of the low-frequency magnetic behavior in YBCO are found.[6,19] These are the mean field (MF) regime at high temperatures, which gives way at T_{cr} to a pseudoscaling (PS) regime, existing down to a temperature T_*, and at temperatures below T_* a pseudogap (PG) re-

gime, characterized by a change in the spectrum of magnetic fluctuations and by the presence of a strong temperature variation of the band structure of the quasiparticles, which should lead to evolution of the Fermi surface.[20,21]

In this approach the NAFL theory successfully explains both the anomalous Hall effect and the temperature dependence of the resistivity. According to the NAFL theory, in the MF and PS regimes the temperature dependence $\rho_{xx}(T)$ should be linear, as is observed in experiment. In the pseudogap regime the effective size of the Fermi surface should decrease as the temperature decreases. This actually leads to a closing of some of the scattering channels for charge carriers, and that can explain the observed deviation of $\rho_{xx}(T)$ down from a linear trend for $T_{*0} \leqslant T_*$. Thus the linear dependence of $\rho_{xx}(T)$ can be considered a reliable indicator of the normal state of the system, which, accordingly, is characterized by stability of the Fermi surface in the MF and PS regimes. This conclusion is important for analysis of the fluctuation conductivity, in which the determination of the normal state plays an important role.

All of the critical temperatures separating the temperature regimes mentioned above depend strongly on the oxygen concentration in the sample and decrease rapidly with increasing oxygen index, probably because of a lessening of the influence of the magnetic interaction with increasing doping.[1,22–24] For the optimally doped YBCO system ($T_c \cong 90$ K) the theory[6,19] gives $T_* \cong 110$ K and $T_{cr} \cong 150$ K, showing that in this case the crossover in the magnetic behavior of the system and the transition to the pseudogap regime occur very close to T_c. It should be noted that from the standpoint of studying the mechanism of superconducting pairing it is the pseudogap regime that is of greatest interest, since, as we suppose, it is in the temperature interval $T_c < T < T_{*0}$ that the nucleation of the superconducting state occurs in YBCO systems. However, the parameters of the HTSC in the pseudogap regime vary so unpredictably that neither the NAFL nor the other theories that satisfactorily describe the scattering of charge carriers in the normal region, i.e., above T_{*0}, can describe the experiment in this temperature interval.

At the same time, as we have shown previously,[9] for optimally doped systems the interval $T_c < T < T_{c0} = (110 \pm 5)$ K is precisely that temperature region in which the temperature dependence of the resistivity is governed by superconducting fluctuations, leading to the onset of fluctuation conductivity $\sigma' = \sigma(T) - \sigma_N(T)$. Thus the study of fluctuation conductivity (FC) can yield information about the scattering and fluctuational pairing mechanisms as T approaches T_c. The equation determining the FC is conveniently written as

$$\sigma'(T) = [\rho_N(T) - \rho(T)]/[\rho_N(T)\rho(T)], \qquad (1)$$

where $\rho(T) = \rho_{xx}(T)$ is the actually measured resistivity, and $\rho_N(T) = \alpha T + b$ is the normal-state resistivity of the sample extrapolated to low temperatures. Although such a definition of $\rho_N(T)$ is widely used for calculating $\sigma'(T)$ in HTSCs,[25–31] it has long remained in dispute, especially for lightly doped systems, for which a deviation of $\rho_{xx}(T)$ from a linear dependence is observed for $T_{*0} \gg T_c$. With the adoption of the NAFL theory this definition of $\rho_N(T)$ can be considered fully justified.

To obtain information about the mechanisms for scattering and superconducting pairing in HTSCs we have analyzed the fluctuation conductivity, which was first measured for well structured $YBa_2Cu_3O_{7-y}$ films with different oxygen concentrations. There are two fluctuation contributions to $\sigma'(T)$. The direct contribution, which was given a theoretical foundation by Aslamazov and Larkin (AL),[32] arises as a result of the spontaneous formation of fluctuation-induced Cooper pairs above T_c. An additional contribution, introduced by Maki and Thompson (MT)[33] in an extension of the AL theory, is interpreted as being the result of an interaction of already existing fluctuational pairs with normal charge carriers and is governed by pair-breaking processes in the particular sample. The MT contribution depends on the lifetime τ_φ of the fluctuational pairs and is dominant in the region of two-dimensional (2D) fluctuations,[34] especially in well-structured samples, i.e., in the case of weak pair-breaking, whereas the AL mechanism dominates in three-dimensional (3D) region of fluctuation conductivity near T_c. In layered structures, including HTSCs, the AL contribution is usually determined by the Lawrence–Doniach (LD) model,[35] which predicts a smooth dimensional crossover from 2D to 3D fluctuation behavior for $T \to T_c$. Here the MT contribution is assumed to be insignificant and, naturally, the question of a changeover of fluctuation mechanisms does not arise.

In the first papers on the measurement of the fluctuation conductivity in HTSCs[26–28] it was observed that the temperature dependence of σ' is described rather well by the LD model. However, a significant quantitative discrepancy between theory and experiment is observed, probably because of the nonuniform flow of current over the sample due to the inhomogeneities of its structure, which cannot be taken into account theoretically. Therefore, it has been proposed to introduce a scaling factor, the so-called C factor,[26] by which the experimental data are multiplied in order to agree with the theoretical calculations. Clearly, the more the value of C differs from unity, the poorer the structure of the sample.

Thus, measurement of the fluctuation conductivity in the case of observation of a dimensional crossover provides a rather simple method of obtaining reliable information about the coherence length $\xi_c(0)$ along the c axis, τ_φ, and the dimensionality of the electronic system of the HTSC, and also about the structural imperfection of the sample, from the value of the C factor. A comparison of τ_φ and the transport relaxation time τ of the charge carriers is decisive for understanding the scattering and superconducting pairing mechanisms in HTSCs. At present, however, except for measurements on YBCO–PrBCO superlattices,[9,30] it has remained impossible to observe the MT contribution and, accordingly, the MT–AL crossover in measurements of the fluctuation conductivity, both in single crystals[31] and in thin films.[25–29] Besides, all of the previous experiments have been done on optimally doped samples. There are no data on the behavior of the fluctuation conductivity in systems with a low T_c (~ 60 K), even though such information is exceptionally important.

SAMPLES AND EXPERIMENTAL TECHNIQUES

For these experiments it was necessary to prepare YBCO films having different oxygen concentrations and demonstrating the explicit presence of the MT fluctuation contribution to the temperature dependence $\sigma'(T)$. Samples with thicknesses from 650 Å ($T_c \sim 54.2$ K) to 1050 Å ($T_c \sim 87.4$ K) were prepared at the Max-Planck-Institute in Stuttgart, Germany by pulsed laser deposition on $SrTiO_3$ (100) substrates, a method which is widely covered in the literature[36] and reproducibly yields *c*-oriented epitaxial films of YBCO, as was monitored by studying the x-ray and Raman spectra. To provide for resistive measurements and measurements of the Hall effect the films were processed photolithographically to yield samples with dimensions of 1.68×0.2 mm and the necessary number of contacts. The resistive measurements were made by the standard four-probe scheme on a fully computerized setup. Careful shielding of the equipment lowered the noise level to ~ 500 nV. The special care in preparing the samples, this made it possible to obtain reproducible, reliable, and systematic results.

Figure 1 shows the $\rho_{xx}(T)$ curves for the most typical YBCO films with different oxygen concentrations. To obtain the optimal information we chose samples F1 ($T_c \cong 87.4$ K), close to the optimally doped system, and sample F6 ($T_c \cong 54.2$ K), representing a very lightly doped system. By comparing the results with the analogous curves obtained for single crystals,[37] one can estimate the oxygen index of these samples as $(7-y) \cong 6.85$ (sample F1) and $\cong 6.56$ (sample F6). As expected, sample F1 exhibits the resistive behavior typical of almost optimally doped systems, for which the magnetic interaction is gradually replaced by a correlation interaction as the number of charge carriers increases,[1,23,24] and the region of pseudogap behavior turns out to be rather small.[6,22] As a consequence, the $\rho_{xx}(T)$ curve is linear above

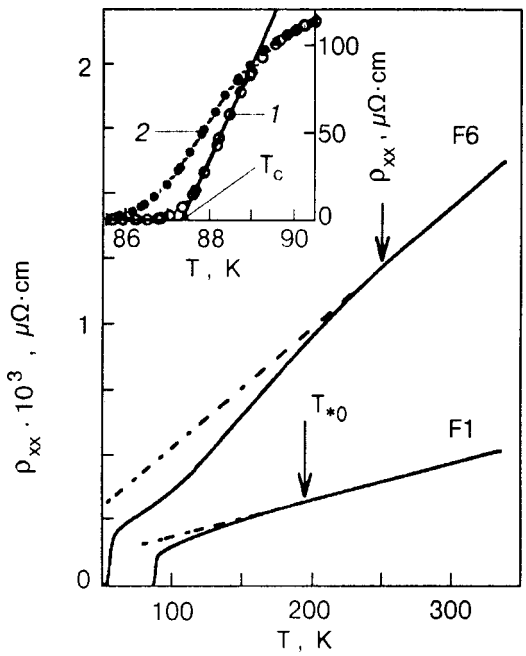

FIG. 1. Temperature dependence of the resistivity for samples F1 and F6; the dashed line is the extrapolation of the resistivity in the normal state into the low-temperature region. The inset shows the resistive transition of sample F1 in zero magnetic field (curve *1*) and in a field $H = 0.6$ T (curve *2*).

$T_{*0} = (190 \pm 0.2)$ K and in the temperature interval 190–330 K it is well extrapolated by the function $\rho_N(T) = \alpha T + b$ (dashed line in Fig. 1) with a relative rms error of 6.52×10^{-4}. In accordance with the concepts of the NAFL theory, this linear dependence extrapolated to the low-temperature region defines $\rho_N(T)$, used in calculating $\sigma'(T)$ according to Eq. (1). A similar procedure for determining $\rho_N(T)$ was used in calculating $\sigma'(T)$ from experiment for sample F6 as well. We note also that $\rho_N(T)$ intersects the T axis near zero, and the ratio $\rho_{300}/\rho_{100} \cong 3.2$. Both of these facts are additional evidence of the good quality of the samples.[36]

As the oxygen concentration decreases, one observes the expected rapid increase in T_c, which in this case is determined by extrapolation of the resistive transition to its intercept with the temperature axis, as is shown in the inset of Fig. 1. At the same time, ρ_{xx} and T_{*0} (indicated by arrows on the curves) increase rapidly, in good agreement with the conclusions of NAFL theory. This means that the scattering mechanism for normal carriers in the HTSC at low T_c is determined mainly by the magnetic interaction. Indeed, sample F6 exhibits resistive behavior typical for very lightly doped YBCO systems[22,37] and is characterized by a wide temperature interval ($T < T_{*0}$) in which spin fluctuations are dominant, leading to the observed peculiar shape of the resistive curve (Fig. 1). Nevertheless, above $T_{*0} = (250 \pm 0.3)$ K the $\rho_{xx}(T)$ curve is linear, as before. According to the NAFL theory, the extrapolation of this linear dependence to the low-temperature region (dashed line in Fig. 1) defines $\rho_N(T)$, as before. We note that all of our attempts to to draw the dashed line in some other way did not give reasonable results for the determination of σ'. In our view, this fact is an additional argument in favor of the correctness of the definition of the normal state of the system. We also note that, despite the low T_c and low oxygen concentration, especially in the case of sample F6, the width ΔT of the resistive transition, determined in the presence of an applied magnetic field, as is shown in the inset in Fig. 1, is extremely narrow. This confirms the good structural quality of our samples, which is important for analysis of the fluctuation conductivity. The parameters of the samples are given in the tables.

ANALYSIS OF THE RESULTS

The general theory of the fluctuation conductivity in layered superconductors was developed by Hikami and Larkin (HL)[34] and considers both the AL and MT fluctuation mechanisms. In the absence of magnetic field the AL contribution is given by

$$\sigma'_{AL} = [e^2/(16\hbar d)](1+2\alpha)^{-1/2}\varepsilon^{-1}, \tag{2}$$

and the MT contribution is given by the theory as

$$\sigma'_{MT} = \{e^2/[8\hbar d(1-\alpha/\delta)]\} \times \ln\left\{\frac{(\delta/\alpha)[1+\alpha+(1+2\alpha)^{1/2}]}{1+\delta+(1+2\delta)^{1/2}}\right\}\varepsilon^{-1}. \tag{3}$$

Here $\alpha = 2\xi_c^2(T)/d^2 = 2[\xi_c(0)/d]^2\varepsilon^{-1}$ is the coupling parameter, $\varepsilon = \ln(T/T_c^{mf}) \approx (T - T_c^{mf})/T_c^{mf}$ is the reduced temperature, T_c^{mf} is the critical temperature in the mean-field approximation, $d \cong 11.7$ Å is the distance between conducting

layers in the HTSC, and $\delta = 1.203(l/\xi_{ab})(16/\pi\hbar) \times [\xi_c(0)/d]^2 k_B T \tau_\varphi$ is the depairing parameter. The factor $1.203(l/\xi_{ab})$, where l is the mean free path and ξ_{ab} is the coherence length in the ab plane, takes into account the clean-limit approximation introduced in the theory of Bieri, Maki, and Thompson (BMT).[38] Equation (2) actually reproduces the result of the LD model,[35] which assumes the presence of a Josephson interaction between conducting layers. This is the most probable situation for the 3D region, since $\xi_c(T) > d$ near T_c, whereas the MT mechanism dominates for $k_B(T - T_c^{mf}) \gg \hbar/\tau_\varphi$ (Ref. 34), where pair tunneling between layers cannot occur, since $\xi_c(T) < d$ (2D region). Thus the HL theory predicts both a change in the electron dimensionality of the sample (2D–3D crossover) and a change of the fluctuation mechanism (MT–LD crossover) as the temperature approaches T_c. Accordingly, the 2D–3D crossover should occur at

$$T_0 = T_c\{1 + 2[\xi_c(0)/d]^2\}, \tag{4}$$

where $\alpha = 1/2$, i.e., $\xi_c(0) = (d/2)\varepsilon_0^{1/2}$, while the MT–LD crossover should occur at a temperature where $\delta \cong \alpha$, which gives

$$\varepsilon_0 = (\pi\hbar)/[1.203(l/\xi_{ab})(8k_B T\tau_\varphi)] \tag{5}$$

and makes it possible to determine τ_φ.[34]

It follows from Eqs. (2) and (3) that outside the region of critical fluctuations, $\sigma'(T)$ depends only on $\varepsilon = (T - T_c^{mf})/T_c^{mf}$, with T_c^{mf} being the temperature that separates the region of fluctuation conductivity from the region of critical fluctuations. Thus the determination of T_c^{mf} is exceptionally important for analysis of the fluctuation conductivity. We determined T_c^{mf} by extrapolation of the linear part of the $\sigma'^{-2}(T)$ curve to its intercept with the temperature axis,[26] since in the 3D region near T_c the dependence of $\sigma'(T)$ should diverge as $(T - T_c^{mf})^{-1/2}$ [Eq. (2)]. The data points in Fig. 2 show a plot of $\sigma'^{-2}(T)$ for sample F1. One can clearly see the extended 3D region, extrapolated by a straight line whose intercept with the T axis immediately gives $T_c^{mf} \cong 88.46$ K. The observed deviation of the data to the right of the straight line at T_0 can be regarded as a reliable indication that the scattering mechanism for the fluctuational pairs at $T > T_0$ is indeed of the MT type. If the fluctuational MT mechanism is absent in the sample, then the data always deviate to the left at T_0.[26] As we have said, before the present studies were done, the fluctuation mechanism of the MT type and, accordingly, the MT–AL crossover, had never been observed in single crystals and thin films: the $\sigma'(T)$ curves only show the smeared 2D–3D transition predicted by the LD model.[26–30]

In contrast to the previous studies, our samples exhibited a pronounced MT–AL transition (indicated by an arrow on the curves in Figs. 3 and 4), which, as a rule, is simultaneously a 2D–3D crossover.[9] This fact allows us to determine ε_0 quite accurately and, using Eq. (4), to obtain reliable values of $\xi_c(0)$. However, we still can't determine τ_φ [see Eq. (5)], since neither l nor $\xi_{ab}(0)$ is measured experimentally in a study of fluctuation conductivity. To find τ_φ we proceed as follows: we denote $[1.203(l/\xi_{ab})] = \beta$; we assume as before that $\tau_\varphi(T) \propto 1/T$,[6,9,39] and for our subsequent estimate of $\tau_\varphi(100\text{K})$ we assume that $\tau_\varphi T = \text{const}$. Equation (5) can be rewritten as

$$\tau_\varphi \beta T = \pi\hbar(8k_B\varepsilon_0) = A\varepsilon_0^{-1}, \tag{6}$$

where $A = \pi\hbar/(8k_B) = 2.988 \times 10^{-12}$ s. Now the parameter $\tau_\varphi(100\text{K})\beta$ is also clearly determined by the measured value of ε_0 and can be used for analysis of the fluctuation conductivity. Thus in the given case the only adjustable parameter is the C factor. We note that, as compared to the previous studies, we introduce the C factor in a more logical manner as the factor by which Eqs. (2), (3), and (7) must be multiplied for agreement with the experimental data.

Figure 3 shows the temperature dependence $\sigma'(T)$ for sample F1 in comparison with the calculated dependence

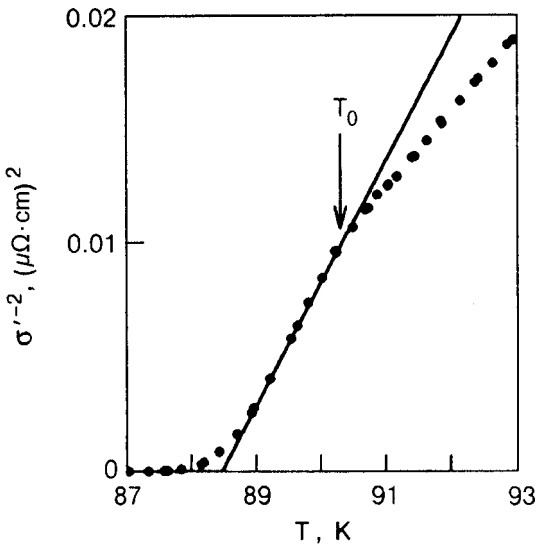

FIG. 2. Plot of σ'^{-2} versus T for sample F1; the solid straight line is the extrapolation of the 3D region; its intercept with the T axis determines T_c^{mf}.

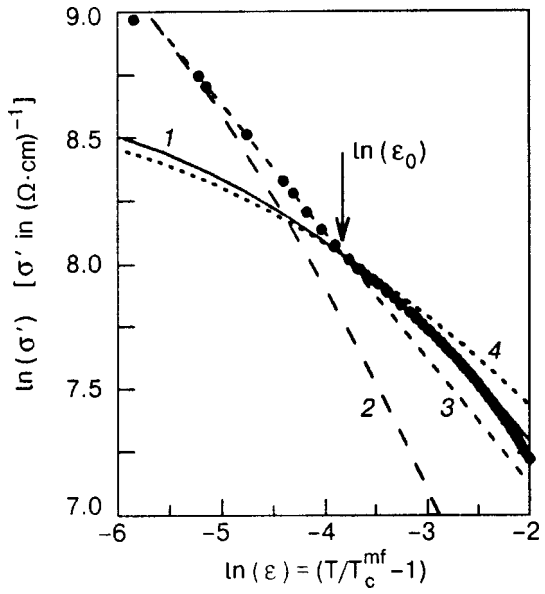

FIG. 3. Comparison of the experimental curves of $\ln(\sigma')$ versus $\ln(\varepsilon)$ (points) for sample F1 ($T_c^{mf} = 88.46$ K) with the fluctuation theories: curve *1* — the MT contribution ($C_{2D} = 0.544$, $d = 11.7$ Å), curve *2* — the LD contribution ($C_{3D} = 0.55$, $d = 11.7$ Å), curve *3* — the AL contribution (3D) ($C_{3D} = 1$), curve *4* — the MT contribution ($C_{2D} = 0.494$, $d = 4.2$ Å).

obtained using the HL theory in the clean limit. The solid curve *1* in the figure is the MT term, and the dashed curve *2* is the LD term. As expected, the MT–AL (2D–3D) crossover is clearly seen on the curve at $\ln\varepsilon_0 \cong -3.92$ ($T_0 \cong 90.22$ K). It is also seen that, in contrast to all the previous measurements of the fluctuation conductivity in HTSCs, the curve determined by the LD model does not agree with the experimental data in any temperature interval. In addition, the value $\xi_c(0) \cong 0.825$ Å determined by the LD model according to Eq. (4) is extremely small. On the other hand, it is clearly seen that in the 3D region the $\sigma'(T)$ curve is linear and is extrapolated beautifully by the standard equation of the AL theory (line *3*), which determines the fluctuation conductivity in any 3D system:[32]

$$\sigma'_{AL} = \{e^2/[32\hbar\xi_c(0)]\}\varepsilon^{-1/2}. \tag{7}$$

This means that the ordinary 3D fluctuation superconductivity is realized in HTSCs at $T \to T_c$. The result also means that in the case of well-structured samples the relation between $\xi_c(0)$ and d does not so strongly influence the pairing processes in this temperature region as would follow from the LD model.[35] Therefore, we denote the observed crossover as MT–AL, unlike the MT–LD transition predicted by the HL theory.[34] It is clear on physical grounds that with increasing temperature the 3D fluctuation regime will persist until $\xi_c(T) > d$.[40] Thus in this case the crossover should occur at $\xi_c(T) \cong d$, i.e., at

$$\xi_c(0) \cong d\varepsilon_0^{1/2}, \tag{8}$$

which is larger by a factor of two than is predicted by the LD and HL theories. Now from Eq. (8) we obtain $\xi_c(0) = (1.65 \pm 0.01)$ Å, in good agreement with the published data.[9,28,29,41] As expected, using the value found for $\xi_c(0)$ we can reconcile the experimental data on $\sigma'(T)$ with the theory in all the temperature intervals studied (Fig. 3). The most important result in this case is that $C_{3D} \equiv 1$, i.e., in the 3D region the experimental data are unambiguously described by the theory on account of the good structure of the sample. On the other hand, we can conclude from the equality $C_{3D} = 1$ that $\xi_c(0)$ has been chosen correctly. In fact, for sample F1 we did not need to use any adjustable parameters. For this reason we take F1 as the base sample.

Above T_0, all the way up to $\ln\varepsilon_{c0} \cong -2.3$ ($T_{c0} \cong 97.3$ K), the $\sigma'(T)$ curve is well extrapolated by the MT contribution of HL theory (curve *1* in Fig. 3) with the parameters $\xi_c(0) = 1.65$ Å and $\tau_\varphi(100\text{K})\beta = 15.06 \times 10^{-13}$ s determined from the measured value of ε_0, and $d = 11.7$ Å. As we have said, the temperature region above T_0 is a region of 2D fluctuations. Thus the result obtained permits the conclusion that the scattering mechanism for fluctuational pairs near T_c, i.e., in the region of the 3D fluctuation conductivity, is different from that in the region of 2D fluctuation conductivity above T_0, as a consequence of the internal nature of the fluctuation conductivity in HTSCs.[9,42] Figure 3 also shows the MT term calculated for $d = 4.2$ Å (curve *4*), which is the distance between the 1D CuO chains in YBCO. We see that in this case the theory does not agree with experiment, indicating that the 1D chains do not contribute directly to the fluctuation conductivity even in the case of optimally doped YBCO systems. It must also be emphasized that the fluctuation mechanism of the MT type, corresponding to a 2D electronic state of the sample, obviously requires that the CuO_2 conducting planes not have defects. Thus the observation of an MT contribution can serve as an additional indication of good structure of the sample. Nevertheless, in the given case it was necessary to use a factor $C_{2D} \cong 0.544$ in order for the theory to correctly describe the experiment. This fact provides a second important result of the analysis of the fluctuation conductivity: $C^* = C_{3D}/C_{2D} \cong 1.84$, from which one may conclude that the effective volume of the sample in the 2D region of fluctuation conductivity is equal to approximately one-half of the actually measured volume. In fact, $\sigma'_{\text{exp}}(T) \propto 1/d_0$ [see Eq. (1)], where d_0 is the geometric thickness of the sample, and $\sigma'_{\text{th}}(T) \propto 1/d_{\text{eff}}$. Since $C_{2D} \cong 0.544$, we have $\sigma'_{\text{exp}}(T) \approx \frac{1}{2}\sigma'_{\text{th}}(T)$, and hence $d_{\text{eff}} \approx \frac{1}{2}d_0$. From this result we can conclude that above T_0 the fluctuational pairs, like the normal carriers, lie within the CuO_2 planes, whereas in the 3D fluctuation region, where $\xi_c(T) > d$ and pair tunneling along the c axis is allowed, the fluctuational pairs interact throughout the entire volume of the sample.

Despite the very low value of T_c, sample F6 exhibits extremely similar behavior of the fluctuation conductivity (Fig. 4), thus confirming the correctness of the analysis developed in this paper. At $\ln\varepsilon_0 \cong -2.98$ ($T_0 \cong 58.72$ K) one can clearly see the MT–AL (2D–3D) crossover on the plot, from which the values $\xi_c(0) = (2.64 \pm 0.02)$ Å and $\tau_\varphi(100\text{K}\beta \cong 5.9 \times 10^{-13}$ s can be obtained with the use of Eqs. (8) and

TABLE I. Resistive parameters of the samples.

Sample	d_0, Å	T_c	ΔT	T_c^{mf}	ρ(100 K)	ρ(300 K)	T^*_0,
		K			$\mu\Omega\cdot$cm		K
F1	1050	87.4	2.3	88.46	148	476	190
F6	650	54.2	3.5	55.88	364	1460	250

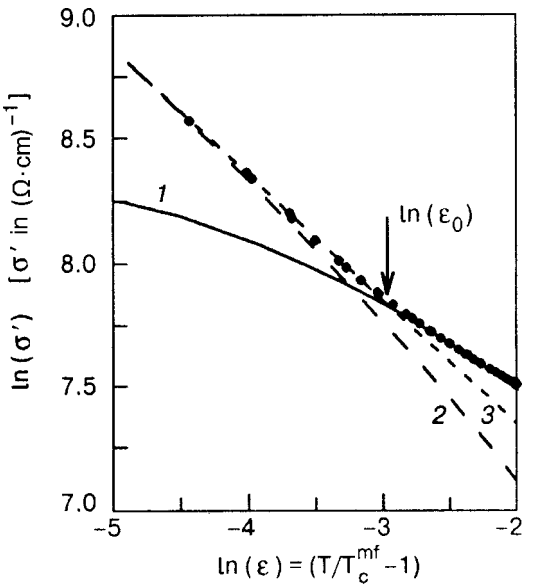

FIG. 4. Comparison of the experimental curves of $\ln(\sigma')$ versus $\ln(\varepsilon)$ (points) for sample F6 ($T_c^{mf} = 55.88$ K) with the fluctuation theories: curve *1* — the MT contribution ($C_{2D} = 1.105$, $d = 11.7$ Å), curve *2* — the LD contribution ($C_{3D} = 2.04$, $d = 11.7$ Å), curve *3* — the AL contribution (3D) ($C_{3D} = 2$).

(6), respectively. Using the parameters found and assuming that $d=11.7$ Å, one can match up the experimental and calculated results both below and above T_0. Near T_c the temperature dependence of $\sigma'(T)$ is determined, as before, by the 3D contribution of the AL theory [see Eq. (7)] (curve *3* of Fig. 4). The LD term, even when constructed with this same value of $\xi_c(0)$ (curve *2* of Fig. 4) again fails to fit the experiment. Above T_0 the fluctuation contribution of the MT type [see Eq. (3)] is a good extrapolation of $\sigma'(T)$ up to $\ln\varepsilon_{c0}\simeq-2.25$ ($T_{c0}\cong 61.9$ K), although the 2D region itself is rather short. Nevertheless $C^*=C_{3D}/C_{2D}\cong 1.81$, as before, confirming the universality of this ratio for HTSCs. However, the absolute values of the C factors in this case are twice those for sample F1: $C_{3D}=2$ and $C_{2D}=1.105$. We assume that the main reason for this result is the growth of the resistivity of the sample by nearly a factor of two for $T>62$ K (see Fig. 1), which, in turn, may be due to several causes. These are a strong influence of spin fluctuations,[6] an appreciable decrease in the carrier density,[1,43] and possibly the inability of the 1D CuO chains to participate in the transport of normal carriers, since, according to Ref. 43, the chains are clearly unlinked in underdoped YBCO systems. In the present case most likely all three mechanisms influence the transport of normal carriers, which, as a result, is extremely complex.[6]

Another aspect of the behavior that is common to both samples is the practically equal values of the relative temperature at which the experimental data deviate from the calculated results with increasing T: $\ln\varepsilon_{c0}=\ln\delta\cong(-2.3\pm 0.05)$. We recall that the pair-breaking parameter δ was initially introduced[33] as $\delta=(T_{c0}-T_c)/T_c$, where T_{c0} is the hypothetical critical temperature in the absence of any pair-breaking processes. This result also suggests that the pair-breaking processes and, possibly, the formation of fluctuational pairs are identical in the two samples. Thus the study of the fluctuation conductivity in samples with a low oxygen concentration permits the conclusion that spin fluctuations and other possible types of magnetic interaction in HTSCs, while strongly influencing the transport properties, have practically no effect on the fundamental mechanism of fluctuational pairing in cuprates and, in the final analysis, lead only to a proportional increase in the C factors.

Considering these arguments, in the analysis of the Hall-effect results for sample F6 we, as before, used $C_{3D}=1$ and not 2. This approach seems reasonable, since it allows one to obtain a self-consistent picture of the behavior of the two samples.

In order to obtain the values of $\tau_\varphi(100\text{K})$ in explicit form, it is necessary to determine the values of the parameter $\beta(100\text{K})$, for which we used the results of the Hall-effect measurements. It is knwon[44] that the Hall resistivity is given by the expression

$$\rho_H(T)\sim[V_{xy}(T)/I_{xx}]=R_{xy}=R_H(T)d_0^{-1}B_z, \tag{9}$$

where $V_{xy}(T)$ is the transverse voltage measured in the experiment, I_{xx} is the current along the sample, d_0 is the thickness of the sample, and B_z is the magnetic field. Thus the Hall coefficient

$$R_H=R_{xy}d_0/B_z \tag{10}$$

can easily be determined. In HTSCs all of the parameters, including R_H, are functions of temperature, and the subsequent estimates were therefore made at $T=100$ K, as is customary in the literature. Here we give a detailed analysis for sample F1. The corresponding parameters obtained in a similar way for sample F6 are given in the tables. According to the theory of Ref. 45, the density of charge carriers is given by $\eta=r[1/(eR_H)]$, where e is the electron charge, the coefficient $r=\langle\tau^2\rangle/\langle\tau\rangle^2$, and τ is the mean time between the charge carrier collisions. Thus r actually reflects the scattering mechanism in the normal state. For purely phonon scattering $r=1.18$, while in the presence of ionized impurities $r=1.93$.[45] Knowing that the samples in question do not contain impurities, in the analysis of the results we shall assume that $r_1=1$ and $r_2=1.18$.

Using the value $R_H(100\text{K})=2.45\times10^{-9}$ m^3/C measured for sample F1, we obtain $n_1=-2.55\times10^{21}$ cm^{-3} ($r_1=1$) and $n_2=3.01\times10^{21}$ cm^{-3} ($r_2=1.18$). The carrier density normalized to the unit cell volume is $n_0=nV_0$, where $V_0=1.74\times10^{-22}$ cm^3. Accordingly, $n_{01}=n_1V_0=0.44$ and $n_{02}=0.52$. To determine the real value of the r factor one can consider the $T_c(n_0)$ diagram.[43] Using this diagram, one can easily find $T_{c1}=85$ K and $T_{c2}=95$ K. Thus the experimentally measured value $T_c=87.4$ K lies right in the investigated temperature interval, but the value $T_{c2}=95$ K determined for $r_2=1.18$ is clearly overestimated. Using the diagram, we find that the real value of T_c corresponds to $r\cong 1.06$ and, hence, $n\cong 2.7\times10^{21}$ cm^{-3}. Clearly both estimates actually represent average values. In the analysis below we consider only the parameter values corresponding to $\langle r\rangle=1.06$. Using a similar approach for sample F6 we obtain $\langle r\rangle=1.07$. Thus the scattering mechanism of the Hall carriers seems to be the same in the two samples. Comparing this result with the theory of Ref. 45, we can conclude that, as expected, the samples are free of impurities. In addition, the electron–phonon interaction is extremely weak ($r\ll 1.18$), as was shown in our previous studies.[9]

Continuing our analysis of sample F1, we obtain for the surface density of carriers $n_s=nd\cong 3.16\times10^{14}$ cm^{-3}. Using the measured value $\rho(100\text{ K})C_{3D}=148$ $\mu\Omega\cdot$cm, since in this case $C_{3D}=1$, we obtain the Hall mobility $\mu_H=r/(\rho ne)\cong 16.55$ cm^2/(V·s). According to the formula $l=(\hbar\mu/e)(2\pi n_s)^{1/2}$ we easily obtain the mean free path of the charge carriers in sample F1: $l=v_F\tau\cong 48.6$ Å, where v_F is the Fermi velocity. Finally, for sample F1 we chose the average value from the literature:[29,46,47] $\xi_{ab}=13.0$ Å. In the general theory of superconductivity[48]

$$\xi_0\sim\hbar v_F/[\pi\Delta(0)], \tag{11}$$

where $\Delta(0)$ is the order parameter at $T=0$ K. Taking into consideration that $2\Delta(0)/k_BT_c\cong 5$–5.5 in HTSCs,[49] and assuming that $\xi_0=\xi_{ab}$, we obtain for the Fermi velocity $v_F=(1.17$–$1.28)\times10^7$ cm/s, and for the effective mass of the carriers $m^*/m_0=(\rho\ln e^2)/(v_Fm_0)=4.68$–$4.23$. After this it is easy to calculate the transport time of the normal carriers: $\tau(100\text{ K})=l/v_F=(0.42$–$0.38)\times10^{-13}$ s. All of the estimates obtained above are in good agreement with the analogous results obtained for optimally doped YBCO systems.[1,9,28,30,39] The only exception is $l(100\text{ K})$ (Table II), which came out somewhat smaller. Nevertheless, $l(0)$

TABLE II. Electronic parameters of the samples.

Sample	C_{3D}	R_H(100 K), 10^{-9} m^3/C	n(100 K), 10^{21} cm^{-3}	n_0 (100 K)	$\xi_c(0)$, Å	r (100 K)	l(100 K), Å	μ_H(100 K), cm^2/(V·s)
F1	1	2.45	2.7	0.47	1.65	1.06	48.6	16.55
F6	2(1)	5.80	1.15	0.20	2.64	1.07	30.5	15.93

$>l(100\ \mathrm{K}) \gg \xi_{ab}$ as before, so that it can be stated that the investigated films are in fact type-II superconductors in the clean limit. Ultimately we find that $\beta(100\ \mathrm{K}) = [1.203(l/\xi_{ab})] = 4.5$. Using the value $\tau_\varphi(100\ \mathrm{K})\beta \cong 15.06\times 10^{-13}$ s found above, we obtain the desired value $\tau_\varphi(100\ \mathrm{K}) \cong 3.35\times 10^{-13}$ s, which is in good agreement with the analogous results obtained in measurements of the magnetoresistance on YBCO–PrBCO superlattices.[41] Similar calculations for sample F6 give $\tau_\varphi(100\ \mathrm{K}) \cong 3.36\times 10^{-13}$ s (see Tables II and III), i.e., the value of $\tau_\varphi(100\ \mathrm{K})$ is indeed the same for the two samples.

We can now analyze the parameters of the fluctuation conductivity. It is clear that, in accordance with the results of analogous measurements,[37,43] the sample with the lower T_c corresponds to the larger R_H, while the carrier density n_0, l, and $\tau(100\ \mathrm{K})$ decrease accordingly. However, μ_H and v_F are practically the same for the two samples. This result can be regarded as additional evidence of the correctness of our approach to the analysis of the fluctuation conductivity, since $\mu_H = R_H/(\rho C_{3D})$, where all of the parameters are measured independently. Finally, in spite of the significant difference of all the initial parameters, the values $\tau_\varphi(100\ \mathrm{K}) = (3.35 \pm 0.01)\times 10^{-13}$ s and $C^* = (1.82 \pm 0.02)$ were found for both samples; this is the main experimental result of this study and confirms the conclusion reached previously that spin fluctuations and other possible types of quasiparticle interactions in HTSCs, while strongly influencing the scattering mechanisms for normal carriers with changing oxygen concentration, have practically no effect on the mechanism of superconducting fluctuational pairing, which is just characterized by the quantity τ_φ. Another result is that the ratio between ξ_c and T_c for the two samples was found to be in complete agreement with the general theory of superconductivity [see Eq. (11)]. It is easily found that their values in samples F1 and F6 have the ratios $T_c(\mathrm{F1})/T_c(\mathrm{F6}) = 1.61$ and $\xi_c(0)(\mathrm{F6})/\xi_c(0)(\mathrm{F1}) = 1.6$, which indicates a clear relation between ξ_c and T_c. This result suggests that the mechanisms of superconducting pairing in HTSCs is to some degree analogous to the pairing mechanisms in conventional superconductors.

CONCLUSION

We have developed an approach to the analysis of fluctuation conductivity in $YBa_2Cu_3O_{7-y}$ HTSC films with different oxygen content and used it to detect a clear MT–AL (2D–3D) dimensional crossover on the $\sigma'(T)$ curves. We have shown that in well-structured samples the LD model does not describe the experimental data in any of the temperature regions. Near T_c a 3D fluctuation superconductivity is realized, which is extrapolated beautifully by the 3D equation of the Aslamazov–Larkin theory. Above T_0 the data are extrapolated by the Maki–Thompson equation, showing that here a 2D fluctuation conductivity is realized. This conclusion is confirmed by the ratio $C^* = C_{3D}/C_{2D} \cong 1.82$ obtained for both samples; this in turn allows us to say that in the 2D region the effective volume of the sample is approximately one-half of its real volume. We can thus conclude that in this temperature region the fluctuational pairs are two-dimensional and, like normal carriers, are located in the CuO_2 planes, since, as we have shown, the 1D CuO chains do not contribute to the fluctuation conductivity. The analysis for the two samples gives a value $\tau_\varphi(100\ \mathrm{K}) = (3.35 \pm 0.01)\times 10^{-13}$ s, which allows us to say with a high probability that the magnetic interaction in HTSCs, while strongly influencing the scattering of normal carriers at low T_c, does not have an appreciable effect on the fluctuational pairing processes.

TABLE III. Electronic parameters of the samples.

Sample	v_F, 10^7 cm/s	m^*/m_0	τ(100 K), 10^{-13} s	β(100 K)	τ_φ(100 K), 10^{-13} s	C^*
F1	1.17–1.28	4.68–4.23	0.42–0.38	4.5	3.35	1.84
F6	1.15–1.27	3.1–2.8	0.26–0.24	1.76	3.36	1.81

In closing the authors thank Prof. V. M. Dmitriev for valuable comments made in a discussion of the results of this study.

*E-mail: solovjov@ilt.kharkov.ua

[1] Y. Iye, in *Physical Properties of High Temperature Superconductors III*, D. M. Ginsberg (Ed.), World Scientific, Singapore (1992), p. 285.
[2] C. P. Slichter, in *Strongly Correlated Electronic Systems*, edited by K. S. Bedell, Addison-Wesley, New York (1994).
[3] M. Acquarone (Ed.), *High Temperature Superconductivity: Models and Measurements*, World Scientific, Singapore (1994).
[4] T. R. Chien, Z. Z. Wang, and N. P. Ong, Phys. Rev. Lett. **67**, 2088 (1991).
[5] S. J. Hagen, A. W. Smith, M. Rajeswari, J. L. Peng, Z. J. Li, R. L. Greene, S. N. Mao, X. X. Xi, S. Bhattacharya, Qi Li, and C. J. Lobb, Phys. Rev. B **47**, 1064 (1993).
[6] B. P. Stojkovic and D. Pines, Phys. Rev. B **55**, 8576 (1997).
[7] S. Yu. Davydov and E. I. Leonov, Fiz. Nizk. Temp. **15**, 536 (1989) [Sov. J. Low Temp. Phys. **15**, 302 (1989)].
[8] G. M. Eliashberg, J. Supercond. **7**, 525 (1994).
[9] A. L. Solovjov, V. M. Dmitriev, H.-U. Habermeier, and I. E. Trofimov, Phys. Rev. B **55**, 8551 (1997).
[10] P. Coleman, A. J. Schofield, and A. M. Tsvelik, Phys. Rev. Lett. **76**, 1324 (1996).
[11] S. G. Kaplan, S. Wu, H.-T. S. Lihn, H. D. Drew, Q. Li, D. B. Fenner, Julia M. Phillips, and S. Y. Hou, Phys. Rev. Lett. **76**, 696 (1996).
[12] A. S. Alexandrov, A. M. Bratkovsky, and N. F. Mott, Phys. Rev. Lett. **72**, 1734 (1994).
[13] P. W. Anderson, Phys. Rev. Lett. **67**, 2092 (1991).
[14] G. A. Levin and K. F. Quader, Phys. Rev. B **46**, 5872 (1992).
[15] D. M. Newns, H. C. Pattnaik, and C. C. Tsuei, Phys. Rev. B **43**, 3075 (1991).
[16] A. Carrington, A. P. Mackenzie, C. T. Lin, and J. R. Cooper, Phys. Rev. Lett. **69**, 2855 (1992).

[17] R. Hlubina and T. M. Rice, Phys. Rev. B **51**, 9253 (1995); *ibid.* **52**, 13043 (1995).
[18] M. Lercher and J. M. Wheatley, Phys. Rev. B **52**, R7038 (1995).
[19] V. Barzykin and D. Pines, Phys. Rev. B **52**, 13585 (1995).
[20] O. Narikiyo and K. Miyake, Solid State Commun. **90**, 333 (1994).
[21] J. R. Engelbrecht, A. Nazarenko, M. Randeria, and E. Dagotto, Phys. Rev. B **57**, 13406 (1998).
[22] B. Bucher, P. Steiner, J. Karpinski, E. Kaldis, and P. Wachter, Phys. Rev. Lett. **70**, 2012 (1993).
[23] V. V. Eremenko, V. N. Samovarov, V. N. Svishchev, V. L. Vakula, M. Yu. Libin, and S. A. Uyutnov, Fiz. Nizk. Temp. **26** 739 (2000) [Low Temp. Phys. **26**, 541 (2000)].
[24] V. V. Eremenko, V. N. Samovarov, V. L. Vakula, M. Yu. Libin, and S. A. Uyutnov, Fiz. Nizk. Temp. **26**, 1091 (2000) [Low Temp. Phys. **26**, 809 (2000)].
[25] P. P. Freitas, C. C. Tsuei, and T. S. Plaskett, Phys. Rev. B **36**, 333 (1987).
[26] B. Oh, K. Char, A. D. Kent, M. Naito, M. R. Beasley, T. H. Geballe, R. H. Hammond, A. Kapitulnik, and J. M. Graybeal, Phys. Rev. B **37**, 7861 (1988).
[27] Y. Matsuda, T. Hirai, and S. Komiyama, Solid State Commun. **68**, 103 (1988).
[28] J. Sugawara, H. Iwasaki, N. Kabayashi, H. Yamane, and T. Hirai, Phys. Rev. B **46**, 14818 (1992).
[29] W. Lang, G. Heine, P. Schwab, X. Z. Wang, and D. Bauerle, Phys. Rev. B **49**, 4209 (1994).
[30] H.-U. Habermeier, A. L. Solovjov, and V. M. Dmitriev, Physica C **235–240**, 1959 (1994).
[31] K. Winzer and G. Kumm, Z. Phys. B - Condensed Matter **82**, 317 (1991).
[32] L. G. Aslamazov and A. I. Larkin, Phys. Lett. A **26**, 238 (1968).
[33] K. Maki, Prog. Theor. Phys. **39**, 897 (1968); R. S. Tompson, Phys. Rev. B **1**, 327 (1970).
[34] S. Hikami and A. I. Larkin, Mod. Phys. Lett. B **2**, 693 (1988).
[35] W. E. Lawrence and S. Doniach, in *Proceedings of the Twelfth International Conference on Low Temperature Physics; Kioto (1971)*, p. 361.
[36] H.-U. Habermeier, Appl. Surf. Sci. **69**, 204 (1993).
[37] T. Ito, K. Takenaka, and S. Uchida, Phys. Rev. Lett. **70**, 3995 (1993).
[38] J. B. Bieri, K. Maki, and R. S. Thompson, Phys. Rev. B **44**, 4709 (1991).
[39] Y. Matsuda, T. Hirai, S. Komiyama, T. Terashima, Y. Bando, K. Iijima, K. Yamamoto, and K. Hirata, Phys. Rev. B **40**, 5176 (1989).
[40] V. M. Dmitriev, A. L. Solov'ev, and A. I. Dmitrenko, Fiz. Nizk. Temp. **11**, 682 (1985) [Sov. J. Low Temp. Phys. **11**, 374 (1985)].
[41] W. Volz, F. S. Razavi, G. Quirion, H.-U. Habermeier, and A. L. Solovjov, Phys. Rev. B **55**, 6631 (1997).
[42] Y. B. Xie, Phys. Rev. B **46**, 13997 (1992).
[43] Z. Z. Wang, J. Clayhold, and N. P. Ong, Phys. Rev. B **36**, 7222 (1987).
[44] A. L. Solovjov, Fiz. Nizk. Temp. **24**, 215 (1998) [Low Temp. Phys. **24**, 161 (1998).]
[45] S. M. Sze, *Physics of Semiconductor Devices*, Wiley-Intercience, New York (1969), p. 45.
[46] K. Semba and A. Matsuda, Phys. Rev. B **55**, 11103 (1997).
[47] J. Axnas, B. Lundqvist, and O. Rapp, Phys. Rev. B **58**, 6628 (1998).
[48] P. G. De Gennes, *Superconductivity of Metals and Alloys*, Benjamin, New York–Amsterdam (1966).

Translated by Steve Torstveit

LOW TEMPERATURE MAGNETISM

Inhomogeneous states for small magnetic particles with exchange anisotropy

B. A. Ivanov[1)]

Institute of Magnetism of the National Academy of Sciences of Ukraine, pr. Vernadskogo 36 b, 03142 Kiev, Ukraine; Taras Shevchenko Kiev University, pr. Glushkova 2, 03127 Kiev, Ukraine

A. Ya. Volk and A. Yu. Merkulov

Taras Shevchenko Kiev University, pr. Glushkova 2, 03127 Kiev, Ukraine

(Submitted June 5, 2001)
Fiz. Nizk. Temp. **28**, 36–41 (January 2002)

In a ferromagnetic particle with exchange anisotropy a state with a nonuniform distribution of spins can arise in the presence of a magnetic field perpendicular to the easy axis. The presence of inhomogeneous states substantially modifies the standard dependence of the magnetization of the particle on the magnetic field. The form of the boundary conditions on the macroscopic equations for the magnetization is refined on the basis of a comparison of the results with the solutions in the continuum approximation. © *2002 American Institute of Physics*.
[DOI: 10.1063/1.1449181]

Artificial magnetic structures containing ferromagnetic elements (films, granules, magnetic dots) with a characteristic size of the order of tens or hundreds of nanometers and separated by nonmagnetic spacers have attracted a great deal of attention in the last ten years. Such materials are important for practical applications (high-density magnetic recording; the use of the giant magnetoresistance and giant magnetoimpedance effects) and are also interesting as fundamentally new objects for the basic physics of magnetism.[1–7] Of course, for materials of this kind the role of the surface becomes much more important than for bulk materials. In real magnets the surface comes into play for two reasons. First, even on an ideal atomically smooth surface the spins have different coordination numbers than in the bulk, and consequently the intensity of the exchange interaction is different. Second, in real magnets the surface atoms have a different environmental symmetry, which leads to a specific single-ion anisotropy for the spins on the surface with a preferred axis coinciding with the vector normal to the surface.

In the physics of magnetism there are two approaches to the analysis of the static and dynamic problems: microscopic and macroscopic. The microscopic approach is based on the use of a discrete spin Hamiltonian in which the spins $\mathbf{S_l}$ (quantum or treated quasi-classically) are specified at the lattice sites $\mathbf{l}$. In discrete models the magnetic anisotropy can be introduced in two different ways: as single-ion anisotropy, and as anisotropy of the exchange interaction. In the spin Hamiltonian these anisotropies are described by terms $H_a^{(SI)}$ and $H_a^{(e)}$, respectively. In the case of a ferromagnet with exchange anisotropy of the easy-axis type the Hamiltonian is chosen in the form

$$H=-\frac{J}{2}\sum_{\mathbf{l},\boldsymbol{\delta}}\left[S_{\mathbf{l}}^{z}S_{\mathbf{l}+\boldsymbol{\delta}}^{z}+\gamma\left(S_{\mathbf{l}}^{x}S_{\mathbf{l}+\boldsymbol{\delta}}^{x}+S_{\mathbf{l}}^{y}S_{\mathbf{l}+\boldsymbol{\delta}}^{y}\right)\right], \tag{1}$$

where J is the exchange integral, γ is the anisotropy parameter of the exchange interaction, and $\boldsymbol{\delta}$ are the vectors of the nearest neighbors. In this case the anisotropic Hamiltonian $H_a^{(e)}$ (the second term of the sum) is determined by the inequality of the interaction constants of the spin components $S_{\mathbf{l}}^{x,y}$ and $S_{\mathbf{l}}^{z}$, i.e., by the quantity $1-\gamma$, with $\gamma<1$. The single-ion anisotropy is taken into account by adding to the isotropic (with $\gamma=1$) exchange Hamiltonian H_e in (1) a term $H_a^{(SI)}$,

$$H_a^{(SI)}=-\frac{K}{2}\sum_{l}\left[(S_l^z)^2\right], \quad K>0. \tag{2}$$

A study of the substantially inhomogeneous states for the microscopic Hamiltonian (1) was done by Gochev. He constructed exact one-dimensional solutions describing a domain wall[8] and inhomogeneous states localized near the surface.[9] In particular, a unique property of model (1), consisting in the fact that for any, even a very large, value of the anisotropy, when the thickness of the domain wall is comparable to the lattice constant there is no pinning of the wall. Apparently this demonstrates special properties of the model, which are close to the properties of exactly integrable models. Gochev's results cannot be generalized to more general models, e.g., incorporating the single-ion anisotropy (2) or, what is of interest here, an external magnetic field perpendicular to the easy axis. Those papers[8,9] are therefore an exceptional case, and the study of the microscopic Hamiltonian is usually done numerically, for large but finite lattices. In that case the special role of the surface is manifested directly for the first mechanism; the specifics of the single-ion anisotropy can easily be taken into account by the replacement $K\rightarrow K_s\neq K$ for the spins on the surface. We note that in the description of the macroscopic inhomogeneities of the magnetization in weakly anisotropic materials with $H_a\ll H_e$, both of the aforementioned ways of incorporating anisotropy are completely equivalent, as has been mentioned repeatedly

in the literature, but models with exchange anisotropy are considerably more convenient for numerical study.

In the macroscopic approach, which has long been the main approach used to study the macroscopic inhomogeneities of the magnetization, such as domains and domain structures, magnetic solitons, etc., the state of a magnet is described by a normalized (unit) magnetization vector $\mathbf{m}(\mathbf{r})$, $\mathbf{m}^2=1$. For describing the macroscopic inhomogeneities of the magnetization in weakly anisotropic materials (for $1-\gamma \ll 1$ or $K \ll J$) both of the ways of introducing anisotropy described above are completely equivalent and give a magnetic anisotropy energy density of the form

$$\omega_a = -\frac{1}{2}\beta m_z^2,$$

where the constant $\beta = Z(1-\gamma)JS^2/2a^3$ (Z is the coordination number of the lattice, and a is the lattice constant) or $\beta = KS^2/a^3$ for the cases of exchange or single-ion anisotropy, respectively. We shall show below that when the surface is taken into account, this equivalence is lost, and that leads to important effects—in particular, to the appearance of a new mechanism for the formation of inhomogeneous states of small magnetic particles.

In this paper we show that in the case of exchange anisotropy, in the presence of a magnetic field perpendicular to the easy axis a state of the particle can arise in which the spin distribution is nonuniform, while this effect is absent in the case of single-ion anisotropy. We note that analysis of the inhomogeneous states resulting from the magnetic dipole–dipole interaction is one of the most important problems of the physics of magnetism. In recent years interest in such states for submicron particles has risen significantly.[5,6,10–14] Our proposed mechanism is different, and the inhomogeneous states arise solely because of the presence of a surface and an external magnetic field and are not due to a dipole interaction. To explain this mechanism, we note that in the presence of a magnetic field $H < H_a$ (H_a is the anisotropy field) the magnetic moment makes an angle θ_0 with the easy axis,

$$\sin\theta_0 = \frac{H}{H_a}, \tag{3}$$

where in the case of exchange anisotropy $H_a = (1-\gamma)SZJ/2\mu_B$, where μ_B is the Bohr magneton. It is clear that the coordination number Z' near the surface is smaller than that in the bulk: $Z' < Z$. Therefore, one expects that the deviation of the spins from the easy axis will be larger near the surface than in the bulk. The character of the spin distribution in this state is determined both by the difference of the anisotropy fields at the surface and in the bulk and by the exchange interaction of the spins. Our analysis of this problem is based on numerical and analytical studies of the discrete Hamiltonian without the assumption that the anisotropy is small. Based on a comparison of the results with the solutions in the continuum approximation, we refine the form and character of the boundary conditions for the magnetization.

Let us consider a model ferromagnet occupying the half space $x > 0$, in which the surface is an ideally smooth atomic plane coincident with the plane $x = 0$; the interatomic distance is equal to a. To ascertain the basic relationships of the problem it is sufficient to consider a semi-infinite chain of atoms (Fig. 1). We shall assume that the magnetic anisotropy arises because of anisotropy of the exchange interaction, i.e., the system is described by Hamiltonian (1). We also take into account an external magnetic field perpendicular to the easy axis, which in our case is the z axis. We assume that the atoms on the surface are in no way different from the atoms in the bulk, except that they have a different number of nearest neighbors. The Hamiltonian of the chain is written in the form

$$\hat{H} = -J\sum_{n=1}^{\infty}[\cos\theta_n\cos\theta_{n+1} + \gamma\sin\theta_n\sin\theta_{n+1} \times\cos(\varphi_n - \varphi_{n-1}) + h\sin\theta_n\cos\varphi_n]. \tag{4}$$

Here θ_n and θ_n are the angle variables for the atomic spins in the chain; $h = 2\mu_B H/J$ is the dimensionless magnetic field. The boundary atom is assigned the number $n=1$. It is obvious that the ground state corresponds to $\varphi_n = 0$, and we must minimize the given energy with respect to the angles θ_1, θ_2, θ_3, etc. Thus we obtain an infinite system of transcendental equations which is impossible to solve analytically. We shall therefore analyze this problem numerically; here, of course, the problem will be solved for a chain of relatively large, but finite, length. However, there is an important limiting case in which the problem can be solved analytically.

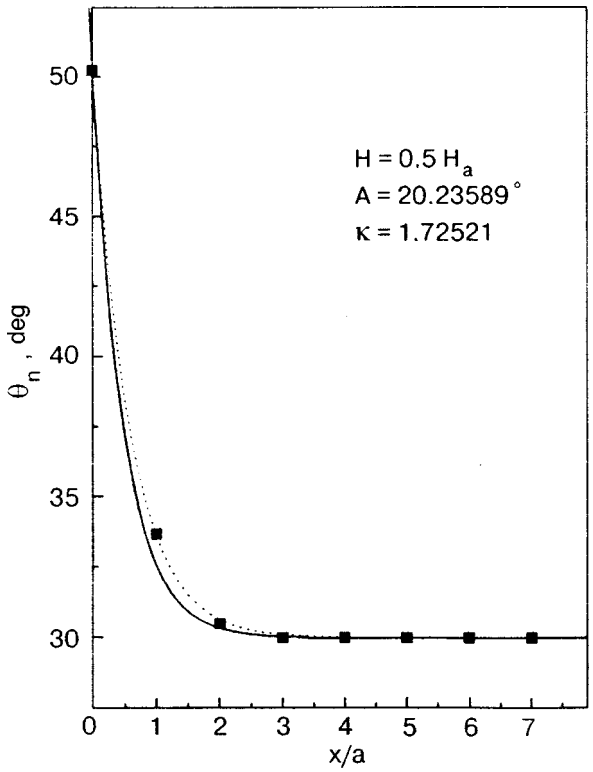

FIG. 1. Deviations of the spins from the anisotropy axis for the Ising model at a value of the magnetic field $H = 0.5H_a$. The points are the deviations in the positions of the atoms found numerically; the solid curve was constructed using the exponential dependence (7), and the dotted curve represents a fit of the function (7) to the numerical values through choice of the parameters A, θ, and κ. The values of A and κ found from the fit are given in the upper right-hand corner of the figure.

Both numerical analysis and simple arguments show that in the presence of a surface the deviations of the variables θ_n from θ_0 are small (θ_0 is the angle of deviation (3) of the spin from the easy axis in the magnet when the surface is not taken into account). Of course, if the applied magnetic field is small, then the deviation θ_0 will also be small. However, if H is large, then the characteristic size of the inhomogeneity increases, and the role of the surface states becomes insignificant; as a result, the deviation of θ_n from θ_0 becomes smaller and smaller. Therefore, the angles of deviation θ_n from the equilibrium position can be decomposed into two terms,

$$\theta_n = \theta_0 + \xi_n, \tag{5}$$

where it is assumed that the ξ_n are small. Since the surface spins are found in a somewhat different position than all the others, it is necessary to write separate equations for ξ_1, ξ_2 and for ξ_n for all the remaining atoms with $n \geqslant 3$. For these last the equations do not contain the surface deviation ξ_1 and have the same form as in an unbounded magnet:

$$\frac{\partial H}{\partial \xi_n} = 2(\gamma-1)\cos^2\theta_0 \xi_n - [1+(\gamma-1)\cos^2\theta_0] \times (2\xi_n - \xi_{n-1} - \xi_{n+1}) = 0. \tag{6}$$

By virtue of this circumstance the solution of our system of equations may be sought in the form

$$\xi_n = A e^{-(n-1)\kappa}, \tag{7}$$

where A is a constant. The exponential dependence (7) for spins in the interior of the crystal follows from the Bloch theorem. The quantity κ, which determines the character of the exponential damping, is found from Eq. (6):

$$\sinh^2\frac{\kappa}{2} = \frac{0.5(1-\gamma)\cos^2\theta_0}{\sin^2\theta_0 + \gamma\cos^2\theta_0}. \tag{8}$$

In the absence of magnetic field ($\theta_0 = 0$) this formula corresponds to Gochev's expression[8] for the thickness of the domain wall in model (1) for an arbitrary value of the anisotropy parameter γ. If the anisotropy is small, i.e., in the case $\gamma - 1 \ll 1$, expression (8) assumes the standard form:

$$\kappa = \sqrt{2(1-\gamma)}.$$

An analysis showed that the exponential substitution is also consistent with Eq. (6) for $n = 2$, and the constant A can be evaluated from the equation obtained by variation with respect to the value of the boundary spin θ_1:

$$A = \frac{(1-\gamma)\sin\theta_0\cos\theta_0}{e^{\kappa} - 1 - (1-\gamma)(e^{\kappa}\cos^2\theta_0 - \sin^2\theta_0)}. \tag{9}$$

This awkward expression simplifies somewhat for the Ising model ($\gamma = 0$), which corresponds to the limiting case of large anisotropy:

$$A^{\text{Ising}} = \frac{\sin\theta_0\cos\theta_0}{\sin^2\theta_0 + \cos\theta_0\sqrt{1+\sin^2\theta_0}}. \tag{10}$$

In this case for $\theta_0 \to 0$, i.e., for a weak field, we have $A \to \theta_0$, and for a field close to the anisotropy field ($\theta_0 \to \pi/2$) the value of A is small, $A \to \cos\theta_0$. A substantial simplification arises in the limiting case of a weakly anisotropic magnet, for $1 - \gamma \ll 1$:

$$A^{\omega a} = \frac{\sqrt{1-\gamma}\sin\theta_0}{2} \ll \theta_0. \tag{11}$$

It follows from these limiting expressions that the assumption that A is small is sensible over a wide interval of parameter values. Consequently, for a weakly anisotropic magnet it holds automatically [see Eq. (11)] because in that case κ is small and the surface spin aligns itself with the bulk spins. This is valid for high fields, when $\kappa \ll 1$ even for large anisotropy, including the Ising model. On the other hand, for small fields the value of θ_0 is itself small, and although it can happen that A is of the order of θ_0 (for the Ising model, $A \to \theta_0$ in the low-field limit), the condition $A \ll 1$, which is sufficient for applicability of the linear approximation, remains in force. Thus it is found that the linear approximation we have used and the formulas (9)–(11) obtained on the basis of it are applicable, at least qualitatively, for a wide class of models, including strongly anisotropic ones.

To check the assumption that the linear approximation is applicable we also carried out a numerical analysis of the problem for the Ising model. A field value $H = 0.5H_a$, i.e., $\theta_0 = 30°$, was chosen, which from the standpoint of applicability of the linear theory corresponds to the least favorable situation: on the one hand, the value of κ is not small—it follows from Eq. (8) that $\kappa = 2.0634$—and on the other hand, the value of A is not small—a calculation on the basis of Eq. (10) gives $A = 20.365°$. We see that the numerical calculations (see Fig. 1) are in good agreement with the analytical formula obtained, even for the case when κ is not very small, and the characteristic scale of variation of the magnetization, a/κ, is smaller than the lattice constant a.

If we consider a real (nonideal) small particle bounded on all sides, then the situation become more complicated, and the problem may be analyzed only numerically. We investigated the distribution of spins in a 10×10 square particle described by the Ising model Hamiltonian. Figure 2 shows the projection of the atomic spins on the field direction in a two-dimensional lattice. In each of Figs. 2a–2c, which correspond to different values of the field, the arrows showing the spin projections are represented in different scales. These arrows reflect the relative lengths of the vectors corresponding to different points of the same figure. The absolute values of the deviations at the characteristic points for each figure are presented in the caption. Figure 3 shows the magnetization curves of the particle, from which we see that the presence of inhomogeneous states substantially modifies the standard dependence (which is linear, by virtue of the relation $\sin\theta_0 = H/H_a$ for a uniform distribution).

The numerical analysis showed that the deviation of the atomic spins on the surface differs from the deviation of the spins in the bulk. However, the greatest value of the deviation occurs for spins located at the corners of the lattice. Intuitively this result is clear: the corner spins have an even smaller coordination number than the spins at regular points of the surface. In this connection the problem arises of how to go from the discrete to the macroscopic description of effects of this kind, if only in that region of parameters of the

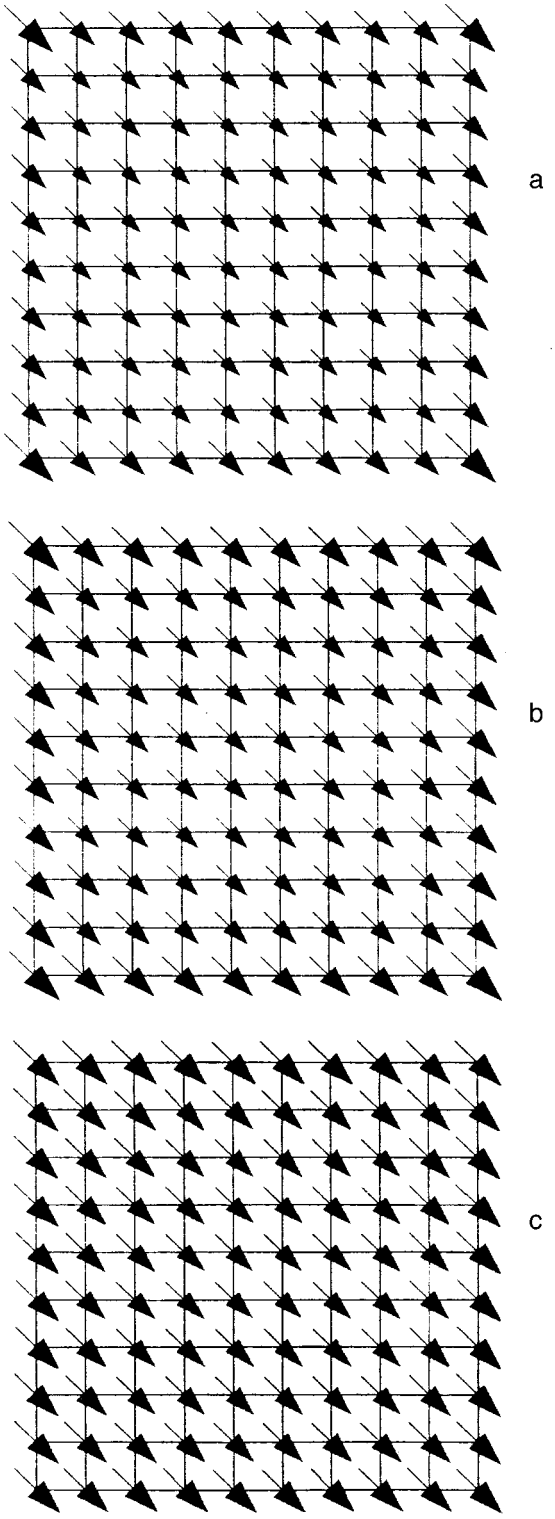

FIG. 2. Inhomogeneous states for a square particle at different values of the field; the arrows describe the relative scale of the inhomogeneity of the spin components in the field direction; the values of θ at the corners, at the center of the boundaries, and in the center of the square for parts a, b, and c are: a—$H/H_a=0.2$; 22.6°, 15.4°, 11.5°; b—$H/H_a=0.5$; 53.5°, 39.9°, 30°; c—$H/H_a=0.8$; 79.9°, 68.6°, 53.3°.

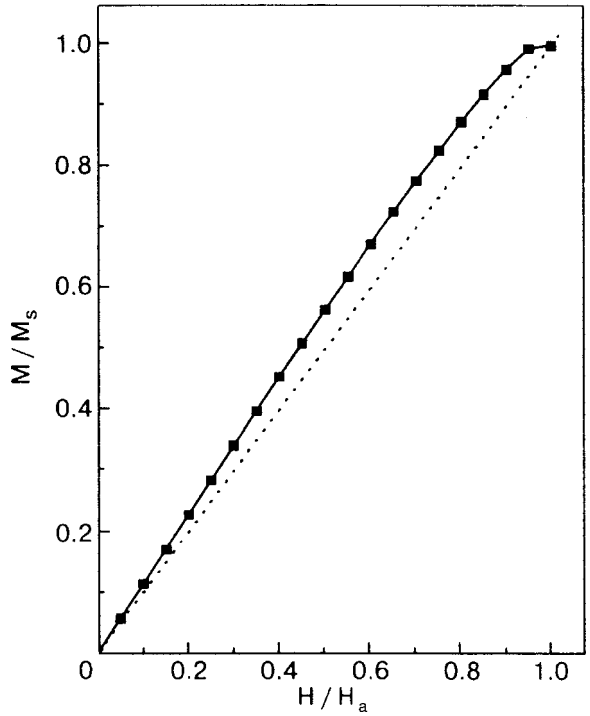

FIG. 3. Magnetization curve for a square particle; the curve with the symbols was found numerically for a particle with exchange anisotropy in an inhomogeneous state, while the dotted curve corresponds to the theoretical linear dependence of the magnetization on field when inhomogeneous states are not taken into account.

problem where $\kappa \ll 1$, the gradients are small, and, at least for the bulk region of the particle, the macroscopic approach should be adequate.[15–17]

In the macroscopic approach the form of the function $\mathbf{m}(\mathbf{r})$ is determined by the solution of differential micromagnetic equations, and the properties of the surface are taken into account through the choice of the particular boundary conditions for these solutions. The question of taking the surfaces into account was posed back in the 1950s and can be regarded as thoroughly investigated. In particular, it is generally accepted that for an ideal atomically smooth surface, the properties of the atoms on which are the same as in the bulk, one must choose free boundary conditions for the magnetization, $n_i(\partial_i \mathbf{m}/\partial x_i)=0$, where $\mathbf{n}$ is the vector normal to the surface.[15–17] If it is instead assumed that there is a specific single-ion surface anisotropy with a volume density

$$\omega_s=\frac{1}{2}K_s^*(\mathbf{m}\cdot\mathbf{n})^2\delta(|\mathbf{r}-\mathbf{r}_s|), \tag{12}$$

where $\mathbf{r}_s$ is a vector parametrizing the surface, the boundary conditions are chosen in the form

$$\mathbf{m}\times\left(An_i\frac{\partial \mathbf{m}}{\partial r_i}+K_s^*(\mathbf{n}\cdot\mathbf{m})\mathbf{n}\right)=0, \tag{13}$$

where A is the inhomogeneous exchange constant. Boundary conditions (13) entail a universal characteristic of the magnet, $\kappa^*=K_s^*/A$. Thus it is regarded as established that the boundary conditions are characterized by a single parameter with dimensions of length, $1/\kappa^*$, and differ from free boundary conditions only in the presence of a specific single-ion surface anisotropy.

Our analytical and numerical results for a spin chain can be described on this basis with the use of an effective anisotropy energy $w_a=-\beta m_z^2/2$, $\beta=2(1-\gamma)JS^2/2a^3$, if it is taken into account that the direction of the axis of the surface anisotropy coincides with that of the bulk anisotropy and not

with the normal to the surface, and a certain modification is made to the boundary conditions, which we now take as

$$\mathbf{m}\times\left(JS^2 a n_i \frac{\partial \mathbf{m}}{\partial r_i} + K_s(\mathbf{e}_z\cdot\mathbf{m})e_z \right) = 0, \tag{14}$$

with the value $K_s=(1-\gamma)JS^2$. This is also valid for non-one-dimensional problems for the corresponding choice $K_s=(Z-Z')(1-\gamma)JS^2$, but only in the case that the irregular points of the surface, such as the points at the corners of a square particle, are not taken into consideration. For macroscopic samples those points are clearly not very important, but for nanometer particles the macroscopic theory is in need of modification.

We thank N. A. Usov for helpful discussions. This work was supported by the grant INTAS 97-31 311.

[1)]E-mail: bivanov@i.com.ua

[1] A. E. Berkowitz, J. R. Mitchell, M. J. Carey, A. P. Young, S. Zhang, F. E. Spada, F. T. Parker, and G. Thomas, Phys. Rev. Lett. **68**, 3745 (1992).
[2] B. Hillebrands, C. Mathieu, C. Hartmann, M. Bauer, O. Buettner, S. Riedling, B. Roos, S. O. Demokritov, B. Bartenlian, C. Chappert, D. Decanini, F. Rosseaux, E. Cam, A. Muller, B. Hoffmann, and U. Hartmann, J. Magn. Magn. Mater. **75**, 10 (1997).
[3] M. Grimsditch, Y. Jaccard, and I. K. Shuller, Phys. Rev. B **58**, 11539 (1998).
[4] C. Mathieu, C. Hartmann, M. Bauer, O. Buettner, S. Riedling, B. Roos, S. O. Demokritov, B. Hillebrands, B. Bartenlian, C. Chappert, D. Decanini, F. Rousseaux, E. Cambril, A. Muller, B. Hoffman, and U. Hartman, Appl. Phys. Lett. **70**, 2912 (1997).
[5] E. F. Wassermann, M. Thielen, S. Kirsch, A. Pollmann, H. Weinforth, and A. Carl, J. Appl. Phys. **83**, 1753 (1998).
[6] K. Runge, Y. Nozaki, Y. Otani, H. Miyajima, B. Pannetier, T. Matsuda, and A. Tonomura, J. Appl. Phys. **79**, 5075 (1996).
[7] R. P. Cowburn, A. O. Adeyeye, and M. E. Welland, Phys. Rev. Lett. **81**, 5415 (1998).
[8] I. G. Gochev, Zh. Éksp. Teor. Fiz. **85**, 199 (1983) [Sov. Phys. JETP **58**, 115 (1983)].
[9] I. G. Gochev, Fiz. Nizk. Temp. **10**, 615 (1984) [Sov. J. Low Temp. Phys. **10**, 320 (1984)].
[10] N. A. Usov and S. E. Peschany, J. Magn. Magn. Mater. **130**, 275 (1994); R. P. Cowburn and M. E. Welland, Phys. Rev. B **58**, 9217 (1998); R. P. Cowburn, A. O. Adeyeye, and M. E. Welland, Phys. Rev. Lett. **81**, 5415 (1998).
[11] N. A. Usov and S. E. Peschany, J. Magn. Magn. Mater. **118**, L290 (1993).
[12] A. Fernandez and C. J. Cerjan, J. Appl. Phys. **87**, 1395 (2000).
[13] Jing Shi, S. Tehrani, and M. R. Scheinfein, Appl. Phys. Lett. **76**, 2588 (2000).
[14] T. Pokhil, D. Song, and J. Nowak, J. Appl. Phys. **87**, 6319 (2000).
[15] A. I. Akhiezer, V. G. Bar'yakhtar, and S. V. Peletminskiĭ, *Spin Waves* [in Russian], Nauka, Moscow (1967).
[16] W. F. Brown Jr., *Micromagnetics*, Wiley, New York (1963).
[17] A. Aharoni, J. Appl. Phys. **81**, 830 (1997); **87**, 5526 (2000).

Translated by Steve Torstveit

Metallic ferromagnetism in a generalized Hubbard model

L. Didukh* and O. Kramar

Ternopil State Technical University, Department of Physics, 56 Rus'ka Str., Ternopil 46001, Ukraine
(Submitted June 20, 2001; revised July 16, 2001)
Fiz. Nizk. Temp. **28**, 42–50 (January 2002)

The possibility of realization of a metallic ferromagnetic state in a generalized Hubbard model with correlated hopping and exchange interaction integrals is investigated. The single-electron energy spectrum recently obtained by means of the mean-field approximation is applied for the description of ground-state and finite-temperature properties of the system. An expression for the Curie temperature is found, and the behavior of the temperature dependences of the magnetization and paramagnetic susceptibility is analyzed. Taking the correlated hopping into account allows one to explain certain peculiarities of the ferromagnetic behavior of transition metals and their compounds. © *2002 American Institute of Physics.*
[DOI: 10.1063/1.1449182]

1. INTRODUCTION

An important problem in the explanation of ferromagnetism in a single band of electrons is that of correctly taking into account the Coulomb correlations between electrons. The Hubbard model,[1,2,3] which describes a single nondegenerate electron band with local Coulomb interaction, is oversimplified and requires generalization. It is natural to generalize the Hubbard Hamiltonian by taking into account other matrix elements of electron–electron interaction (in addition to the intra-atomic Coulomb repulsion) and to consider the ferromagnetism in the generalized Hubbard model (for a review of this problem see Refs. 4–6).

Note that the problem of metallic ferromagnetism in the single-band Hubbard model and its generalizations has attracted much attention to a series of papers employing the dynamical mean-field theory,[7,8] the Gutzwiller variational wave function approximation,[9,10] the spectral density approximation,[11,12] the exact diagonalization method,[13] and mean-field theory.[14–16] In the papers of Hirsch[14–16] a generalization of Stoner–Wolfarth theory[17,18] was carried out. The Stoner–Wolfarth theory has been used for the description of itinerant electron magnetism (note in this connection that the calculations in this theory essentially depend on the shape and peculiarities of the density of states; in particular, it is known that the incomplete ferromagnetism in this model is absent if the density of states is rectangular[18]). This generalization[14–16] has shown that the interatomic exchange interaction plays an important role for obtaining a ferromagnetic state with partial polarization. Using the mean-field theory, Hirsch has obtained the condition for realization of a ferromagnetic state, nonmonotonic behavior of the concentration dependence of the magnetization, an expression for the Curie temperature, and the temperature dependences of the magnetization and magnetic susceptibility. Using a local approximation developed from the Gutzwiller wave function method, the authors of Ref. 10 suggest also (in agreement with Ref. 14) the importance of the interatomic exchange interaction for stabilization of the ferromagnetic state with partial spin polarization. In Ref. 19 the case of strong correlation was studied and the criterion of ferromagnetism and magnetization of the system in the ground state was derived; in this paper the importance of interatomic exchange interaction is also emphasized.

At the same time, from our point of view it is in principle necessary to consider (in addition to the interatomic exchange interaction) the matrix elements which describe the correlated hopping of electrons[20] for explanation of ferromagnetism in a single-band model. In this model an electron hopping from one site to another is correlated both by the occupation of the sites involved in the hopping process and the occupation of the nearest-neighbor sites. Taking into account the correlated hopping allows one to obtain an additional mechanism[21,22] for the stabilization of ferromagnetic ordering.

The importance of correlated hopping for understanding of metallic ferromagnetism was discussed in Ref. 13, where the results obtained by means of exact diagonalization for small one-dimensional chains were compared with mean-field theory results. It has been shown that in the strong-coupling regime, correlated hopping favors ferromagnetism more strongly for electron concentration $n>1$ than for $n<1$ (the reverse situation occurs for weak interactions[13]); this result agrees with conclusions of Ref. 23. Using the Gutzwiller approach, the authors of Ref. 9 have shown that the correlated hopping strongly favors the ferromagnetic ordering close to the point of half filling.

The magnetic properties of the system at nonzero temperature have been analyzed in a series of papers.[7,8,11,12] However, the important question concerning the influence of correlated hopping on the Curie temperature and on the behavior of the magnetization and magnetic susceptibility at nonzero temperature has not yet been considered.

In this paper the theory of metallic ferromagnetism in a model which includes the intra-atomic Coulomb interaction, the interatomic exchange interaction of electrons, and the electron–electron interaction due to electron hopping (correlated hopping) is formulated. The application of the mean-field approximation to this generalized Hubbard model with

correlated hopping leads to a correct description of ferromagnetism for zero temperature (in this case our results agree with the results obtained by Hirsch[14,15]) and can also eliminate the problem of overestimation of the Curie temperature (in consequence of taking into account the correlated hopping). Besides, the mean-field analysis of this model, in spite of its limitations, allows one to reproduce the behavior of the magnetic moment and Curie temperature with changing electron concentration and obtain the correct temperature dependence of the magnetic moment of the system. Note that the mean-field treatment of models which include only the band part of the Hamiltonian and intra-atomic Coulomb interaction (or exchange interaction) predicts values for the Curie temperature which are larger than those observed in transition metals by an order of magnitude.

The paper is organized as follows. In Sec. 2 the Hamiltonian of the generalized Hubbard model with correlated hopping and interatomic exchange interaction is written, and the single-electron energy spectrum obtained by means of the Green function technique is analyzed. In Sec. 3 the ground-state properties of the system are considered, the equation for the critical parameters of the system, and the expression for the magnetization are derived. In Sec. 4 the finite-temperature properties of the system are considered, and expressions for the Curie temperature and the temperature dependences of the magnetization and magnetic susceptibility are obtained. Sec. 5 is devoted to the conclusions.

2. THE MODEL HAMILTONIAN AND SINGLE-ELECTRON ENERGY SPECTRUM

Consider the Hamiltonian proposed in Ref. 24, generalized by taking into account a weak magnetic field:

$$H=-\mu\sum_{i\sigma} a_{i\sigma}^{+}\alpha_{i\sigma}+\sum_{ij\sigma}{}' t_{ij}(n)a_{i\sigma}^{+}a_{j\sigma} + \sum_{ij\sigma}{}' (T_2(ij)a_{i\sigma}^{+}a_{j\sigma}n_{i\bar{\sigma}}+\text{h.c.})+U\sum_{i} n_{i\uparrow}n_{i\downarrow} + \frac{J}{2}\sum_{ij\sigma\sigma'}{}' a_{i\sigma}^{+}a_{j\sigma'}^{+}a_{i\sigma'}a_{j\sigma}-h\sum_{i}(n_{i\uparrow}-n_{i\downarrow}), \qquad (1)$$

where $a_{i\sigma}^{+}$, $a_{i\sigma}$ are the creation and annihilation operations of an electron on site i, $\sigma=\uparrow,\downarrow$, $n_{i\sigma}=a_{i\sigma}^{+}a_{i\sigma}$ is the number operator for electrons with spin σ on site i, $n=\langle n_{i\uparrow}+n_{i\downarrow}\rangle$, μ is the chemical potential, $t_{ij}(n)=t_{ij}+nT_1(ij)$ is the effective hopping integral of an electron from site j to site i, t_{ij} is the band hopping integral of an electron from site j to site i, $T_i(ij)$ and $T_2(ij)$ are the parameters of correlated hopping of electrons, U is the intra-atomic Coulomb repulsion, J is the exchange integral for the nearest neighbors, and h is the external magnetic field (the units of h are such that the magnetic moment per electron is unity). The prime on the sums in Eq. (1) signifies that $i\neq j$. The concentration dependence of the effective hopping integral $t_{ij}(n)$ is caused by the correlated hopping[24] of electrons.

The peculiarities of the model described by Hamiltonian (1) are the taking into account of the influence of site occupation on the hopping process (correlated hopping) and the direct exchange interaction between electrons on the neighboring sites. To characterize the value of correlated hopping we introduce dimensionless parameters $\tau_1=T_1(ij)/|t_{ij}|$, $\tau_2=T_2(ij)/|t_{ij}|$ which are independent of the number of the site.

Using the mean-field approximation in the Green function method, we have recently obtained[22] the single-electron energy spectrum. In an external magnetic field it has the form

$$E_\sigma(\mathbf{k})=-\mu+\beta_\sigma+n_{\bar{\sigma}}U-zn_\sigma J-h\eta_\sigma+t(n\sigma)\gamma(\mathbf{k}); \qquad (2)$$

here the spin-dependent shift of the band centers is

$$\beta_\sigma=\frac{2}{N}\sum_{ij} T_2(ij)\langle a_{i\bar{\sigma}}^{+}a_{i\bar{\sigma}}\rangle, \qquad (3)$$

z is the number of nearest neighbors to a site, for the spin $\sigma=\uparrow(\downarrow)$ we have $\eta_\sigma=1(-1)$, $\gamma(\mathbf{k})=\Sigma_R e^{i\mathbf{kR}}$ (the sum goes over the nearest neighbors to a site), and the spin- and concentration-dependent hopping integral is

$$t(n\sigma)=\left(1-\tau_1 n-2\tau_2 n_{\bar{\sigma}}-\frac{zJ}{w}\sum_{\sigma'} A_{\sigma'}\right)t=\alpha_\sigma t, \qquad (4)$$

where $w=z|t|$ is one-half the bandwidth, t is the hopping integral between nearest-neighbor sites, and

$$A_{\sigma'}=\frac{1}{N}\sum_{ij}\left(-\frac{t_{ij}}{w}\right)\left\langle a_{i\sigma'}^{+}a_{j\sigma'}\right\rangle. \qquad (5)$$

Energy spectrum (2) will be used in the next Sections for the description of the model properties in the ground state and at finite temperature.

3. THE GROUND-STATE PROPERTIES OF THE MODEL

The concentration of electrons with spin σ is

$$n_\sigma=\int_{-w}^{w}\rho(\varepsilon)f(E_\sigma(\varepsilon))d\varepsilon, \qquad (6)$$

where $\rho(\varepsilon)$ is the density of states, and $f(E_\sigma(\varepsilon))$ is the Fermi distribution function. Thus the occupation number and the magnetization are expressed, respectively, as

$$n=n_\uparrow+n_\downarrow=\int_{-w}^{w}\rho(\varepsilon)[f(E_\uparrow(\varepsilon))+f(E_\downarrow(\varepsilon))d\varepsilon; \qquad (7)$$

$$m=n_\uparrow-n_\downarrow=\int_{-w}^{w}\rho(\varepsilon)[f(E_\uparrow(\varepsilon))-f(E_\downarrow(\varepsilon))]d\varepsilon. \qquad (8)$$

Let us assume a rectangular unperturbated density of states, $\rho(\varepsilon)=\Theta(\varepsilon^2-w^2)/2w$. In the case of zero temperature one can obtian for the correlation function A_σ and the shift β_σ of the center of the σ subband

$$A_\sigma=n_\sigma(1-n_\sigma), \qquad (9)$$

$$\beta_\sigma=2w\tau_2 A_\sigma=2w\tau_2 n_\sigma(1-n_\sigma), \qquad (10)$$

where the concentration of electrons with spin σ

$$n_\sigma=\frac{\varepsilon_\sigma+w}{2w}, \qquad (11)$$

here $\varepsilon_\sigma=\mu_\sigma/a_\sigma$ is the solution of the equation $E_\sigma(\varepsilon)=0$, where $\mu_\sigma=\mu-\beta_\sigma+zn_\sigma J-n_{\bar{\sigma}}U+h\eta_\sigma$ and $\alpha_\sigma=1-\tau_1 n-2\tau_2 n_{\bar{\sigma}}-zJ/w\Sigma_{\sigma'}A_{\sigma'}$.

On the basis of expressions (7)–(8) using (9)–(10), one can obtain the equation for the system critical parameters:

$$\frac{zJ}{2w}[1+n(2-n)-m^2]=1-n\tau_1-\tau_2(2-n)-\frac{U}{2w}-\frac{h}{w}. \tag{12}$$

Expression (12), which determines the stability condition for ferromagnetism, agrees with the expression obtained from an analysis of the ground-state energy.[22] The condition for onset of ferromagnetic ordering is obtained (replacing the equals sign by an inequality sign) when $m=0$, and the condition for the ferromagnetic state with full spin polarization is derived by putting $m=n$ in expression (12). The peculiar distinction of our expression from the similar condtiion obtained in Refs. 10 and 14–16 for the various generalizations of the Hubbard model is the presence of correlated hopping, which can substantially modify the properties of the model. Taking correlated hopping into account leads to the appearance of a peculiar kinetic mechanism of stabilization of the ferromagnetic ordering. This mechanism is caused by the presence of the spin-dependent shift of the spin subband centers, which is a consequence of correlated hopping (it is analogous to the shift of subband centers in consequence of the interatomic direct exchange interaction).

The spontaneous ground-state magnetization (in the absence of magnetic field) of the system is found from Eq. (12) as

$$m_0=\left[1+n(2-n)-\frac{1-U/2w-\tau_1 n-\tau_2(2-n)}{zJ/2w}\right]^{1/2}, \tag{13}$$

which is valid in the case $J>0$ (when $J=0$ only the transition from the paramagnetic to the fully polarized ferromagnetic state with $m_0=n$ occurs). If the calculated magnetization $m_0>n$, then it is necessary to put $m_0=n$.

The influence of correlated hopping on the properties of the system is illustrated in Figs. 1 and 2. In Fig. 1 the dependence of the critical value of the exchange integral at which the ferromagnetic ordering occurs is plotted (in the absence of magnetic field) as a function of band filling for various values of correlated hopping parameters τ_1, τ_2 and intra-

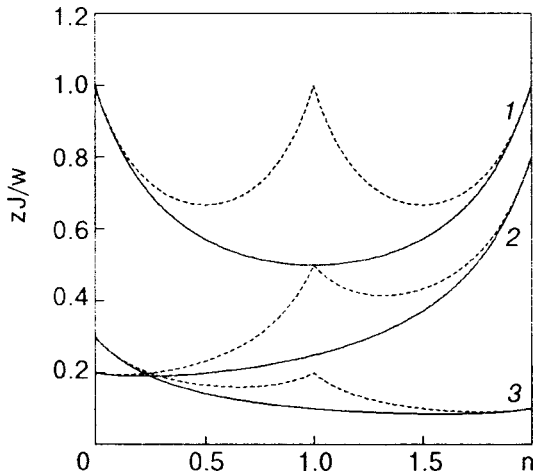

FIG. 1. Critical values of zJ/w as a function of n at fixed value of U/w. $U/w=1$, $\tau_1=\tau_2=0$ (*1*); $U/w=1.2$, $\tau_1=0$, $\tau_2=0.15$ (*2*); $U/w=1.3$, $\tau_1=0.15$, $\tau_2=0.1$ (*3*).

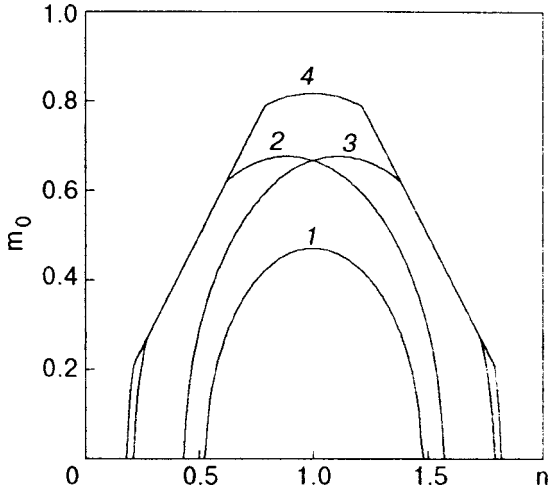

FIG. 2. Ground-state magnetization m_0 as a function of n for $U/w=1.2$ and $zJ/w=0.1$. $\tau_1=\tau_2=0$ (*1*); $\tau_1=0$, $\tau_2=0.05$ (*2*); $\tau_1=0.05$, $\tau_2=0$ (*3*); $\tau_1=\tau_2=0.05$ (*4*).

atomic Coulomb interaction U/w. The solid curves correspond to the onset of spin polarization and the dashed curves to the fully polarized ferromagnetic state (the area below the solid line is paramagnetic, above the dashed line—fully polarized ferromagnetic, between these lines—partially polarized ferromagnetic). Similar phase diagrams were obtained in Refs. 14 and 16, but in those works the correlated hopping was not considered. Note that the presence of correlated hopping (curves *2* and *3* in Fig. 1) leads to a substantial change of the phase boundary of the paramagnet–ferromagnet transition; in particular, to a shift of the minimum point, namely to the inequivalence of the cases $n<1$ and $n>1$.

In Fig. 2 the dependence of the ground-state magnetization m_0 on the electron concentration n for fixed values of exchange and Coulomb interactions, as well as for different values of correlated hopping parameters, is plotted. In Refs. 14 and 16 the concentration dependences of the magnetization were obtained in the framework of the Hubbard model with interatomic exchange, but they are symmetric with respect to half-filling. In Ref. 19 a similar $m_0(n)$ dependence was obtained.

As mentioned above, asymmetry of the cases $n<1$ and $n>1$ is observed; in particular, an increase of parameter τ_1 leads to a shift of the ferromagnetic area to a region of larger electron concentration n, while an increase of parameter τ_2 gives a shift to smaller n. Note also that taking into account the correlated hopping enriches considerably the set of curves $m_0(n)$. The obtained concentration dependences of the magnetization allow one to describe qualitatively the experimental curves for binary ferromagnetic alloys of the transition metals Fe, Co, and Ni (Slater–Pouling curves[26]).

4. THE PROPERTIES OF THE MODEL AT NONZERO TEMPERATURE

For nonzero temperature and unperturbed rectangular density of states the concentration of electrons with spin σ is expressed form (6) as

$$n_\sigma = 1 - \frac{\Theta}{2w\alpha_\sigma}\ln\left[\frac{1+\exp\left(\frac{E_\sigma(w)}{\Theta}\right)}{1+\exp\left(\frac{E_\sigma(-w)}{\Theta}\right)}\right]. \tag{14}$$

Using expression (8), one can obtain the equation for the magnetization

$$\exp\left(-\frac{mJ_{\text{eff}}}{\Theta}\right) = \frac{\sinh\left(\frac{(1-n_\uparrow)\alpha_\uparrow w}{\Theta}\right)\sinh\left(\frac{n_\downarrow\alpha_\downarrow w}{\Theta}\right)}{\sinh\left(\frac{(1-n_\downarrow)\alpha_\downarrow w}{\Theta}\right)\sinh\left(\frac{n_\uparrow\alpha_\uparrow w}{\Theta}\right)}, \tag{15}$$

where $J_{\text{eff}} = zJ + U + 2\tau_2 w(1-n)$. To obtain the temperature dependence of the magnetization it is necessary to apply numerical methods inasmuch as the last equation cannot be solved analytically. The numerical calculations show that the results could be approximately expressed using the approach proposed in Ref. 15. The Curie temperature can be obtained by expanding (8) to lowest order in $m \to 0$:

$$1 = \frac{1}{2w}\frac{U + zJ - 2w\tau_2(n-1)}{\alpha^*}\int_{-w\alpha^*}^{w\alpha^*}\left[-\frac{\partial f(x-\mu^*)}{\partial x}\right]dx - \frac{\tau_2}{w(\alpha^*)^2}\int_{-w\alpha^*}^{w\alpha^*}\left[-\frac{\partial f(x-\mu^*)}{\partial x}\right]x\,dx, \tag{16}$$

where $x = \alpha^*\varepsilon$, $\alpha^* = \alpha_\sigma|_{m=0}$ and $\mu^* = \mu_\sigma|_{m=0}$.

At low temperature one can approximately write

$$1 = \frac{U/2w + zJ/2w - 2w\tau_2(n-1)}{1-(\tau_1+\tau_2)n - 2A^*(\Theta_C)zJ/w}, \tag{17}$$

where $A^*(\Theta_C) = A_\sigma(\Theta)|_{m=0}$, $\Theta = k_B T$, k_B is the Boltzmann constant. In the case of zero temperature the last expression reproduces the criterion of the paramagnetic–ferromagnetic transition obtained in a recent paper.[22]

To find $A_\sigma(\Theta)$, as in Ref. 15, one can apply the Sommerfeld expansion[25]

$$A_\sigma(\Theta) = \int_{-w}^{w}\left[-\frac{\varepsilon}{2w^2}\right]\frac{d\varepsilon}{\exp(E_\sigma(\varepsilon)/\Theta)+1} \simeq n_\sigma(1-n_\sigma) - \frac{\pi^2}{3}\left(\frac{\Theta}{2w}\right)^2 \times \frac{1}{[1-\tau_1 n - 2\tau n_{\bar\sigma} - (A_\uparrow(\Theta)+A_\downarrow(\Theta))zJ/w]^2}. \tag{18}$$

At the Curie point (when the magnetic moment $m \to 0$ and $n_\sigma = n/2$) the last equation is written as

$$A^*(\Theta_C) = \frac{n(2-n)}{4} - \frac{2\pi^2}{3}\left(\frac{\Theta_C}{2w}\right)^2 \times \frac{1}{[1-(\tau_1+\tau_2)n - 2A^*(\Theta_C)zJ/w]^2}. \tag{19}$$

Solving the system of equations (17) and (19), we can express the Curie temperature as a function of the model parameters as

$$\frac{\Theta_C}{2w} = \left[1 + n(2-n) - \frac{1 - U/2w - \tau_1 n - \tau_2(2-n)}{zJ/2w}\right]^{1/2} \times \left(\frac{3}{2\pi^2}\right)^{1/2}\left[\frac{U}{2w} + \frac{zJ}{2w} - 2\tau_2(n-1)\right]. \tag{20}$$

Taking into account expression (13), we finally obtain for the Curie temperature

$$\frac{\Theta_C}{2\omega} = \left(\frac{3}{2\pi^2}\right)^{1/2}\left[\frac{U}{2w} + \frac{zJ}{2w} - 2\tau_2(n-1)\right]m_0. \tag{21}$$

In the absence of correlated hopping, formula (21) reproduces the result of Ref. 15. Note that the Curie temperature is closely related (in the approximation used) to the ground state magnetization of the ferromagnet. The pecularity of formula (21) is the presence of the term containing the correlated hopping parameters τ_2 (m_0 is also dependent on this parameter), which in the case $n > 1$ is negative and therefore lowers the Curie temperature. The consideration of correlated hopping allows one to avoid (for some values of the correlated hopping parameters) overestimation of the Curie temperature and to obtain values which are close to the experimentally observed ones (in this connection see also Ref. 15, where the correlated hopping is not taken into account). Let us assume (as in Ref. 15) that the bandwidth of the ε_g states in $3d$ ferromagnetic transition metals is approximately 2 eV. In our work the band filling $n = 1.2$ corresponds to Fe, and for the values of correlated hopping $\tau_1 = 0.15$, $\tau_2 = 0.2$ our theory would predict values of the Curie temperature between 1000 and 1600 K, depending on the values of the intra-atomic Coulomb repulsion and exchange interaction (these parameters are varied in the ranges from 0 to 0.4 and from 0.14 to 0.37, respectively; the larger the value of the parameter U/w, the smaller the value of parameter zJ/w that is needed). The value of the Curie temperature for some fixed values of the intra-atomic Coulomb interaction and interatomic exchange interaction agrees with the experimental data even quantitatively.

In Fig. 3 the concentration dependence of the Curie temperature is plotted for various values of the exchange interaction. The peculiarity of this dependence is the lowering of

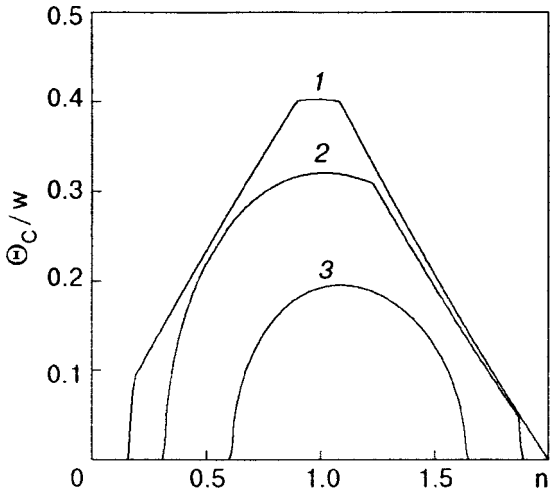

FIG. 3. Curie temperature as a function of n for $U/w = 1$ and $\tau_1 = 0.05$, $\tau_2 = 0.1$. $zJ/w = 0.4$ (*1*); $zJ/w = 0.5$ (*2*), $zJ/w = 0.6$ (*3*).

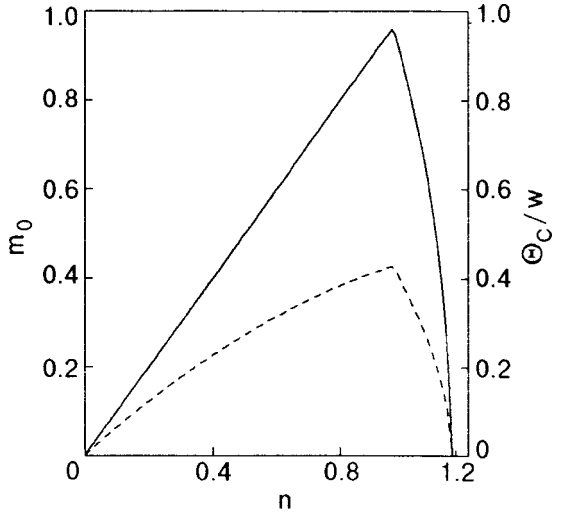

FIG. 4. Dependences of the magnetization (solid curve) and Curie temperature (dashed curve) on electron concentration n for $U/w=1.5$, $\tau_1=0$, $\tau_2=0.8$ and $zJ/w=0.2$.

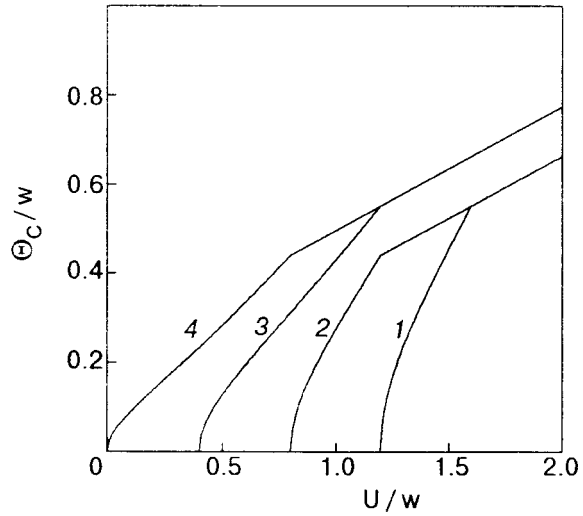

FIG. 5. Curie temperature as a function of U/w at half-filling. $zJ/w=0.4$ $\tau_1=\tau_2=0$ (*1*); $zJ/w=0.4$, $\tau_1=\tau_2=0.1$ (*2*); $zJ/w=0.8$ $\tau_1=\tau_2=0$ (*3*); $zJ/w=0.8$, $\tau_1=\tau_2=0.1$ (*4*).

the Curie temperature with increasing carrier concentration. Besides, taking into account the correlated hopping causes asymmetry of the curve with respect to half-filling which allows one to explain qualitatively the higher Curie temperature in Co as compared to Fe. Note that this fact could not be explained in Ref. 15 without further comments (in particular, taking into account peculiarities of the density of states). On the basis of the expression obtained for the Curie temperature one can explain the peculiarities of the Curie temperature behavior in binary alloys of transition metals.[26] It is reasonable to interpret in the framework of our theory as being due to the paramagnet–ferromagnet transition in metallic phase with increasing temperature for the nonstoichiometric chalcogenide chrome spinel $Cr_{0.5}Fe_{0.5}S$ (where the Curie temperature is of the order of 1000 K).[27]

In principle, our theory allows one to obtain the concentration dependences of the magnetization and Curie temperature, which are similar to those observed experimentally in the compounds $Fe_{1-x}Co_xS_2$ and $Co_{1-x}Ni_xS_2$ with a change of electron concentration in the $3d$ band.[28] In these crystals the same subsystem of electrons is responsible both for conductivity and for the formation of localized magnetic moments. Although these compounds should be described in the framework of a doubly orbitally degenerate model, nevertheless for some values of the model parameters it is also possible to obtain in terms of a single-band model the concentration dependences of the Curie temperature and magnetic moment of the system (see Fig. 4) in qualitative agreement with the experimentally observed ones.[28] The plotted curves show that for the choosen model parameters the values of the above mentioned quantities are reproduced accurately.

The influence of the model parameters on the critical temperature is illustrated in the next figures. In Figs. 5 and 6 the dependences of the Curie temperature on the intra-atomic Coulomb interaction parameter are plotted at half-filling (Fig. 5) and various values of the band filling (Fig. 6); the values of exchange integral and correlated hopping are fixed. The plotted curves have a pecularity; one can distinguish an area of sharp increase of the Curie temperature with increase of the parameter U/w (these values of the model parameters correspond to partial spin polarization of the system) and an area where the Curie temperature changes in proportion to U/w (these values correspond to full spin polarization of the system). Note that increasing the interatomic exchange interaction leads to extension of the partially polarized ferromagnetic area and also to a decrase of the critical value of U required for the development of saturated ferromagnetism. The pecularity of the dependence of the Curie temperature on U/w is the increase of the critical value of U/w with increasing n. Note also that the change of this critical value (for chosen values of correlated hopping) in the case $n>1$ and with increaisng electron concentration is more pronounced than in the case $n<1$. It is also interesting that, depending on the magnitude of U/w, the system with electron concentration $n<1$ can have a larger value of the Curie temperature than the system with $n>1$. However, starting

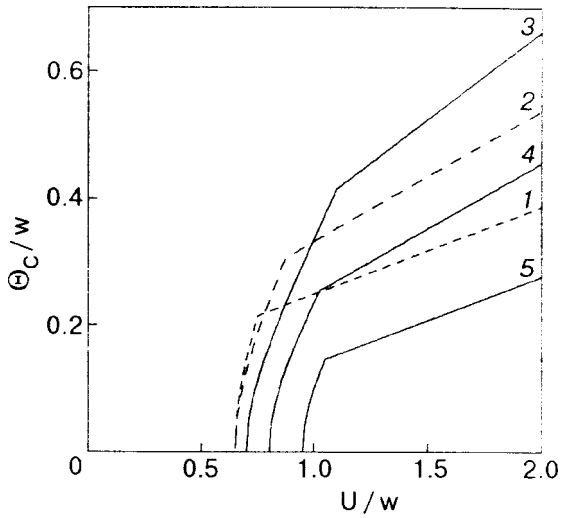

FIG. 6. Curie temperature as a function of U/w at $zJ/w=0.4$, $\tau_1=0.05$, $\tau_2=0.2$ and various band fillings. *1*, *2*, *3*, *4* and *5* — $n=0.5$, 0.75, 1, 1.25. and 1.5, respectively.

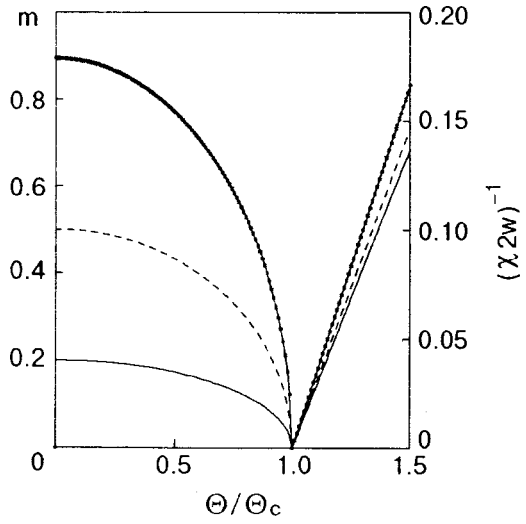

FIG. 7. Dependences of the magnetization and inverse magnetic susceptibility on reduced temperature for $U/w=1$, $zJ/w=0.5$, $\tau_1=0.05$ and $\tau_2=0.1$; the upper, middle and lower curves correspond to the case $n=1$, $n=0.5$, and $n=0.2$, respectively.

from the critical point for the intra-atomic Coulomb interaction, the situation becomes the opposite: the Curie temperature is larger for the system with $n>1$.

Next consider the behavior of the magnetization of the system with change of temperature. To obtain the temperature dependence of the magnetization m let us use the assumption (as in Ref. 15), that Eq. (17) is also valid for nonzero magnetization and for temperatures lower than the critical Θ_C. Then, using (18) one can obtain the equation

$$m=\frac{2\pi}{\sqrt{3}}\left\{\left(\frac{\Theta_C}{2w}\right)^2\frac{1}{(\alpha^*)^2}-\frac{1}{2}\left(\frac{\Theta}{2w}\right)^2 \times\left[\frac{1}{(\alpha^*+\tau_2 m)^2}+\frac{1}{(\alpha^*-\tau_2 m)^2}\right]\right\}^{1/2}. \tag{22}$$

The results of numerical calculations for m are plotted in Fig. 7. It should be noted that if the correlated hopping is not taken into account, expression (22) gives the analytical result of Ref. 15. In the band limit the last expression reproduces the result of Ref. 29, where a similar treatment is applied to the completely itinerant carriers.

To find the magnetic susceptibility let us take the derivative of the magnetization (8) with respect to the magnetic field,

$$\chi(\Theta)=\left.\frac{\partial m(h)}{\partial h}\right|_{h\to 0,m\to 0} =\frac{1}{2w}\,\frac{1}{\alpha^*-U/2w-zJ/2w+2\tau(n-1)}. \tag{23}$$

Using (17) for temperatures which are close to Θ_C one can obtain

$$\chi(\Theta)=\frac{6w[U/2w+zJ/2w-2\tau_2(n-1)]^2}{2\pi^2\Theta_C(\Theta-\Theta_C)zJ/w}. \tag{24}$$

In Fig. 7 the temperature dependences of the magnetization and inverse magnetic susceptibility are plotted. A similar plot was obtained for the transition metals in Ref. 30 using the dynamical mean-field theory combined with the local density approximation. For temperatures higher than the Curie temperature the magnetic susceptibility demonstrates Curie–Weiss-like behavior.

5. CONCLUSIONS

In this paper the ferromagnetic solution in a single-band generalized Hubbard model is derived. The peculiarity of the model is the inclusion in the Hubbard Hamiltonian the interatomic exchange interaction and electron–electron interactions which describe the influence of occupancy of sites on the hopping process. The physical mechanism which leads to realization of the ferromagnetic state is a shift of the electron subband centers caused by the exchange interaction and correlated hopping; in addition, the band narrowing due to correlated hopping is also important.

Taking the correlated hopping into account leads to asymmetry of the cases $n<1$ and $n>1$ for the consideration of ferromagnetism in this model. An increase of the correlated hopping parameter τ_1 leads to a shift of the ferromagnetic area to a region of larger electron concentration n, while an increase of the correlation hopping parameters τ_2 causes a shift to smaller electron concentration n. An important consequence of this study is the conclusion that, for the realization of ferromagnetism the case of a more than half-filled band is more favorable (this is the case of transition metals and their alloys) than the case of $n<1$.

The concentration dependence of the ground-state magnetization m_0 qualitatively agrees with the experimental data for the $3d$ transition metals and their alloys; in particular, our results can explain the Slater–Pouling curves[26] for the binary ferromagnetic alloys of the transition metals Fe, Co, and Ni with other $3d$ metals.

Taking into account the correlated hopping in the calculation of the Curie temperature allows one to obtain values which agree with the experimentally observed ones. The calculated Curie temperature is characterized by peculiarities of the concentration dependence; in particular, asymmetry (in consequence of taking correlated hopping into account) with respect to band half-filling. This result agrees with the experimentally observed values of the critical temperature in the ferromagnetic transition metalas. Besides, our results qualitatively reproduce the a typical concentration dependence of the Curie temperature in the systems $Fe_{1-x}Co_xS_2$ and $Co_{1-x}Ni_xS_2$ (Ref. 28).

In conclusion, the correct taking into account of the above-mentioned matrix elements of electron–electron interactions allows one to explain some peculiarities of the ferromagnetic properties for transition metal and their alloys and compounds both in the case of the ground state and at nonzero temperatures.

*E-mail: didukh@tu.edu.te.ua

[1] J. Hubbard, Proc. R. Soc. London, Ser. A **276**, 238 (1963).
[2] J. Kanamori, Prog. Theor. Phys. **30**, 275 (1963).
[3] M. C. Gutzwiller, Phys. Rev. Lett. **10**, 159 (1963).
[4] H. Tasaki, Prog. Theor. Phys. **99**, 489 (1998).
[5] D. Vollhardt, N. Blumer, K. Held, M. Kollar, J. Schlipf, M. Ulmke, and J. Wahle, Adv. Solid State Phys. **38**, 383 (1999).
[6] V. Yu. Irkhin and Yu. P. Irkhin, *Electronic structure and physical properties of d- and f-transition metals and their compounds*, cond-mat/9812072.
[7] D. Vollhardt, N. Blumer, K. Held, M. Kollar, J. Schlipf, and M. Ulmke, Z. Phys. B **103**, 283 (1997).
[8] J. Wahle, N. Blumer, J. Schlipf, K. Held, and D. Vollhardt, Phys. Rev. B **58**, 12749 (1998).
[9] M. Kollar and D. Vollhardt, Phys. Rev. B **63**, 045107 (2001).
[10] H.-Q. Nie and W.-Y. Zhou, Phys. Rev. B **55**, 59 (1997).
[11] T. Herrman and W. Nolting, J. Magn. Magn. Mater. **170**, 253 (1997).
[12] M. Potthoff, T. Herrman, and W. Nolting, Phys. Status Solidi B **210**, 199 (1997).
[13] J. C. Amadon and J. E. Hirsch, Phys. Rev. B **54**, 6364 (1996).
[14] J. E. Hirsch, Phys. Rev. B **40**, 2354 (1989).
[15] J. E. Hirsch, Phys. Rev. B **40**, 9061 (1989).
[16] J. E. Hirsch, Phys. Rev. B **59**, 6256 (1999).
[17] E. C. Stoner, Proc. R. Soc. London, Ser. A **165**, 372 (1938).
[18] E. P. Wohlfarth, Philos. Mag. **42**, 374 (1951).
[19] V. Ivanov, Ukr. Phys. J. **36**, 751 (1991).
[20] L. Didukh, J. Phys. Stud. **1**, 241 (1997) (in Ukrainian).
[21] L. Didukh, O. Kramar, and Yu. Skorenkyy, J. Phys.: Condens. Matter **4**, 101 (2001).
[22] L. Didukh, O. Kramar, and Yu. Skorenkyy, Phys. Status Solidi B, (2002), in press (cond-mat/0012402).
[23] L. Didukh, Sov. Phys. Solid State **19**, 711 (1977).
[24] L. Didukh, J. Phys.: Condens. Matter **1**, 125 (1998).
[25] N. W. Ashcroft and N. D. Mermin, *Solid State Phys.*, Holt, Rinehart and Winston, New York (1975).
[26] F. Gautier, in *Magnetism of Metals and Alloys*, edited by M. Cyrot, North-Holland, Amsterdam (1982).
[27] G. V. Loseva, S. G. Ovchinnikov, and G. A. Petrakovsky, *Metal-Insulator Transition in Sulfides of 3d Metals* (in Russian), Nauka, Novosibirsk (1983).
[28] H. S. Jarrett, W. H. Cloud, R. J. Bouchard, S. R. Butler, C. G. Frederick, and J. L. Gilson, Phys. Rev. Lett. **21**, 617 (1965).
[29] J. A. Blanco and J. Pisonero, Eur. J. Phys. B **20**, 289 (1998).
[30] A. T. Lichtenstein and M. I. Katsnelson, cond-mat/0102297.

This article was published in English in the original Russian journal. Reproduced here with stylistic changes by AIP.

Effect of light illumination on antiferromagnet-metamagnet phase transitions in the garnet $Ca_3Mn_2Ge_3O_{12}$

V. A. Bedarev,* V. I. Gapon, and S. L. Gnatchenko

B. Verkin Institute for Low Temperature Physics and Engineering, National Academy of Sciences of Ukraine, 47 Lenin Ave., Kharkov 61103, Ukraine

M. Baran and R. Szymczak

Institute of Physics, Polish Academy of Sciences, Al. Lotnikow 32/46, 02-668 Warsaw, Poland

J. M. Desvignes

Laboratory Charles Fabry de l'Institut d'Optique, bat.503, 91403 Orsay, France

H. Le Gall

Laboratory of Magnetism of Bretagne, 6 Avenue Le Gorgeu, 29285 Brest, France
(Submitted June 13, 2001; revised September 13, 2001)
Fiz. Nizk. Temp. **28**, 51–60 (January 2002)

The effect of linearly polarized light illumination on the metamagnetic phase transition in the antiferromagnetic garnet $Ca_3Mn_2Ga_3O_{12}$ is studied. The crystal is exposed to light propagating both along the tetragonal axis [001] and along the [100] direction. In both cases, a change of the field H_t of the metamagnetic phase transition is observed under illumination, and this change depends on the orientation of plane or polarization of the light with respect to the crystal axes. In the first case, $\mathbf{k}\|\mathbf{H}\|[001]$, the value of H_t decreases on exposure to light with the polarization $\mathbf{E}\|[1\bar{1}0]$ and increases on exposure to light with the polarization $\mathbf{E}\|[110]$. In the second case, $\mathbf{k}\|\mathbf{H}\|[100]$, the value of H_t decreases irrespective of the orientation of the plane of polarization of the light with respect to the crystal axes. However, the magnitudes of the change of H_t are different for light with the polarization $\mathbf{E}\|[011]$ and with the polarization $\mathbf{E}\|[0\bar{1}1]$. The change of the field of the metamagnetic phase transition in the second case is much larger than in the first case. A phenomenological theory of the photomagnetic effects observed in the antiferromagnetic garnet $Ca_3Mn_2Ge_3O_{12}$ is developed. It is shown that the effect of light illumination on the metamagnetic phase transition is related to the photoinduced magnetic moment in this antiferromagnet. The magnetic moment induced by linearly polarized light in the garnet $Ca_3Mn_2Ge_3O_{12}$ is detected experimentally by means of a SQUID magnetometer. [DOI: 10.1063/1.1449183]

INTRODUCTION

The study of possibility of controlling the magnetic state of crystals by using light illumination is attracting interest in terms of both a better insight into the nature of the effect and its application. Light-induced phase transitions have been observed in some magnetically ordered crystals.[1] For instance, the linearly polarized light illumination of yttrium iron garnets results in a spin-reorientation phase transition as a result of the photoinduced change of the crystalline magnetic anisotropy.[2,3] The changes in magnetic and electronic states in response to light irradiation was recently observed in manganites with colossal magnetoresistance.[4–7] In these compounds the light induces a phase transition from an insulating antiferromagnetic (AFM) state to a conducting ferromagnetic one. At the moment, the mechanism of the light-induced phase transition in manganites remains unclear. The transition is thought to be a associated with the photoinduced melting of the charge-ordered state caused by optical transitions with charge transfer between Mn^{3+} and Mn^{4+} ions.

The light-induced modification of the magnetic state related to the redistribution of the Mn^{3+} and Mn^{4+} ions in the crystal lattice due to the photoinduced charge transfer between the ions was recently observed in another manganese oxide, namely in the AFM garnet $Ca_3Mn_2Ge_3O_{12}$ (Ref. 8). Linearly polarized light alters the field of the metamagnetic (MM) phase transition. The effect of light on the phase transition in the garnet $Ca_3Mn_2Ge_3O_{12}$ is related to the light-induced magnetic moment that arises in the AFM state.

The mechanisms of the photoinduced phase transitions in the above manganese oxides have some common features; in particular, the optical transitions with charge transfer between the Mn^{3+} and Mn^{4+} ions are of great importance. A comprehensive elucidation of the mechanisms of the photoinduced phase transitions in manganese oxides is of obvious interest for the physics of photoinduced phenomena in magnets and is also necessary for application of these compounds. The photoinduced effects observed in manganese oxides could be used in devices for the storage and processing of information.

The paper reports experimental data on the effect of illumination on the first-order MM phase transitions induced

by magnetic field in the AFM garnet $Ca_3Mn_2Ge_3O_{12}$. The experiments were carried out for two directions of propagation of the inducing light and two directions of magnetic field with respect to the crystallographic axes: along the tetragonal axis [001]($\mathbf{k}\|\mathbf{H}\|$[001]) and normal to this axis, i.e., along the crystallographic direction [100] ($\mathbf{k}\|\mathbf{H}\|$[100]). It was found that the effect of light on the MM phase transition in the above two cases differs substantially. A phenomenological theory has been developed to describe the observed photoinduced effects.

EXPERIMENTAL TECHNIQUE

The effect of light irradiation on the first-order MM phase transitions in calcium-manganese-germanium garnet (CaMnGeG) was investigated by means of magnetooptical and magnetometric techniques. The field dependences of the angle of rotation of the plane of polarization of the light and the field dependences of the magnetization were measured. Visual observations of the two-phase domain structure formed during the MM phase transition were also performed. The samples under study were plates of several tens of microns in thickness. The single crystal plates were cut perpendicular to a direction of type [100]. The elastic stresses generated in the plate surface layers due to mechanical polishing were removed by annealing at a temperature of about 1000 °C as well as by chemical polishing in orthophosphoric acid. It is known that the CaMnGeG crystals display the Jahn–Teller phase transition from the cubic to a tetragonal phase at $T \approx 500$ K.[9] This transition results in the formation of crystal twins in the low-symmetry phase.[9–11] A special thermal treatment was used to obtain single-domain samples.[10] As a result of the treatment, single-domain plates with the tetragonal axis oriented perpendicular or parallel to the plate surface were obtained.

In the magnetooptical and visual experiments the sample was placed on a holder in an optical helium cryostat and was kept in vacuum. Temperature was measured by means of a resistance thermometer with an accuracy of about 0.1 K. A superconducting magnet produced a magnetic field that was perpendicular to the plate surface and parallel to the direction of light propagation.

The optical scheme of the experimental setup for visual observation of the two-phase domain structure is shown in Fig. 1a. The light from filament lamp (1) passes through polarizer (5), the sample (7), and analyzer (9). The sample image is projected by the objective (8) onto the photocathode of a TV camera (10) and is displayed on a monitor (11) and saved by a video recorder (12). To ensure that the magnetic state of the crystal under study remains unchanged, the light flux density is decreased to 0.01 W/cm^2 by means of the filters. To investigate the effect of light illumination on the MM phase transition, the sample is exposed to the light of a helium-neon laser (15) with a wavelength $\lambda = 633$ nm and a light flux density of about 0.1 W/cm^2. The optical system is also equipped with rotary mirrors (13) and (14) and with a field diaphragm (3) having a certain shape which allows local irradiation of a chosen area of the sample. The image of the diaphragm on the sample surface is formed by the lens (4).

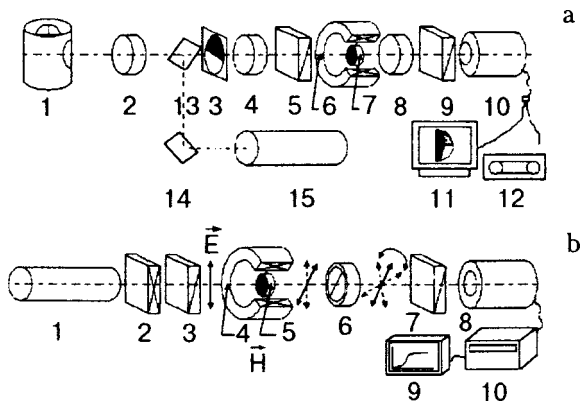

FIG. 1. The optical system of the experimental setup for visual observation of the domain structure: 1 — filament lamp; 2, 4, 8 — lenses; 3 — field diaphragm; 5 — polarizer; 6 — solenoid; 7 — sample; 13, 14 — mirrors; 15 — helium–neon laser (a). The optical system for measuring the angle of rotation of the plane of polarization of the light: 1 — helium–neon laser; 2 — light attenuator; 3 — polarizer; 4 — solenoid; 5 — sample; 6 — modulator; 7 — analyzer; 8 — photomultiplier; 9 — recorder; 10 — lock-in amplifier (b).

When the field dependences of the angle of rotation of the plane of polarization were measured, it was necessary to take into account that several magnetooptical effects (the Faraday effect, Cotton–Mouton effect, and the linear magnetooptical effect (LMOE)[12]) arise in a magnetic field in the antiferromagnet CaMnGeG. Therefore, the incident linearly polarized light became elliptically polarized even in the case when it passed through the crystal along the tetragonal axis. In our experiments we measured the angle of rotation Φ of the ellipse axis of the transmitted light with respect to the plane of polarization of the incident light. The angle Φ depended on the Faraday rotation and linear birefringence. When the measuring beam of light passed through the crystal along the [100] direction, i.e., perpendicular to the tetragonal axis, the plane of polarization of the incident light was chosen parallel to the crystallographic direction [010] or [001]. In this case, the contribution of crystalline birefringence to the modification of the polarization of the transmitted light was minimal. As a rule, the light ellipticity was slight (about 1°) in our experiments. That made possible to use a modulation technique with light modulation in the plane of polarization and synchronous detection of the signal to measure the angle Φ (Fig. 1b). The measurement of field dependences $\Phi(H)$ and the light illumination of the sample were carried out with the use of helium-neon laser of wavelength $\lambda = 633$ nm. The light flux density used for illumination of the sample was about 0.1 W/cm^2. To measure the field dependences $\Phi(H)$, the flux density of the laser beam was attenuated down to 0.01 W/cm^2.

The field dependences of the magnetization and photoinduced magnetic moment were measured by means of a commercial SQUID magnetometer (Quantum Design MPMS-5).

EXPERIMENTAL RESULTS

Before studying the effect of light illumination on the MM phase transitions, we examined these transitions in an unexposed crystal. The data from the magnetooptical and visual studies were used to construct the $H-T$ magnetic

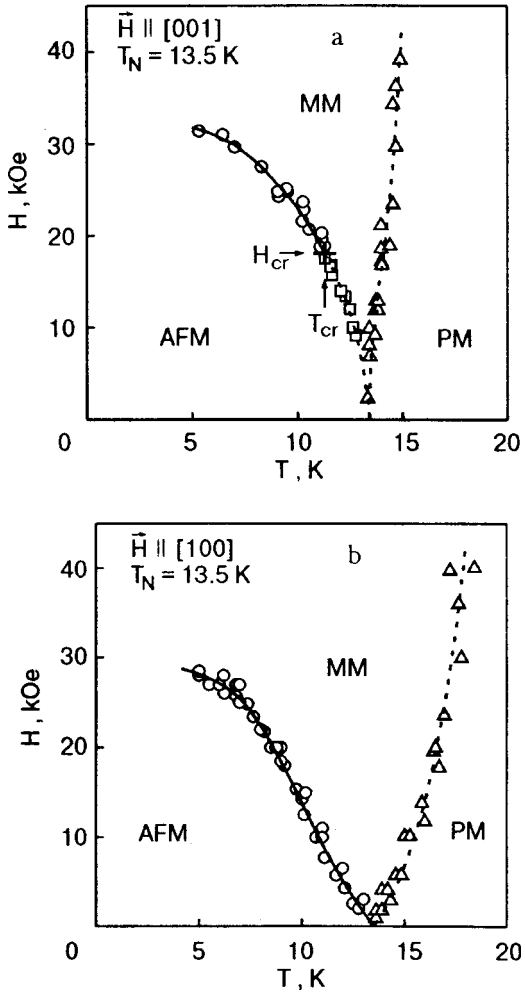

FIG. 2. Magnetic phase diagrams of the garnet $Ca_3Mn_2Ge_3O_{12}$ for $\mathbf{H}\|[001]$ (a) and $\mathbf{H}\|[100]$ (b). The solid and dotted lines correspond to the first- and second-order phase transitions, respectively.

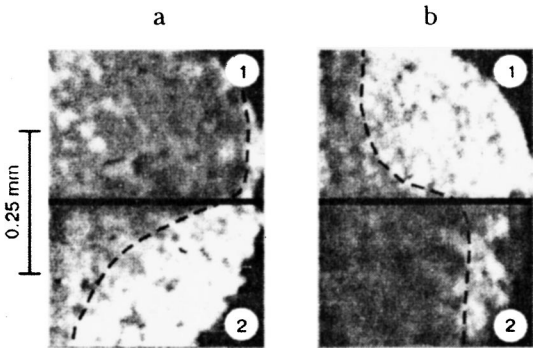

FIG. 3. The two-phase domain structure formed in the $Ca_3Mn_2Ge_3O_{12}$ plate during the MM phase transition after exposure of the crystal to linearly polarized light. The AFM–MM interphase wall is denoted by a dashed line. The sample temperature $T=7$ K; the applied magnetic field $\mathbf{H}\|[001]$. Part 1 (above the solid heavy line) exposed to light with the polarization $\mathbf{E}\|[1\underline{1}0]$ and part 2 (below the solid heavy line) to light with the polarization $\mathbf{E}\|[110]$ (a); part 1 exposed to light with the polarization $\mathbf{E}\|[110]$ and part 2 to light with the polarization $\mathbf{E}\|[110]$ (b).

phase diagrams of CaMnGeG for two orientations of external magnetic field: $\mathbf{H}\|[001]$ and $\mathbf{H}\|[100]$ (Fig. 2). In both cases the transition from the AFM to the MM state is a first-order phase transition at low temperatures. For $\mathbf{H}\|[100]$ the first-order AFM-MM phase transition is observed in the whole temperature range $T<T_N\approx 13.5$ K, where T_N is the Néel temperature. In the case $\mathbf{H}\|[001]$, the $H-T$ phase diagram exhibits a critical point, $H_{cr}\approx 18$ kOe, $T_{cr}\approx 11.5$ K, at which the line of first-order phase transitions passes into a line of second-order ones. Because the effect of light illumination on the first-order MM phase transition was studied, in the case $\mathbf{H}\|[001]$ the experiments were performed at $T<T_{cr}$.

In the first experiment we studied the effect of light irradiation on the MM phase transition induced by a magnetic field $\mathbf{H}\|[001]$. In this case the directions of the inducing light and the measuring light beam were parallel to the [001] crystal axis. The effect of light on the MM phase transition was first studied visually. For this purpose a single domain AFM state was prepared by applying a magnetic field.[12] The process of monodomainization was monitored visually through the LMOE. After the process was completed and the magnetic field was switched off, the upper half of the sample was exposed to laser light with the polarization $\mathbf{E}\|[110]$ and the lower one to light with the polarization $\mathbf{E}\|[\bar{1}10]$. Thereupon we observed visually the magnetic-field-induced phase transition from the AFM to the MM state. The two-phase domain structure formed during the transition in the exposed sample is shown in Fig. 3. The AFM–MM interphase wall is indicated by the dashed line, and the boundary between the crystal parts exposed to the light with the different polarizations is shown by the solid heavy line. As is evident from Fig. 3a, the transition from the AFM to the MM state in the upper part of the sample occurs before that in the lower part. To be sure that the difference in the transition fields between the upper and lower parts of the sample is caused by the light illumination and not accidental factors (internal mechanical stresses, temperature gradient, etc.), in the second stage of the experiments the upper part of the sample was exposed to light with the polarization $\mathbf{E}\|[110]$ and the lower one to light with the polarization $\mathbf{E}\|[110]$. In this case we observed the inverse effect, namely, the magnetic-field-induced phase transition from the AFM to the MM state in the lower part of the sample occurs before that in the upper part (Fig. 3b). Thus the visual observation permits us to conclude that exposure of the crystal to light with the polarization $\mathbf{E}\|[110]$ stimulates the MM phase transition in the garnet $Ca_3\underline{Mn}_2Ge_3O_{12}$, while exposure to light with the polarization $\mathbf{E}\|[110]$ inhibits the transition.

To determine the value of the photoinduced change of the phase transition field, ΔH_t, we measured the field dependences of the rotation angle, $\Phi(H)$, shown in Fig. 4. The dependences were measured in the same area of the sample ($\sim$100 μm in diameter) exposed first to light with the polarization $\mathbf{E}\|[110]$ and then to light with the polarization $\mathbf{E}\|[110]$. In both cases the intensity and the duration of the exposure were the same. The jump in the $\Phi(H)$ curve (Fig. 4) corresponds to a first-order MM phase transition. The transition is accompanied by relatively small hysteresis. The difference in transition fields, $2\Delta H_t=H_{t2}-H_{t1}$, between the cases of exposure of the crystal to light with polarization $\mathbf{E}\|[110]$ and $\mathbf{E}\|[110]$ is about of 180 Oe at the temperature $T=7$ K, i.e., $\Delta H_t\approx 90$ Oe. The values H_{t1} and H_{t2} were determined from the midpoint of the section of sharp change

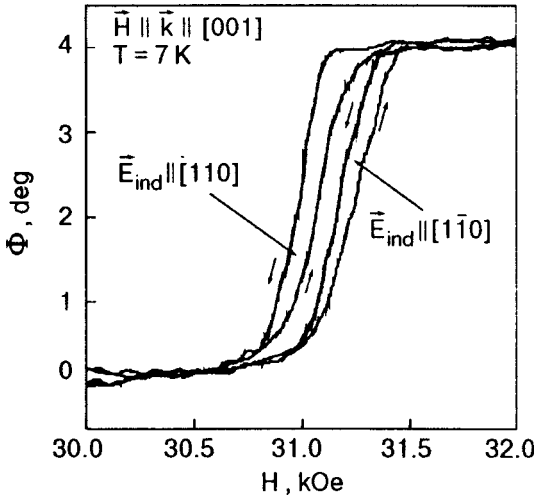

FIG. 4. The field dependences of the rotation angle measured in the case $\mathbf{k}\|\mathbf{H}[001]$ in a sample area of about 100 μm in diameter exposed beforehand to linearly polarized light with the polarization $\mathbf{E}\|[110]$ or $\mathbf{E}\|[110]$. The sample temperature $T=7$ K.

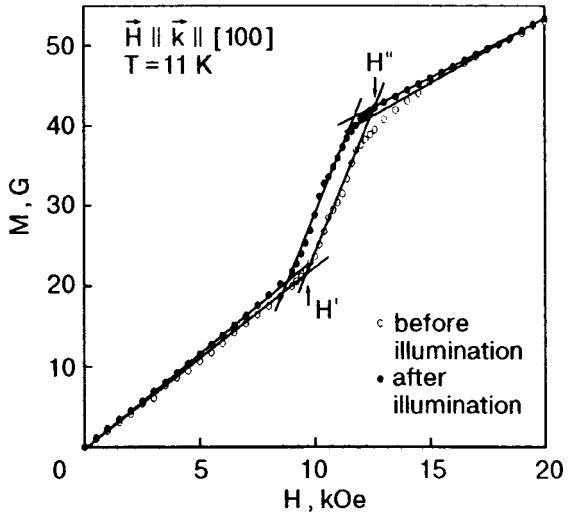

FIG. 6. The field dependences of the magnetization measured in a field $\mathbf{H}\|[100]$ at a temperature $T=11$ K. ○ — unexposed sample; ● — the sample was preliminarily exposed to linearly polarized light with polarization $\mathbf{E}\|[011]$. The direction of propagation of the inducting light $\mathbf{k}\|[100]$.

of the rotation angle on the curve $\Phi(H)$ measured with an increasing (or decreasing) magnetic field for $\mathbf{E}\|[110]$ and $\mathbf{E}\|[110]$ ($H_t=(H'+H'')/2$ [see Figs. 5 and 6)]. The MM phase transition field in the unexposed sample, H_t, was equal to ~31.2 kOe. This is close to the value of $(H_{t1}+H_{t2})/2$.

In the second experiment we investigated the effect of light illumination on the MM phase transition induced by a magnetic field $\mathbf{H}\|[100]$. In this case the studies were performed by means of magnetooptical and magnetometric techniques. The field dependences of the angle of rotation of the plane of polarization and the field the dependences of the magnetization were measured. The direction of propagation of the inducing light was parallel to the crystal axis [100]. In the magnetooptical experiments, the direction of propagation of the measuring light beam was also parallel to the [100] axis.

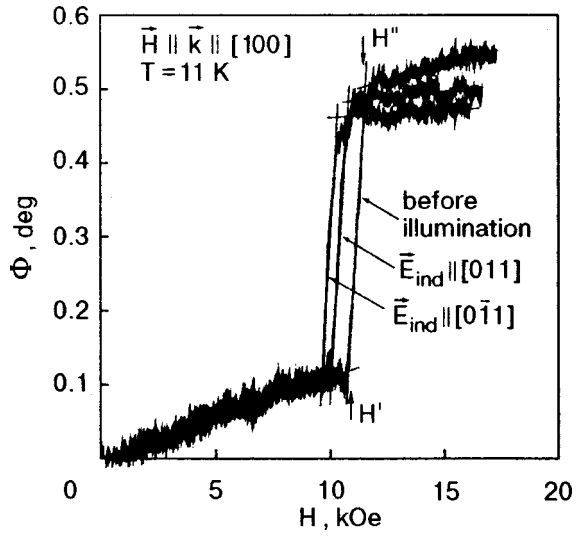

FIG. 5. The field dependences of the rotation angle measured in the case $\mathbf{k}\|\mathbf{H}[100]$ in a sample area about 100 μm in diameter exposed beforehand to linearly polarized light with the polarization $\mathbf{E}\|[011]$ or $\mathbf{E}\|[011]$ as well as in the unexposed sample. The temperature of the sample $T=11$ K.

At $\mathbf{k}\|\mathbf{H}\|[100]$ we also observed a photoinduced change of the MM phase transition field. The value ΔH_t-$H_{t1}-H_{t0}(H_t=(H'+H'')/2)$ also depended on the polarization of the inducing light. However, exposure to light with any linear polarization always resulted in a decrease of the MM transition field. The field dependences of the rotation angle, $\Phi(H)$, measured at the temperature $T=11$ K, are shown in Fig. 5. The jump in the $\Phi(H)$ curves corresponds to the MM phase transition. As it is evident from Fig. 5, after exposing the crystal to light with the polarization $\mathbf{E}\|[011]$ and $\mathbf{E}\|[011]$, the phase transition occurs at a lower field that in the unexposed crystal. The photoinduced decrease in the transition field for $\mathbf{E}\|[011]$ was larger than that for $\mathbf{E}\|[011]$. It is noted that the different magnitudes of the rotation angle Φ in the MM state on the curves shown in Fig. 5 are related to the appearance of photoinduced linear birefringence in the illuminated crystal.[13]

Figure 6 shows the field dependences of the magnetization measured at the temperature $T=11$ K in the unexposed sample and in the sample exposed to light with the polarization $\mathbf{E}\|[011]$. It is also seen in Fig. 6 that a decrease of the MM transition field is observed after illumination of the sample.

In the case $\mathbf{E}\|[0\bar{1}1]$ (larger magnitude of ΔH_t), the values of the photoinduced changes in the transition field, ΔH_t, at different temperatures were determined from the field dependences $\Phi(H)$ measured in the temperature range 7–13 K. The dependence $\Delta H_t(T)$ is shown in Fig. 7. As is seen in Fig. 7, the value of ΔH_t increases with decreasing temperature, peaks at $T=10.5$–11 K, and then decreases with further reduction in temperature. In the case under consideration the maximum value of ΔH_t is about of 1.2 kOe. This is much larger than in the previous case, where the inducing light propagated along the tetragonal axis. The sign of the ΔH_t remains unchanged in the whole temperature range studied.

DISCUSSION

The experimental investigations demonstrated that the exposure of the garnet $Ca_3Mn_2Ge_3O_{12}$ to linearly polarized

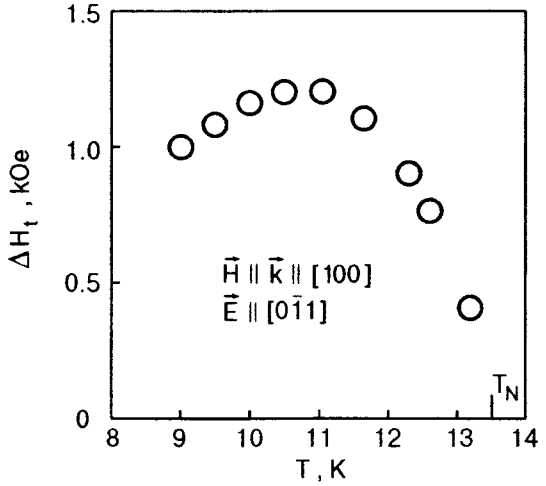

FIG. 7. The temperature dependence of the change in the MM phase transition field caused by light irradiation in the case $\mathbf{k}\|\mathbf{H}\|[100]$ and $\mathbf{E}\|[011]$.

light propagating along the [001] direction resulted in an increase or a decrease in the MM phase transition field, depending on the polarization of the inducing light. On exposure of the crystal to light propagating along [100] the direction, the MM phase transition field decreases without regard to the polarization of the inducing light. The reason why the light irradiation affects the MM phase transition in the CaMnGeG may be magnetic moment stimulation by the light. Depending on the direction of the photoinduced magnetic moment, the AFM phase in the magnetic field is more or less stable in the exposed crystals than in the unexposed crystal, and that results in the variation in the MM phase transition field.

Let us consider a phenomenological model for the appearance of a magnetic moment in this garnet under illumination. It is known that on exposure of the crystal to light, its internal energy per unit volume varies as follows:[14]

$$\Delta F = -(1/16\pi)[d(\omega\varepsilon_{ik})/d\omega]E_iE_k, \tag{1}$$

where ω is the light frequency, E is the electric field strength of the light wave, and ε_{ik} is the dielectric tensor of the crystal. The change in the internal energy under illumination can generate a light-induced magnetic moment ${}^{ph}\mathbf{m}$ in the crystal. The value and the direction of the photoinduced magnetic moment are dependent on the polarization of the inducing light as well as on the crystalline and magnetic symmetry of the crystal.[15,16] Using (1), we can derive an expression for ${}^{ph}\mathbf{m}$. To do this, we first expand the ΔF series to the second-order in $\mathbf{H}$ and then we differentiate the resulting expression with respect to $\mathbf{H}$. As a result we obtain:

$${}^{ph}m_l = C_{lik}E_iE_k + B_{lmik}H_mE_iE_k, \tag{2}$$

where C_{lik} and B_{lmik} are the first and the second derivatives of the expression $(1/16\pi)[d(\omega\varepsilon_{ik})/d\omega]$. Using (2), we can derive an expression for the magnetic moment ${}^{ph}\mathbf{m}$ induced by linear by polarized light propagating along the [001] direction. For this purpose, we rewrite Eq. (2) in the following form:

$${}^{ph}m_l = {}^{ph}m_l^{(1)} + {}^{ph}m_l^{(2)}. \tag{3}$$

In this expression ${}^{ph}m_l^{(1)} = C_{lik}E_iE_k$, where C_{lik} is an axial c-tensor symmetric in i and k, and ${}^{ph}m_l^{(2)} = B_{lmik}E_iE_kH_m = {}^{ph}\Delta\chi_{lm}H_m$, where B_{lmik} is a polar i-tensor symmetric on two pairs of indices i, k and l, m. Let us obtain first ${}^{ph}m_l^{(1)}$. Since CaMnGeG belongs to the point magnetic group $4'/m$, the tensor matrix C_{lik} can be written in the form:

$$C_{l\mu} = \pm\begin{bmatrix} 0 & 0 & 0 & C_{14} & C_{15} & 0 \\ 0 & 0 & 0 & -C_{15} & C_{14} & 0 \\ C_{15} & -C_{15} & 0 & 0 & 0 & C_{14} \end{bmatrix}. \tag{4}$$

The reduction of indices was used in (4). In this expression, "+" and "−" correspond to the two time-inverted antiferromagnetic states, AFM^+ and AFM^-, and $C_{15} = C_{xxz} = C_{yyz} = C_{xzx}$ and $C_{14} = C_{yzx} = C_{xzy} = C_{xyz}$. If the inducing light propagates along the [001] direction, the components ${}^{ph}m_l^{(1)}$ can be written as follows:

$$\begin{aligned} {}^{ph}m_x^{(1)} &= 0 \\ {}^{ph}m_y^{(1)} &= 0 \\ {}^{ph}m_z^{(1)} &= \pm(C_{zxx}E_xE_x - C_{zyy}E_yE_y + 2C_{zxy}E_xE_y). \end{aligned} \tag{5}$$

To determine the second term ${}^{ph}m_l^{(2)}$ in Eq. (3), we calculate ${}^{ph}\Delta\chi_{lm}$ taking into consideration the fact that the Laue crystal class of the garnet under study is C_4:

$$\chi_{lm} = \begin{bmatrix} B_{11} & B_{12} & B_{13} & 0 & 0 & B_{16} \\ B_{12} & B_{11} & B_{13} & 0 & 0 & -B_{16} \\ B_{31} & B_{31} & B_{33} & 0 & 0 & 0 \\ 0 & 0 & 0 & B_{44} & B_{45} & 0 \\ 0 & 0 & 0 & -B_{45} & B_{44} & 0 \\ B_{61} & -B_{61} & B_{63} & 0 & 0 & B_{66} \end{bmatrix}\begin{bmatrix} E_1 & E_1 \\ E_2 & E_2 \\ 0 & \\ 0 & \\ 0 & \\ 2E_1 & E_2 \end{bmatrix}$$

$$= \begin{bmatrix} B_{11}E_1^2 + B_{12}E_2^2 + 2B_{16}E_1E_2 & B_{61}E_1^2 - B_{61}E_2^2 + 2B_{16}E_1E_2 & 0 \\ & B_{12}E_1^2 + B_{11}E_2^2 - 2B_{16}E_1E_2 & 0 \\ & & B_{31}E_1^2 + B_{31}E_2^2 \end{bmatrix}. \tag{6}$$

Then, using (6), we can derive an expression for the magnetic moment ${}^{\rm ph}m_l^{(2)}$:

$$ {}^{\rm ph}m_l^{(2)} = \begin{bmatrix} B_{11}E_1^2 + B_{12}E_2^2 + 2B_{16}E_1E_2 & B_{61}E_1^2 - B_{61}E_2^2 + 2B_{16}E_1E_2 & 0 \\ & B_{12}E_1^2 + B_{11}E_2^2 - 2B_{16}E_1E_2 & 0 \\ & & B_{31}E_1^2 + B_{31} + B_{31}E_2^2 \end{bmatrix} \begin{bmatrix} H_x \\ H_y \\ H_z \end{bmatrix}, \tag{7} $$

where

$$ \begin{aligned} {}^{ph}m_x^{(2)} &= (B_{xxxx}E_x^2 + B_{xxyy}E_y^2 + 2B_{xxxy}E_xE_y)H_x + (B_{xyxx}E_x^2 - B_{xyxx}E_y^2 + 2B_{xxxy}E_xE_y)H_y \\ {}^{\rm ph}m_y^{(2)} &= (B_{xxyy}E_x^2 + B_{xxxx}E_y^2 - 2B_{xxxy}E_xE_y)H_y + B_{xyxx}E_x^2 - B_{xyxx}E_y^2 + 2B_{xxxy}E_xE_y)H_x \\ {}^{\rm ph}m_z^{(2)} &= B_{zzxx}(E_x^2 + E_y^2)H_z . \end{aligned} \tag{8} $$

It should be noted that the matrix of the tensor B_{lmik} is determined only by the crystal symmetry of CaMnGeG. Therefore, the direction of the moment ${}^{\rm ph}m_l^{(2)}$ is independent of the magnetic state of the crystal. If we know the expressions for ${}^{\rm ph}m_l^{(1)}$ and ${}^{\rm ph}m_l^{(2)}$, we can determine the magnetic moment ${}^{\rm ph}\mathbf{m}$ induced by light propagating along the [001] direction. Upon introducing the azimuthal angle φ measured from the axis $\mathbf{x}\|[100]$, the components of this magnetic moment, ${}^{\rm ph}m_x, {}^{\rm ph}m_y, {}^{\rm ph}m_z$, can be given as follows:

$$ \begin{aligned} {}^{\rm ph}m_x &= (B_{xxxx}\cos^2\varphi + B_{xxyy}\sin^2\varphi + B_{xxxy}\sin 2\varphi)|E|^2H_x \\ &\quad + H_y(B_{xyxx} + B_{xxxy})|E|^2\sin 2\varphi + \cos 2\varphi); \\ {}^{\rm ph}m_y &= (B_{xxyy}\cos^2\varphi + B_{xxxx}\sin^2\varphi - B_{xxxy}\sin 2\varphi)|E|^2H_y \\ &\quad + H_x|E|^2(B_{xyxx}\cos 2\varphi + B_{xxxy}\sin 2\varphi); \\ {}^{\rm ph}m_z &= B_{zzxx}|E|^2H_z \pm |E|^2(C_{zxx}\cos 2\varphi + C_{zxy}\sin 2\varphi). \end{aligned} \tag{9} $$

The signs "$\pm$" correspond to the antiferromagnetic states AFM^+ and AFM^-. For $\mathbf{k}\|\mathbf{H}\|[001]$, field components H_x and H_y are equal to zero. Therefore, ${}^{\rm ph}m_x = 0, {}^{\rm ph}m_y = 0$ and ${}^{\rm ph}m_z = B_{zzxx}|E|^2H_z \pm |E|^2(C_{zxx}\cos 2\varphi + C_{zxy}\sin 2\varphi)$ in this case.

If the inducing light propagates along the [100] direction, the induction of a magnetic moment is also allowed by the symmetry. Repeating the line of calculation made for the previous case, we can derive expressions for the photoinduced magnetic moment components:

$$ \begin{aligned} {}^{\rm ph}m_x &= (H_xB_{xxxx} + H_yB_{xyxx})|E|^2\cos^2\varphi \\ &\quad + H_yB_{xxzz}|E|^2\sin^2\varphi + (H_zB_{xzxz} \\ &\quad \pm 2C_{xxz})|E|^2\sin 2\varphi; \\ {}^{\rm ph}m_y &= [(H_xB_{xyxx} + H_yB_{yyxx})|E|^2\cos^2\varphi \\ &\quad + H_yB_{yyzz}|E|^2\sin^2\varphi] + (H_zB_{yzxz} \\ &\quad \pm 2C_{yxz})|E|^2\sin 2\varphi; \\ {}^{\rm ph}m_z &= H_yB_{zzxx}|E|^2 + (H_yB_{yzxz} + H_xB_{xzxz})|E|^2\sin 2\varphi \\ &\quad \pm C_{zxx}|E|^2\cos^2\varphi. \end{aligned} \tag{10} $$

Here the angle φ is measured from the axis $\mathbf{y}\|[010]$, and the signs "$\pm$", as in the previous case, correspond to the two antiferromagnetic states AFM^+ and AFM^-. At $\mathbf{k}\|\mathbf{H}\|[100]$, the field components H_y and H_z are equal zero. Therefore, ${}^{\rm ph}m_x = H_xB_{xxxx}|E|^2\cos^2\varphi \pm 2C_{xxz}|E|^2\sin 2\varphi$, ${}^{\rm ph}m_y = H_xB_{xyxx}|E|^2\cos^2\varphi \pm 2C_{yxz}|E|^2\sin 2\varphi$ and ${}^{\rm ph}m_z = H_xB_{xzxz}|E|^2\sin 2\varphi \pm C_{zxx}|E|^2\cos^2\varphi$, i.e., in this case all components of photoinduced magnetic moments do not equal zero.

Experimental verification of the fact that a magnetic moment is really induced by linearly polarized light in $Ca_3Mn_2Ge_3O_{12}$ came from the magnetic measurements. The photoinduced magnetic moment was measured by means of a SQUID magnetometer. The uniformly magnetized crystal was irradiated along the [001] direction by helium-neon laser light with a wavelength $\lambda = 633$ nm and a light flux density of about 0.1 W/cm^2. The plane of polarization the inducing light was close to the (110) plane of crystal. The magnetiza-

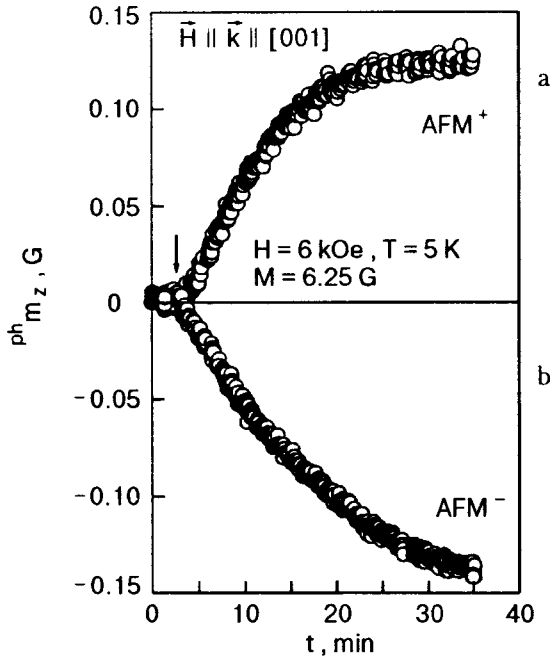

FIG. 8. The time dependences of the photoinduced magnetic moment in the garnet $Ca_3Mn_2Ge_3O_{12}$ exposed to linearly polarized light for two time-inverted antiferromagnetic states AFM^+ and AFM^-. The direction of propagation and the polarization of the inducing light are $\mathbf{k}\|[001]$ and $\mathbf{E}\|[110]$, respectively. The sample temperature $T = 5$ K, and the applied magnetic field is equal to 6 kOe and is oriented along the [001] axis.

tion was measured along the axis $\mathbf{z}\|[001]$. The sample was in a magnetic field $H_z=6$ kOe at a temperature $T=5$ K. The change of the magnetization of crystal under illumination, i.e., the photoinduced magnetic moment, was measured. Figure 8 presents the kinetics of the induced magnetic moment measured for the two antiferromagnetic states of the sample, AFM^+ and AFM^-. It follows from (9) that the value of ${}^{ph}m_z$ changes when the antiferromagnetic state is modified from AFM^+ to AFM^-. Indeed, the same exposure of the crystal induced magnetic moments of opposite directions in the AFM^+ and AFM^- states (Fig. 8). The absolute magnitude of the photoinduced magnetic moment upon saturation was 0.12 and 0.13 G in the AFM^+ and AFM^- states, respectively. Thus the absolute magnitudes of the photoinduced magnetic moments in the antiferromagnetic states AFM^+ and AFM^- are almost identical. One can suggest that the polarization-independent magnetic moment ${}^{ph}m_z^{(2)}$ is appreciably less than ${}^{ph}m_z^{(1)}$ or is equal to zero. It should be noted that in the case $\mathbf{k}\|[001]$ the photoinduced magnetic moment was not found in the MM state.

In the case $\mathbf{k}\|[100]$, the magnetic measurements also revealed a photoinduced magnetic moment. In AFM state the value of ${}^{ph}\mathbf{m}$ was lower than in the previous case. As in the above case, the photoinduced magnetic moments in the antiferromagnetic states AFM^+ and AFM^- are almost the same in value and opposite in direction. Thus, in the case considered, the value of the magnetic moment ${}^{ph}m_x^{(2)}$ is also much lower than ${}^{ph}m_x^{(1)}$ or is also equal to zero. The absolute magnitude of the moment was approximately 0.05 G at $T=5$ K and $H=6$ kOe. In the case under consideration, the magnetic measurements also revealed a photoinduced magnetic moment in the MM state. Its value was approximately 0.25 G at $T=5$ K and $H=35$ kOe.

Using the values of ${}^{ph}\mathbf{m}$ measured with the SQUID magnetometer, one can estimate the change in the MM phase transition field, ΔH_t, caused by the light irradiation in CaMnGeG. The energy of a magnet in a magnetic field can be given in the form of expansion in powers of H:[17]

$$E=E_0-m_i^0H_i-\chi_{ij}H_IH_j+\ldots, \tag{11}$$

where E_0 is the energy of the magnet in the absence of magnetic field; m^0 is the spontaneous magnetic moment; χ_{ij} is the magnetic susceptibility. The photoinduction of a magnetic moment results in a change of the energy of the magnet by a quantity ${}^{ph}m_iH_i$. Taking this addition into consideration and restricting ourselves to the second-order term in the expansion in H, we can rewrite (11) as follows:

$$E=E_0-m_i^0H_i-\chi_{ij}H_iH_j-{}^{ph}m_i(H)H_i, \tag{12}$$

where ${}^{ph}m_i(H)={}^{ph}m_i^{(1)}+{}^{ph}\Delta\chi_{ij}H_i$. Then, the energies of the AFM and MM states in both cases considered above can be written as follows:

$$\begin{aligned} {}^AE&={}^AE_0-{}^A\chi_{ii}H_i^2-{}^{ph}m_i^A(H)H_i;\\ {}^ME&={}^ME_0-m_i^0H_i-{}^M\chi_{ii}H_i^2-{}^{ph}m_i^M(H)H_i. \end{aligned} \tag{13}$$

In (13) the notations A and M refer to the AFM and MM phases, respectively. Equating the energies of the AFM and MM states at the point of the MM phase transition for unexposed and exposed crystal and solving the obtained set of equations, we find the following expression for the photoinduced change in the MM transition field:

$$\Delta H_t=-\frac{{}^{ph}m_i^M(H_t)-{}^{ph}m_i^A(H_t)}{2({}^M\chi_{ii}-{}^A\chi_{ii})+m_i^0/H_t}, \tag{14}$$

where H_t is the field of the MM transition in the unexposed crystal.

Using expression (14), we can estimate the value of ΔH_t in both cases considered, $\mathbf{k}\|\mathbf{H}\|[001]$ and $\mathbf{k}\|\mathbf{H}\|[100]$. In the first case no photoinduced magnetic moment was found in the MM state by means of the SQUID magnetometer. By substituting into Eq. (14) ${}^{ph}m_z^M\approx 0, {}^{ph}m_z^A\approx\pm 0.12$ G, $({}^M\chi_{zz}-{}^A\chi_{zz})=-3.6\times10^{-4}$, and $m_z^0\approx 47$ G, we obtained $\Delta H_t\approx\pm 150$ Oe. The estimated value ΔH_t is somewhat (less than two times) higher than the experimental magnitude $\Delta H_t\approx\pm 90$ Oe. However, taking into account the errors in the determination of the parameters substituted in (14), the agreement between the experimental and the calculated values of the ΔH_t is considered satisfactory. It should be mentioned that ${}^M\chi_{zz}$, ${}^A\chi_{zz}$, and m_z^0 were determined from the field dependence $M(H)$ (m_z^0 was determined by extrapolating the linear field dependence of the magnetization in the MM state to $H=0$).

In the case $\mathbf{k}\|\mathbf{H}\|[100]$, one has $({}^M\chi_{xx}-{}^A\chi_{xx})=-9\times10^{-4}$ and $m_x^0\approx 23$ G at the temperature $T=11$ K (see Fig. 6), as well as ${}^{ph}m_x^M\approx 0.25$ G, ${}^{ph}m_x^A\approx\pm 0.05$ G. By substituting these parameters into Eq. (14), we obtain two values for the change of the transition field, $\Delta H_t\approx -1.2$ kOe and $\Delta H_t\approx -0.8$ kOe. These could correspond either to the two antiferromagnetic states AFM^+ and AFM^- or to the exposure of crystal by the light with the two polarizations $\mathbf{E}\|[011]$ and $\mathbf{E}\|[011]$. The estimated values are in a good agreement with the experimental values $\Delta H_t\approx -1.2$ kOe and $\Delta H_t\approx -0.7$ kOe that were obtained for illumination of the crystal by light with the polarizations $\mathbf{E}\|[011]$ and $\mathbf{E}\|[011]$ at the temperature $T=11$ K. As can be seen from Fig. 7, the magnitude of ΔH_t decreases at higher and lower temperatures. Apparently, the decrease ΔH_t as the temperature increases from 11 K to T_N is related to the decrease of the photoinduced magnetic moment near the Néel temperature. Some decrease of ΔH_t at temperatures $T<10.5$ K can be explained by a decreasing absolute value of $(\chi_M-\chi_A)$ while the photoinduced magnetic moment reaches saturation. For instance, one obtains a calculated value $\Delta H_t\approx -1$ kOe at the temperature $T=9$ K.

CONCLUSION

It follows from a comparison of the experimental results obtained and the results of a theoretical consideration that the change of the MM transition field induced by linearly polarized light in the garnet $Ca_3Mn_2Ge_3O_{12}$ is due to the induction of a magnetic moment under illumination. The appearance of the photoinduced magnetic moment can be explained by the redistribution of the Mn^{4+} ions between the magnetic sublattices in the crystal. The garnet $Ca_3Mn_2Ge_3O_{12}$ contains Mn^{4+} ions in a low concentration.[13] In the ground state these ions are uniformly distributed between the sublattices. Illumination of the crystal by linearly polarized light leads to a non-

uniform distribution of the Mn^{4+} ions between the sublattices as a result of optical transitions with charge transfer.[13,16] As a result of the redistribution, the magnetic sublattices become nonequivalent and a photoinduced magnetic moment appears.

This research was supported in part by the INTAS grant N 97-366.

*E-mail: bedarevilt.kharkov.ua

[1] V. F. Kovalenko and E. L. Nagaev Usp. Fiz. Nauk **148**, 561 (1986) [Sov. Phys. Usp. **29**, 297 (1986)].
[2] V. F. Kovalenko, E. S. Kolezhuk, and P. S. Kuts, Zh. Éksp. Teor. Fiz. **81**, 1399 (1981) [Sov Phys. JETP **54**, 742 (1981)].
[3] V. F. Kovalenko, P. S. Kuts, and V. P. Sokhatskii, Fiz. Tverd. Tela (Leningrad) **24**, 145 (1982) [Sov. Phys. Solid State **24**, 80 (1982)].
[4] K. Mieano, T. Tanaka, and Y. Tokura, Phys. Rev. Lett. **78**, 4257 (1997).
[5] T. Mori, K. Ogawa, K. Yoshida, K. Miyano, Y. Tomioka, and Y. Tokura, J. Phys. Soc. Jpn. **66**, 3570 (1997).
[6] K. Ogowa, W. Wei, K. Miyano, Y. Tomioka, and Y. Tokura, Phys. Rev. B **57**, R15033 (1998).
[7] M. Baran, S. L. Gnatchenko, O. Yu. Gorbenko, A. R. Kaul, R. Szymczak, and H. Szymczak, Phys. Rev. B **60**, 9244 (1999).
[8] V. A. Bedarev, V. I. Gapon, and S. L. Gnatchenko, Fiz. Nizk. Temp **25**, 38 (1999) [Low Temp. Phys. **25**, 28 (1999)].
[9] Z. A. Kazei, P. Novak, and V. I. Sokolov, Zh. Éksp. Teor. Fiz. **83**, 1483 (1982) [Sov. Phys. JETP **56**, 854 (1982)].
[10] S. L. Gnatchenko, V. V. Eremenko, S. V. Sofroneev, N. F. Kharchenko, J. M. Desvignes, P. Feldmann, and H. Le Gall, Zh. Éksp. Teor. Fiz. **90**, 179 (1986) [Sov. Phys. JETP **63**, 102 (1986)].
[11] W. Graeff, J. Kub, and K. Wieteska, Phys. Status Solidi A **126**, 477 (1991).
[12] V. V. Eremenko, N. F. Kharchenko, Yu. G. Litvinenko, and V. M. Naumenko, *Magneto-Optics and Spectroscopy of Antiferromagnetics*, Springer-Verlag, New York (1992).
[13] S. L. Gnatchenko, V. V. Eremenko, S. V. Sofroneev, and N. F. Kharchenko, JETP Lett. **38**, 233 (1983).
[14] L. D. Landau and E. M. Lifshitz, *Electrodynamics of Continuous Media* [Pergamon Press, Oxford (1960), Gostekhizdat, Moscow (1959)].
[15] A. M. Balbashov, B. A. Zon, V. Ya. Kupershmid, G. V. Pakhomov, and T. T. Urazbayev, Zh. Éksp. Teor. Fiz. **94**, 304 (1988) [Sov. Phys. JETP **67**, 1039 (1988)].
[16] N. F. Kharchenko and V. A. Bedarev, Fiz. Nizk. Temp. **19**, 78 (1993) [Low Temp. Phys. **19**, 52 (1993)].
[17] G. Gorodetsky, B. Sharon, and S. Strikman, Solid State Commun. **5**, 739 (1967).
[18] V. V. Eremenko, S. L. Gnatchenko, N. F. Kharchenko, S. V. Sofroneev, J. M. Desvignes, P. Feldmann, and H. Le Gall, Acta Phys. Pol. A **68**, 419 (1985).
[19] N. F. Kharchenko, V. V. Eremenko, S. L. Gnatchenko, A. A. Milner, and S. V. Sofroneev, Fiz. Nizk. Temp. **11**, 215 (1985) [Sov. J. Low Temp. Phys. **11**, 116 (1985)].

This article was published in English in the original Russian journal. Reproduced here with stylistic changes by AIP.

Magnetic phase diagram of the system of manganites $Nd_{0.6}Ca_{0.4}(Mn_{1-x}Cr_x)O_3$

I. O. Troyanchuk and M. V. Bushinsky

Institute of Solid State Physics and Semiconductors, National Academy of Sciences of Belarus, ul. P. Brovki 17, 220072 Minsk, Belarus

V. V. Eremenko and V. A. Sirenko*

B. Verkin Institute for Low Temperature Physics and Engineering, National Academy of Sciences of Ukraine, pr. Lenina 47, 61103 Kharkov, Ukraine

H. Szymczak

Institute of Physics, Polish Academy of Sciences, al. Lotnikow 32/46, 02-688 Warsaw, Poland
(Submitted August 31, 2001)
Fiz. Nizk. Temp. **28**, 61–65 (January 2002)

The following sequence of phase transformations is observed in the $Nd_{0.6}Ca_{0.4}(Mn_{1-x}Cr_x)O_3$ system: antiferromagnet ($x=0$), mixed magnetic state ($0.015\leqslant x\leqslant 0.04$), ferrimagnet ($0.04\leqslant x\leqslant 0.8$), and spin glass ($x=1$). At chromium concentrations near $x\sim 0.5$ the Néel temperature increases sharply, and the contribution from the Nd sublattice increases substantially. Since the chromium and manganese ions have a tendency to order, these results can be interpreted in a model of superexchange interactions.
[DOI: 10.1063/1.1449184]

INTRODUCTION

There have by now been several papers on the study of manganites in which the manganese ions are substituted by ions of Fe, Al, Cr, Ru, Ti, Mo, Cu, Sn, Co, Ni, etc.[1–4] Depending on the ground state of the base compound, these substitutions have different effects. For charge-ordered antiferromagnets the replacement of a small fraction of the manganese ions by other ions leads to stabilization of the ferromagnetic phase. This effect is manifested most clearly when the manganese ions are substituted by chromium and ruthenium.[5–7] Stabilization of the ferromagnetic state gives rise to metal-like properties and a colossal magnetoresistance effect. The mechanism by which various substitutions affect the magnetic ground state is a matter of dispute. Some authors assume that double exchange can occur through the Mn^{3+}–O–Cr^{3+} configuration if the energy difference between the Mn^{3+} e_g band and the Cr^{3+} e_g band is not too large.[8] In another approach it is assumed that the Cr^{3+} ions are stable and the e_g-like conduction electrons cannot move through the chromium position, so that the chromium ions can create only a deficit in the orbital subsystem.[9] In that approach the chromium ions are a source of random fields that disrupt the orbital and charge ordering. However, the diamagnetic ions Al^{3+} and Ti^{4+} act on the ground state of manganites much more weakly than do chromium ions. It should be noted that there have been no published comprehensive studies of systems in which manganese has been substituted by other ions in a large concentration interval ($0\leqslant x\leqslant 1$). This makes it hard to interpret the results. The goal of the present study was to construct the magnetic phase diagram of the $Nd_{0.6}Ca_{0.4}(Mn_{1-x}Cr_x)O_3$ system over a wide range of chromium concentration. As the base compound we chose $Nd_{0.6}Ca_{0.4}MnO_3$, which is a charge-ordered antiferromagnet. It has been shown previously that a large external magnetic field induces a metamagnetic transition to a ferromagnetic metallic state.[8]

EXPERIMENTAL TECHNIQUES

Samples of the series $Nd_{0.6}Ca_{0.4}(Mn_{1-x}Cr_x)O_3$ were synthesized by the usual ceramic technology from simple oxides and carbonates in air at 1550 °C. To minimize the deviation from stoichiometry, the samples were cooled slowly at a rate of 50 °C/h. An x-ray phase analysis on a DRON-3 apparatus in CrK_α radiation did not reveal any traces of extraneous phases. The $Nd_{0.6}Ca_{0.4}(Mn_{1-x}Cr_x)O_3$ samples had an orthorhombically distorted unit cell. The magnetic measurements were made on a Foner magnetometer. The electrical conductivity was measured by the usual four-contact method. The contacts were formed the ultrasonic deposition of indium.

RESULTS AND DISCUSSION

Figure 1 shows the temperature dependence of the magnetization for the $Nd_{0.6}Ca_{0.4}(Mn_{1-x}Cr_x)O_3$ system in a field of 14 kOe. In this system substituting a small amount of manganese by chromium leads to a sharp change in the magnetic ground state. Samples with $0<x<0.04$ behave as metamagnetic materials. The critical fields inducing the transition decrease sharply with increasing chromium concentration. A spontaneous moment appears in the sample at $x=0.015$. The spontaneous magnetization of samples with $0.04\leqslant x\leqslant 0.42$ corresponds to a magnetic state in which an antiparallel ordering of the magnetic moments of the manganese and chromium ions is realized. Figure 2 shows the dependence of the field-cooled (FC) magnetization measured in a field of 100 Oe. It is seen that the samples in the interval

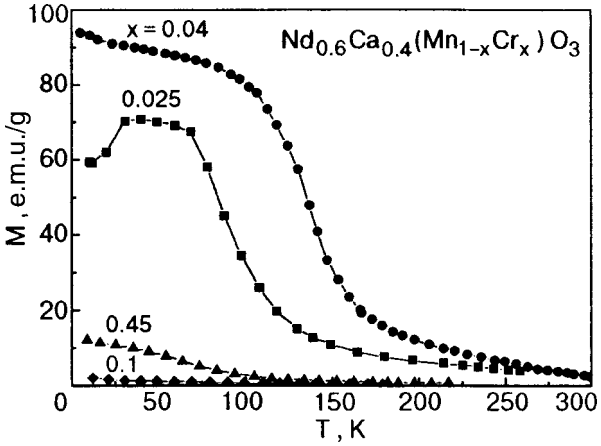

FIG. 1. Temperature dependence of the magnetization on heating after cooling in a magnetic field $H=14$ kOe (FC).

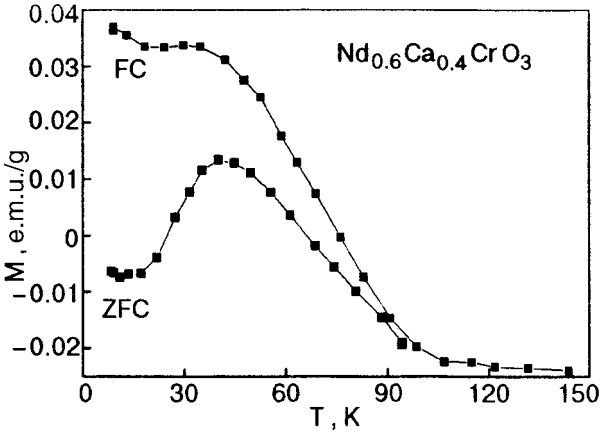

FIG. 3. Temperature dependence of the magnetization in $Nd_{0.6}Ca_{0.4}(Mn_{1-x}Cr_x)O_3$, measured in a field $H=100$ Oe and for different regimes: zero-field cooling (ZFC), and field cooling (FC).

$0<x\leqslant 0.42$ have a positive magnetization (see Fig. 2a), whereas for samples with $x\geqslant 0.48$ (Fig. 2b) at low temperatures the magnetization is directed counter to the magnetic field, which is possible in the presence of two magnetic sublattices with a large magnetic anisotropy. In the samples with $0.04<x\leqslant 0.3$ the transition to the paramagnetic state is rather sharp, while in the sample with $x=0.42$ the magnetization decreases smoothly with increasing temperature. The coercive force increases with increasing chromium concentration. In samples with $0.1\leqslant x\leqslant 0.3$ the FC magnetization decreases sharply with decreasing temperature, an effect which cannot

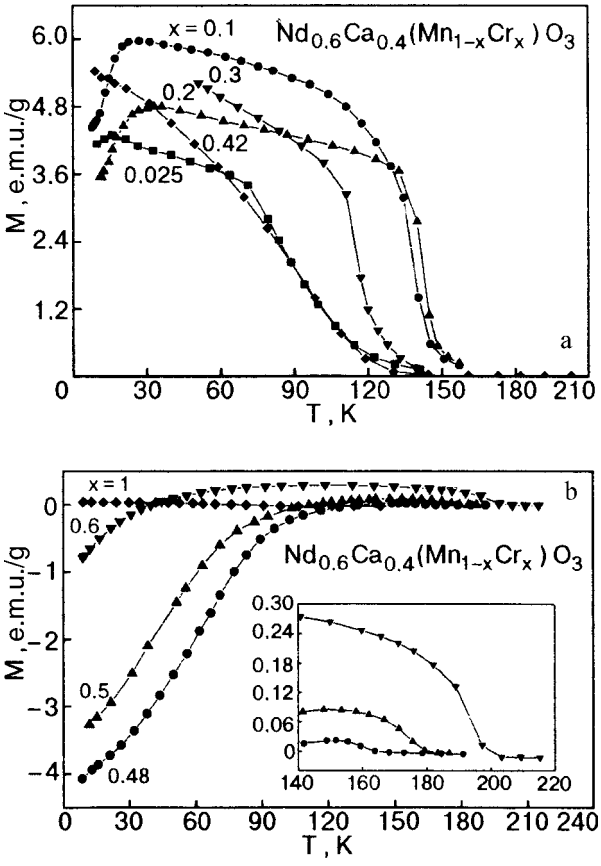

FIG. 2. Temperature dependence of the FC magnetization in a magnetic field $H=100$ Oe for samples with $x\leqslant 0.42$ (a) and in the concentration interval $0.48\leqslant x\leqslant 1$ (b).

be due to frustrations of the exchange interactions, since the measurements were made after cooling in a magnetic field. The anomalous behavior of the magnetization at low temperatures can only be due to negative polarization of the neodymium sublattice or to an orientational phase transition brought on by a change in anisotropy. An argument in favor of the latter cause is that the samples with $x=0.04$ and $x=0.42$ did not show anomalous behavior of the FC magnetization in the low-temperature region.

At concentrations near $x=0.48$ the temperature of the transition to the paramagnetic state increases sharply (Fig. 2). The transition to the paramagnetic state is quite rapid, as is typical for homogeneous magnets. It follows from the measured $M(H)$ curves at different temperatures that the spontaneous magnetization does not exceed 5 e.m.u./g. Such a value of the spontaneous magnetization is typical for rare-earth orthochromites $RCrO_3$, in which the weak ferromagnetism is due to the Dzyaloshinskii–Moriya interaction.[10]

However, the anomalous behavior of the magnetic properties at chromium concentrations near $x=0.5$ is apparently due to a different cause. We made careful x-ray structural studies of samples with $x=0.48$ and $x=0.6$. These revealed two superstructural reflections of low intensity, which can be interpreted as being the result of ordering of the manganese and chromium ions in a checkerboard pattern. In this type of ordering each chromium ion prefers a surrounding of manganese ions. We assume that the tendency toward ordering of the manganese and chromium ions is the cause of the anomalous behavior of the magnetic properties in samples with $x\geqslant 0.48$.

At a temperature T_C the spontaneous magnetization goes to zero. Compensation of the magnetic moment in rare-earth magnets is ordinarily due to a competition between the contributions from $3d$ and $4f$ ions. This is apparently true for the sample with $x=0.48$ as well. The magnetization compensation temperature decreases with increasing chromium concentration. Figure 3 shows the results of a study of the magnetization of samples with $x=1$ in a magnetic field $H=100$ Oe. The curves do not exhibit any sharp anomalies that could be due to a magnetic phase transformation. The zero-field-cooled (ZFC) and FC magnetization diverge smoothly, as is typical of inhomogeneous spin glasses. The

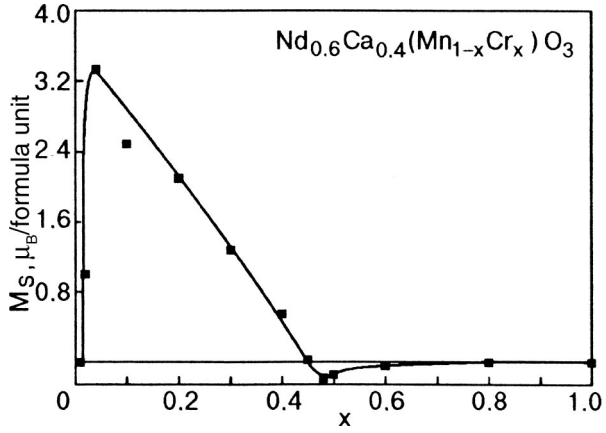

FIG. 4. Concentration dependence of the spontaneous magnetization in the system $Nd_{0.6}Ca_{0.4}(Mn_{1-x}Cr_x)O_3$.

magnetic moments are gradually blocked in the random anisotropy fields. At a temperature $T \sim 40$ K the blocking process is sharply enhanced. Figure 4 shows the magnetic phase diagram of the system $Nd_{0.6}Ca_{0.4}(Mn_{1-x}Cr_x)O_3$. The base compound $Nd_{0.6}Ca_{0.4}MnO_3$ is an antiferromagnet with a Néel temperature of 160 K.[10] The Mn^{3+} and Mn^{4+} ions order at a temperature of 240 K.[10] Samples with $0.015 \leqslant x \leqslant 0.04$ are most likely found in a mixed magnetic state in which antiferromagnetic and magnetic domains coexist. Samples with $0.04 < x < 0.4$ are found in a ferrimagnetic state characterized by antiparallel ordering of the manganese and chromium ions. In samples with $0.1 < x < 0.3$ at low temperatures there is possibly a spin reorientation due to a change of the axis of easy magnetization. Samples with $0.48 \leqslant x \leqslant 0.8$ are ferrimagnets in which the magnetic moment of the neodymium sublattice is directed antiparallel to the moment due to the $3d$ ions. It should be noted that a metal–insulator transition near T_C is observed only in a narrow concentration interval $0.02 \leqslant x \leqslant 0.07$. The other samples all remain insulating as the temperature is lowered.

The magnetic properties of manganites are usually explained by a competition of the positive exchange interactions arising as a result of ''dual exchange'' and the negative superexchange interactions via oxygen. However, as was shown by Goodenough,[12] the Mn^{3+}–O–Mn^{3+} and Mn^{3+}–O–Mn^{4+} interactions should be ferromagnetic even

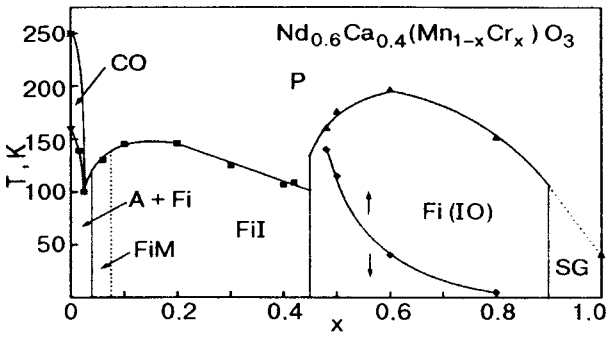

FIG. 5. Magnetic phase diagram of the $Nd_{0.6}Ca_{0.4}(Mn_{1-x}Cr_x)O_3$ system: CO — charge-ordered phase, P — paramagnetic, A — antiferromagnetic, FiM — ferrimagnetic metal, FiI — ferrimagnetic insulator, Fi(IO) — ferrimagnetic insulator with ordering of the Cr^{3+} and Mn^{4+} ions; SG — cluster spin glass.

in the superexchange model if the orbital ordering is lifted. This assumption agrees with the insulator behavior of samples with $0.07 < x \leqslant 0.42$. The highest Curie point T_C in manganites is not over 370 K. This temperature characterizes the positive Mn^{3+}–Mn^{4+} exchange interaction. Spectroscopic studies show that the chromium ions enter the lattice of manganites in the trivalent state.[13] The Mn^{4+} and Cr^{3+} ions each have three unpaired t_{2g} electrons. The negative exchange interactions are Mn^{4+}–Mn^{4+}, Mn^{3+}–Cr^{3+}, Cr^{3+}–Cr^{3+}, and Cr^{3+}–Mn^{4+}. The strength of the Cr^{3+}–Cr^{3+} and Mn^{4+}–Mn^{4+} exchange interactions can be judged from the Néel points of $LaCrO_3$ (300 K)[11] and $Sr_{0.5}Ca_{0.5}MnO_3$ (250 K).[14] Apparently the same value of the energy interactions can be expected in the case of the isoelectronic $3d$ ions Cr^{3+} and Mn^{4+}. Therefore, one can assume that the positive and negative exchange interactions are comparable in strength. If all of the nearest neighbors of a chromium ion are manganese ions, then the magnetic moments of the chromium are directed counter to the magnetic moments of manganese. Since the magnetic structure of $Nd_{0.6}Ca_{0.4}MnO_3$ is of the CE type, small admixtures of chromium should effectively destroy the antiferromagnetic state in manganites. The destruction of the antiferromagnetic state should be accompanied by destruction of the orbital and charge orderings on account of the rigid coupling between the orbital and spin degrees of freedom. In the case when two chromium ions are nearest neighbors, frustrations of the exchange interactions can arise, which are characteristic of a state of the spin glass type. It should be noted that with increasing chromium content the fraction of Mn^{4+} ions increases sharply. For example, for samples with $x = 0.6$ the nominal chemical formula is $Nd_{0.6}C_{0.4}(Mn^{4+}_{0.4}Cr^{3+}_{0.6})O_3$, i.e., there are no Mn^{3+} ions. The ordering of the Cr^{3+} and Mn^{4+} ions should lead to a sharp increase in the role of the antiferromagnetic interactions. In the case of an ideal checkerboard order (NaCl type) of the system in respect to the arrangement of the Cr^{3+} and Mn^{4+} ions for samples with $x = 0.5$, the exchange interaction between chromium and manganese becomes dominant, while the frustrations of the exchange interactions will be minimal. Apparently the tendency toward ordering of the chromium and manganese ions is more pronounced in compounds where the tetravalent manganese is larger and the distortion of the unit cell is stronger. Samples of $Nd_{0.6}Ca_{0.4}CrO_3$ are characterized by properties inherent to cluster systems (Fig. 4), while it is known that $NdCrO_3$ is a weak ferromagnet with a Néel temperature of around 200 K. This means that the exchange interaction between chromium ions of different valence is a strong ferromagnetic interaction, as is observed in the case of Mn^{3+}–Mn^{4+}. It should be noted that further neutron-diffraction studies are needed for a more precise determination of the magnetic ground state of $Nd_{0.6}Ca_{0.4}Mn^{3+}_{0.4}Cr^{4+}_{0.6}O_3$.

Thus the properties of the system $Nd_{0.6}Ca_{0.4}(Mn_{1-x}Cr_x)O_3$ can be obtained in a superexchange interaction model, assuming that the Cr^{3+}–O–Cr^{3+} and Cr^{3+}–O–Mn^{4+} magnetic interactions are negative and comparable in strength.

This study was done with the support of the Foundation for Basic Research of the Republic of Belarus (Project F99R-038).

*E-mail: sirenko@ilt.kharkov.ua

[1] J. Blasco, J. García, J. M. de Teresa, M. R. Ibarra, J. Pérez, P. A. Algarabel, and C. Marquina, Phys. Rev. B **55**, 8905 (1997).
[2] M. Rubinstein, D. J. Gillespie, J.W. Snyder, and T. M. Tritt, Phys. Rev. B **56**, 5412 (1997).
[3] K. Ghosh, S. B. Ogale, R. Ramesh, R. L. Greene, T. Venkatesan, K. M. Gapshup, R. S. Bathe, and S. I. Patil, Phys. Rev. B **59**, 533 (1999).
[4] I. O. Troyanchuk, L. S. Lobanovsky, D. D. Khalyavin, S. N. Pastushonok, and H. Szymczak, J. Magn. Magn. Mater. **210**, 63 (2000).
[5] C. N. R. Rao, A. Arlurraj, P. N. Santosh, and A. K. Chettham, Chem. Mater. **10**, 2714 (1998).
[6] B. Raveau, A. Maignan, C. Martin, and M. Hervieu, Chem. Mater. **10**, 2641 (1998).
[7] P. V. Vanitha, R. S. Singh, S. Natarajan, and C. N. R. Rao, Solid State Commun. **199**, 135 (1999).
[8] Young Sun, Wei Tong, Xiaojun Xu, and Yuheng Zhang, Phys. Rev. B **63**, 17443 (2001).
[9] T. Kimura, R. Kumai, Y. Okimoto, Y. Tomioka, and Y. Tokura, Phys. Rev. B **62**, 15021 (2000).
[10] M. Tokunaga, N. Miura, Y. Tomioka, and Y. Tokura, Phys. Rev. B **57**, 5259 (1998).
[11] A. K. Zvezdin, V. M. Matveev, A. A. Mukhin, and A. I. Popov, *Rare-Earth Ions in Magnetically Ordered Crystals* [in Russian], GFML, Moscow (1985).
[12] J. B. Goodenough, *Magnetism and the Chemical Bond*, Interscience, New York (1963); Metallurgiya, Moscow (1968).
[13] A. Barnabe, M. Hervieu, C. Martin, A. Maignan, and B. Raveau, J. Mater. Chem. **8**, 1405 (1998).
[14] I. O. Troyanchuk, N. V. Samsonenko, H. Szymczak, and A. Nabialek, Solid State Chem. **131**, 144 (1997).

Translated by Steve Torstveit

QUANTUM EFFECTS IN SEMICONDUCTORS AND DIELECTRICS

EPR spectrum of the Fe^{3+} ion in bromcresol green ($C_{21}H_{14}Br_4O_5S$) and features in the dynamics of the surrounding molecules

V. V. Chabanenko[1)] and V. N. Vasyukov

A. A. Galkin Physicotechnical Institute, National Academy of Sciences of Ukraine, ul. R. Lyuksemburg 72, 83114 Donetsk, Ukraine

R. O. Kochkanjan and M. M. Nechitailov

L. M. Litvinenko Institute of Physics and Organic Chemistry and Carbon Chemistry, ul. R. Lyuksemburg 70, 83114 Donetsk, Ukraine

H. Szymczak, S. Piechota, and A. Nabialek

Institute of Physics, Polish Academy of Sciences, al. Lotnikow 32/46, 02-668 Warsaw, Poland
(Submitted April 9, 2001; revised September 18, 2001)
Fiz. Nizk. Temp. **28**, 66–72 (January 2002)

The EPR spectrum of an Fe^{3+} impurity in the organic substance bromcresol green ($C_{21}H_{14}Br_4O_5S$) is investigated in the temperature interval 4.2–295 K. At a temperature of 4.2 K the spectrum is a superposition of two lines with effective g factors $g_1=4.39$ and $g_2=2.03$. As the temperature is lowered a redistribution of the intensity between line occurs. The integral intensity of the first line decreases with increasing temperature, while that of the second line increases. Another feature of the temperature dependence of the EPR spectrum of the Fe^{3+} ion in $C_{21}H_{14}Br_4O_5S$ is manifested in the exponential growth of the width of the second resonance line with decreasing temperature. The observed properties of the EPR spectrum in $C_{21}H_{14}Br_4O_5S$ are typical for systems with a multiwell potential and permit one to characterize the dynamics of the molecules of the environment of the magnetic ion. © *2002 American Institute of Physics.* [DOI: 10.1063/1.1449185]

Unusual temperature dependence of the EPR spectrum of the Fe^{3+} ion in the metalorganic substance $Na[FeO_6(C_{10}H_8N_3)]$ and polyaniline was observed in Refs. 1 and 2. In these substances the EPR spectrum is a superposition of two lines. With decreasing temperature the intensity of one of them increases and the other decreases, so that one line is more strongly expressed in the region of low (helium) temperatures and the other at room temperature. The first line is called the low-temperature (LT) component of the spectrum of the substance, and the second, the high-temperature (HT) component.[1,2] Changing the temperature leads to a redistribution of the intensity of the absorption between the LT and HT components of the spectrum. This sort of behavior of the EPR spectrum is indicative of unusual dynamics of the molecules surrounding the Fe^{3+} ion, and that can have a considerable influence on the various properties of the substance.

In addition, we note that the study of such dynamic transitions is of independent value, since systems that exhibit the given properties as a rule are systems with a multiwell potential. Such systems have not yet been completely studied. They can be of different physical natures, but a common property they share is motion in a potential well with several minima separated by potential barriers. The most studied system of this type is the Jahn–Teller ion of divalent copper in an octahedral environment.[3]

The features in the EPR spectrum for a system with a many-well potential are: (1) the presence of LT and HT components of the EPR spectrum; (2) a redistribution of intensity between the LT and HT spectra as the temperature is changed.

For the Fe^{3+} ion the Jahn–Teller effect does not appear. The cause of the temperature transition in the EPR spectrum is due, according to Refs. 1 and 2, to features of the spectrum of the magnetic centers and is determined by the dynamics of the molecules surrounding the magnetic ion. In Refs. 1 and 2 the structure of the magnetic centers was not determined completely enough. This makes it difficult to construct a model describing the behavior of the magnetic centers. To ascertain the salient properties of the magnetic centers it is necessary to study these centers in different molecular substances. In this paper we investigate the EPR spectrum of magnetic centers in $C_{21}H_{14}Br_4O_5S$.

A study of the temperature dependence of the EPR spectrum of impurity Fe^{3+} in $C_{21}H_{14}Br_4O_5S$ is of interest in connection with the manifestation of a temperature-induced transition from the low-temperature distorted state of the magnetic center to a high-temperature symmetric state and the possibility of characterizing the features of the dynamics of the nearest-neighbor environment of the Fe^{3+} ion in $C_{21}H_{14}Br_4O_5S$ in more detail.

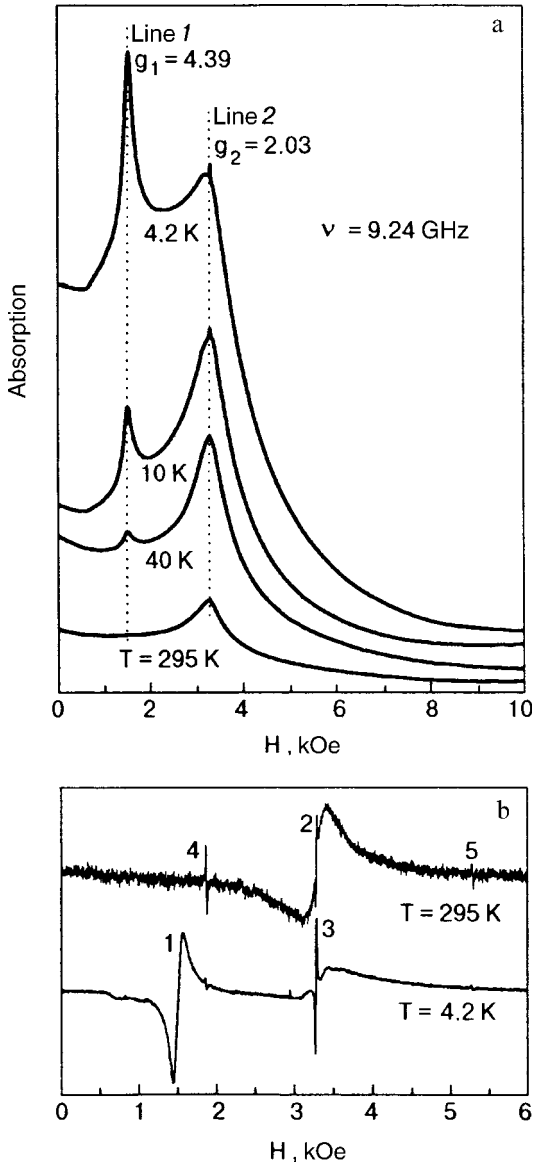

FIG. 1. The EPR spectrum of the Fe^{3+} ion in $C_{21}H_{14}Br_4O_5S$: the absorption line shapes for temperatures $T=4.2$, 10, 40, and 295 K (a); the derivatives of the absorption lines for $T=4.2$ and 295 K (b). Lines *3*, *4*, and *5* were applied for calibration of the magnetic field.

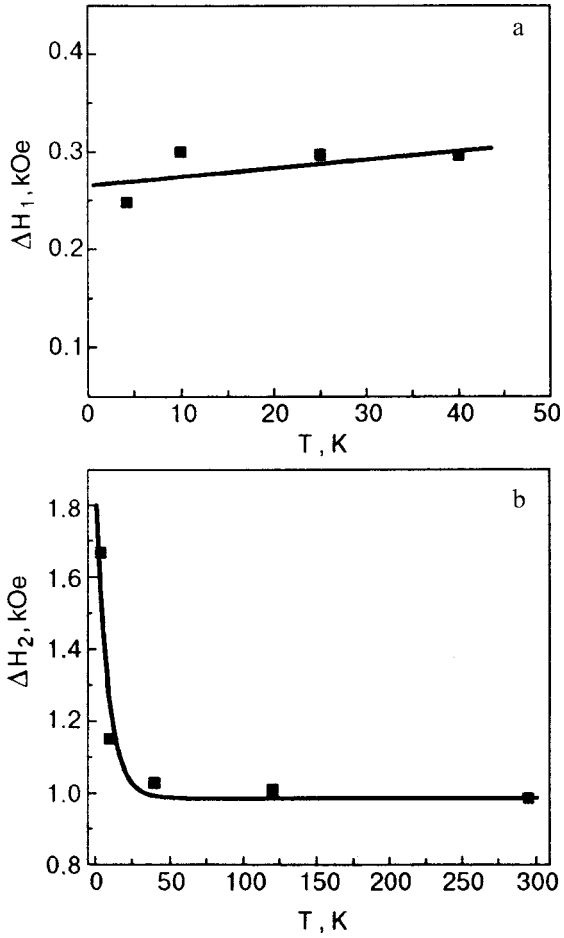

FIG. 2. Temperature dependence of the linewidths (widths at half height) for lines *1* (a) and *2* (b).

2. EXPERIMENTAL RESULTS

The EPR spectrum was studied on a spectrometer with a frequency of the microwave field $\nu=(9.242\pm0.001)$ GHz in the temperature interval $T=4.2$–295 K.

Figure 1 shows the absorption lines at temperatures of 4.2, 10, 40, and 295 K and their derivatives at room and helium temperatures. The absorption lines [Fig. 1a] were obtained by numerical integration of the experimentally recorded lines [Fig. 1b]. It follows from the data that the EPR spectrum of $C_{21}H_{14}Br_4O_5S$ at $T=4.2$ K is a superposition of two resonance lines. The value of the g factor of line *1* is $g_1=4.39\pm0.03$. The second line is described by a g factor $g_2=2.08$. Lowering the temperature leads to a redistribution of the intensities of the lines so that only resonance line *2* remains at 295 K. At this temperature it has a g factor $g_2=2.03\pm0.02$ and a width $\Delta H_{pp}=0.31$ kOe.

The three narrow ($\Delta H_{pp}\approx15$ Oe) resonance lines *3*, *4*, and *5* of the EPR spectrum in Fig. 1b were used for calibration of the magnetic field and belong to magnetic centers that are not incorporated in the structure of the substance under study.

The g factors of resonance lines *1* and *2* of the spectrum remain practically unchanged with temperature (Fig. 1). Analysis of the behavior of the temperature dependence of the intensities of the two lines reveals changes which are unusual for a spin–lattice relaxation mechanism. For example, the intensity of the resonance line *1* decreases with increasing temperature and has vanished completely at $T=295$ K. At the same time, the intensity of line *2* increases with temperature. The width of line *1* increases slightly with increasing temperature [Fig. 2a].

For a quantitative analysis of the observed features [Fig. 1a] the observed absorption spectra were decomposed into components throughout the temperature range investigated. The results of this decomposition for the two extreme values of the temperature, 4.2 and 295 K, are shown in Fig. 3. One can discern two resonance lines *1* and *2* and a nonresonant ''background.'' The intensity of the ''background'' and of the resonance lines *1* and *2* and the shape of these lines were calculated under the condition of minimum deviation of the experimental resultant absorption line (the dashed curve) from the theoretically calculated model absorption line.

The usual broadening mechanism for a line of the EPR spectrum, involving spin–lattice relaxation processes, leads to an increasing linewidth and a decreasing peak intensity

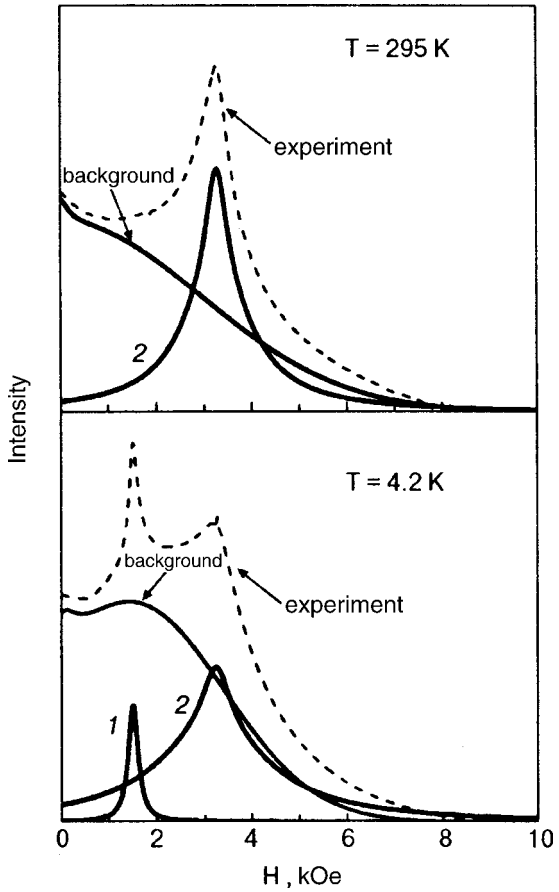

FIG. 3. Decomposition of the resultant absorption line of the EPR spectrum of the Fe^{3+} ion in $C_{21}H_{14}Br_4O_5S$ (– – –) for the components of resonance lines *1* and *2* and the nonresonant "background."

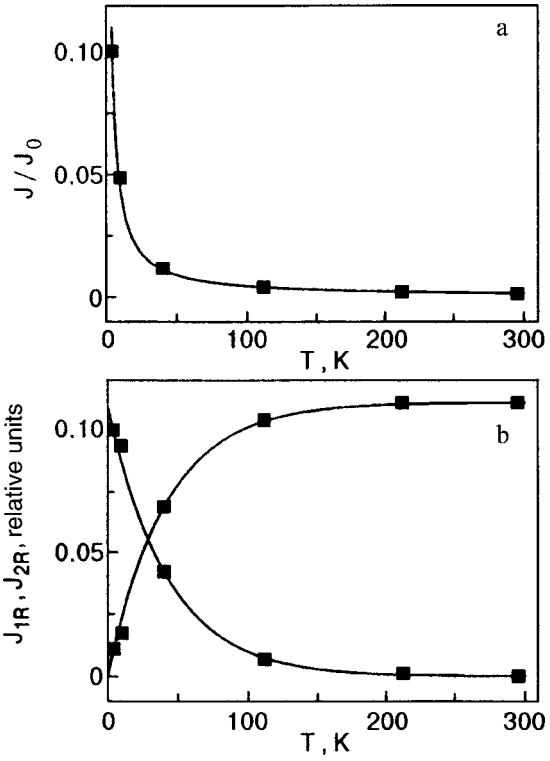

FIG. 4. Temperature dependence of the total intensity $J(T)/J_0 = \tanh(h\nu/2kT)$ of lines *1* and *2* (a) and the relative integrated intensities of lines *1* (J_{1R}) and *2* (J_{2R}) (b); ■—experiment, $J_{1R}=J_1/(J_1+J_2)$; $J_{2R}=J_2/(J_1+J_2)-0.889$.

with increasing temperature. The observed behavior of line *1* of the spectrum [a slight ($\approx$17%) broadening as the temperature is lowered] is evidence that the change of its intensity is not due to the ordinary relaxation mechanism of resonance line broadening.

To explain the observed features of the absorption in this substance we consider a model in which the temperature dependence of the EPR spectrum of the Fe^{3+} ion in $C_{21}H_{14}Br_4O_5S$ can be described by two mechanisms. The first mechanism leads to the usual decreasing of the integral intensity of all the contributions to the resultant absorption line with increasing temperature and is governed by the temperature dependence of the population difference of the resonant states. The temperature dependence of the total integral intensity of the absorption line of the Fe^{3+} ion is presented in Fig. 4a. The intensity represented by the solid curve is described by a function $J(T)=J_0\tanh(h\nu/2kT)$.

The second mechanism of temperature dependence of the EPR spectrum of the Fe^{3+} ion in $C_{21}H_{14}Br_4O_5S$ is due to a process of redistribution of the integral intensity between lines *1* and *2* [see Fig. 4b]. The curves in the figure show the temperature dependence of the relative integrated intensities of the first J_{1R} and second J_{2R} lines: $J_{1R}=J_1/(J_1+J_2)$, $J_{2R}=J_2/(J_1+J_2)-0.889$. These functions can be approximated by the following relations:

$$J_{1R}=0.11(1-e^{-E_0/kT}), \quad J_{2R}=0.11e^{-E_0/kT}, \tag{1}$$

where k is Boltzmann's constant, and $E=15$ cm^{-1} is the effective activation energy.

Besides the above-mentioned features of the temperature distribution of the intensities of the resonance lines *1* and *2*, the EPR spectrum of the Fe^{3+} ion in $C_{21}H_{14}Br_4O_5S$ shows an unusual change in the width of line *2*. This dependence [shown in Fig. 2b] is obtained as a result of a numerical decomposition of the resultant absorption line into components. We see that the width of line *2* at half height increases exponentially with decreasing temperature. The temperature dependence of ΔH_2 can be approximated by the relation

$$\Delta H_2=0.986+0.498e^{-(T-5)/8.14}, \tag{2}$$

(the solid curve in Fig. 2b).

The unusual behavior of the intensity of resonance line *1* and of the width of resonance line *2* of the EPR spectrum suggests that lines *1* and *2* are interrelated. At high temperatures one observes only line *2*, and it can therefore be called the "high-temperature" spectrum of the magnetic centers of the Fe^{3+} ion in $C_{21}H_{14}Br_4O_5S$. Resonance line *1* appears as the temperature is lowered and reaches its highest intensity at $T=4.2$ K; it can therefore be called the "low-temperature" EPR spectrum.

3. DISCUSSION OF THE RESULTS

The EPR spectrum investigated in this paper consists of two resonance lines (Fig. 1). One line has an effective g factor $g_1\approx4.3$, and the other $g_2\approx2$. EPR lines with these g factors are characteristic for Fe^{3+} ions in a polycrystalline material.

1. The resonance line with g_2 is typical for many magnetic centers, among them the Fe^{3+} ion. Line *1* with g_1, unlike the case of line *2* with g_2, is characteristic only for ions with spin $S=5/2$. For example, a resonance line with $g=4.3$ has been observed in a number of studies[4–6] of the EPR spectrum of the iron ion in silicate glasses, which, like the polycrystalline sample studied here, have no long-range order. A detailed analysis of the results of a study of the EPR spectrum of iron ions in amorphous substances is given in Ref. 7. In that paper it is shown that the spectrum consisting of two resonance lines with $g\approx 2$ and $g\approx 4.3$ belong to the Fe^{3+} ion. The authors of Ref. 7 also assume that the resonance lines with the given g factors can be assigned to different magnetic centers that differ in the value of the low-symmetry component of the crystalline field acting on the magnetic ion. The line with $g\approx 2$ corresponds to a center at which the low-symmetry component of the crystalline field is much less than the Zeeman energy. The line with $g\approx 4.3$ corresponds to a center at which the low-symmetry component of the crystalline field is much larger than the Zeeman energy.

2. The transition from the low-temperature to the high-temperature form of the spectrum does not occur abruptly, but gradually [Figs. 1a and 4b]. Therefore structural phase transitions cannot be responsible for this change of the intensity of the EPR spectrum with temperature.

It should be noted that the temperature-related changes shown in Fig. 1 cannot be due to temperature dependence of the parameters D and E of the initial splitting.[2] In that case the spectrum would consist of a single resonance line which would coincide with line *1* at low temperatures and would go over smoothly to line *2* as the temperature was raised.

In the usual situation the intensity of an EPR resonance line is proportional to the number of magnetic ions for the given transition. The observed redistribution of the intensities of lines *1* and *2* [Figs. 1a and 4b] is indicative of a change of the number of magnetic ions corresponding to the different centers.

Analysis of the temperature dependence of the EPR spectrum shown in Figs. 1 and 4 and the results of Ref. 7 lead one to the conclusion that, at least for some of the magnetic centers, the low-symmetry component of the crystalline field acting on the Fe^{3+} ion in $C_{21}H_{14}Br_4O_5S$ is much larger than the Zeeman energy at low temperatures and much smaller than the Zeeman energy at high temperatures.

It is apparently more correct to interpret the described changes in the EPR spectrum with temperature not as the motion of the Fe^{3+} ions from one inequivalent position to another but as the transition of the magnetic center from one state to another.

3. It should be emphasized that the magnetic centers under study have a number of peculiar properties: (a) the existence of a low-temperature, low-symmetry and a high-temperature, high-symmetry state of the magnetic centers; (b) the presence of a temperature region in which the EPR spectrum of both states is observed; (c) a decrease of the intensity of the low-temperature component of the spectrum and an increase of the intensity of the high-temperature component with increasing temperature.

The described characteristic behavior of the magnetic centers is inherent to systems with multiwell potentials. The most-studied system with a multiwell potential is the Jahn–Teller ion of divalent copper in an octahedral crystalline environment. The temperature-induced changes in the intensity of the spectra corresponding to the low- and high-symmetry states for such systems is usually described with the aid of the ''dynamic averaging'' model.[8] According to that model, the spectrum and deformation are averaged as a result of rapid ''hops'' of the system from one potential well to another. This mechanism of dynamic averaging of the deformations has been described in many papers.

The fact that the temperature-related changes in the EPR spectrum of the Fe^{3+} ion in $C_{21}H_{14}Br_4O_5S$ agree with the analogous changes of the EPR spectrum of a well-studied system with a multiwell potential suggests that the molecules surrounding the Fe^{3+} ion in $C_{21}H_{14}Br_4O_5S$ have several energy-equivalent deformations corresponding to low symmetry of the environment of the Fe^{3+} ion. In that case the unusual temperature dependence of the spectrum is due to a feature of the dynamics of the molecules surrounding the Fe^{3+} ion.

It should be noted here that Fe^{3+} is an S ion and, according to the usual concepts, the appearance of the Jahn–Teller effect is improbable for this ion. However, it is possible that a multiwell system exists in $C_{21}H_{14}Br_4O_5S$. The nature of this system is apparently analogous to that described in Ref. 9 and observed in the EPR spectrum of the Fe^{3+} ion in polyparaphenylene. According to Ref. 9, the Fe^{3+} ion has a stationary position between two aromatic fragments of neighboring polyparaphenylene molecules. A calculation[9] of the energy of the magnetic center shows that at a certain value of the distance between aromatic fragments the stationary position of the Fe^{3+} ion does not lie at the center but is displaced toward one of the fragments. If the aromatic fragments are equivalent, then the magnetic ion has two stationary positions separated by a potential barrier.

In the framework of a system with a multiwell potential one can explain the unusual temperature dependence of the intensity of the resonance line *1* (Fig. 1) of the EPR spectrum, the unusual behavior of the width of resonance line *2* [Fig. 2b], and a number of other features of the temperature dependence of the spectrum. The physical picture of the phenomena that occur here is as follows.

At helium temperature the surrounding molecules are ''frozen'' at the bottoms of the potential wells corresponding to the largest value of the low-symmetry component of the crystalline field. Here the anisotropy of the electric field is maximum and one therefore observes resonance line *1*. As the temperature is raised, some of the magnetic centers go into excited vibronic states. The excited states of systems with a multiwell potential are, as a rule, less anisotropic than the ground state.[3] Above-barrier states (states whose energy is higher than the height of the barrier separating the potential wells)[3] are the least anisotropic. Occupation of the above-barrier states increases the contribution to resonance line *2* of the EPR spectrum [Figs. 1a and 4b]. Increasing the number of magnetic centers found in the excited state leads to a decrease in the number of magnetic centers in the ground state. This circumstance is the cause of the decrease

of the intensity of resonance line *1* with increasing temperature [see Figs. 1a and 4b].

The unusual temperature dependence of the width of resonance line *2* [Fig. 2b] is due to the distribution of magnetic centers over excited states. The higher the energy of the excited state, the less the magnetic ion feels the low-symmetry electric field. If the energy of excitation is greater than the height of the barrier between potential wells (above-barrier states), the influence of this component becomes minimal or zero.

At high temperatures a large fraction of the magnetic centers are found in the above-barrier states. The EPR spectrum of these centers is determined by the g factor of the transition $+1/2 \leftrightarrow -1/2$. The value of the g factor of the resonance line corresponding to this transition is close to the value $g=2.0$. Here the linewidth due to the contribution from this transition is small, amounting to $\Delta H_2 = 0.986$ kOe [see Fig. 2b].

At low temperatures an appreciable fraction of the magnetic centers are found in above-barrier excited states. The lower the excitation energy, the larger in the influence of the low-symmetry component of the electric field and the farther the resonance lines of the transitions $\pm 5/2 \leftrightarrow \pm 3/2$ lie from the line of the transition $+1/2 \leftrightarrow -1/2$. As a result of the orientational averaging over directions of the symmetry axes, the contribution of the transitions $\pm 5/2 \leftrightarrow \pm 3/2$ and $\pm 3/2 \leftrightarrow \pm 1/2$ in the low-temperature region will lead to broadening of resonance line *2*. The lower the temperature, the larger the contribution to line *2* from below-barrier excited states in comparison with the above-barrier states. This is the reason for the broadening of resonance line *2* with decreasing temperature.

It should be noted that the mechanism described above for the temperature-related changes in the EPR spectrum should, in pure form, lead to the complete vanishing of line *2* at low temperatures. Such a change was observed in Ref. 1. A similar redistribution of the energy is observed in $C_{21}H_{14}Br_4O_5S$. However, even at $T=4.2$ K line *2* still has significant intensity. This is apparently due to the presence of a static distribution of deformations of the molecular environment of the magnetic ion, which, as in Ref. 9, leads to the appearance of two types of magnetic centers: a symmetric center, which contributes to line *2*, and an asymmetric center, which manifests the properties of a multiwell system.

4. CONCLUSION

Studies of the microwave absorption resonance lines of impurity Fe^{3+} in bromcresol green have made it possible to characterize the dynamics of the molecules of this substance. We have shown that in the framework of the proposed model of dynamic transitions one can explain the temperature dependence of the EPR spectra of a number of molecular substances having in common the presence of physical systems with multiwell potentials.

[1)]E-mail: chaban@host.dipt.donetsk.ua

[1] V. P. D'yakonov, V. N. Vasyukov, V. A. Shapovalov, E. I. Aksiment'eva, G. Shimchak, and S. Pekhota, Fiz. Tekh. Vysokikh Davlenii **8**, 60 (1998).
[2] V. N. Vasyukov, V. P. D'yakonov, V. Shapovalov, E. I. Aksiment'eva, and H. Szymczak, S. Piehota, Fiz. Nizk. Temp. **26**, 363 (2000) [Low Temp. Phys. **26**, 265 (2000)].
[3] V. N. Vasyukov and B. Ya. Sukharevskiĭ, Fiz. Nizk. Temp. **20**, 821 (1994) [Low Temp. Phys. **20**, 644 (1994)].
[4] T. Castner, G. S. Newell, W. C. Holton, and C. P. Slechter, J. Chem. Phys. **32**, 668 (1960).
[5] E. Burzo, M. Chipara, D. Ungur, and I. Ardelean, Phys. Status Solidi B **124**, K117 (1984).
[6] R. Sing, J. Phys. D: Appl. Phys. **17**, 157 (1984).
[7] Ya. G. Klyava, *EPR Spectroscopy of Disordered Solids* [in Russian], Znanie, Riga (1988).
[8] A. Abragam and B. Bleaney, *Electron Paramagnetic Resonance of Transition Ions*, Vol. 2 [Clarendon Press, Oxford (1970); Mir, Moscow (1973)].
[9] V. N. Vasyukov, V. A. Shapovalov, V. P. Dyakonov, A. F. Dmitruk, E. I. Aksimentjeva, H. Szymczak, and S. Piechota, "Investigation of structure of Fe^{3+} magnetic center in polyparaphenylene" [in English], *Third V. A. Fock All-Russia School–Seminar on Quantum and Computational Chemistry* [title in Russian], V. Novgorod, May 21–25, 2001, p. 39.

Translated by Steve Torstveit

Interaction of Pr^{3+} optical centers in the Y_2SiO_5 crystal

Yu. V. Malyukin,[1)] P. N. Zhmurin, A. N. Lebedenko, M. A. Sholkina, and B. V. Grinev

Institute of Single Crystals, National Academy of Sciences of Ukraine, pr. Lenina 60, 61001 Kharkov, Ukraine

N. V. Znamenskiĭ, É. A. Manykin, Yu. V. Orlov, E. A. Petrenko, and T. G. Yukina

Kurchatov Institute Russian Research Center, pl. Kurchatova 1, 123182 Moscow, Russia

(Submitted September 6, 2001)
Fiz. Nizk. Temp. **28**, 73–78 (January 2002)

It is shown on the basis of studies of the optical spectra and luminescence decay of nonequivalent Pr^{3+} optical centers in the Y_2SiO_5 crystal that the occupation of the nonequivalent cation sites of the crystal lattice by the activator ions is irregular. For excitation in the region of the optical transitions $^3H_4 \rightarrow {}^1D_2$in the temperature interval 6–80 K there is no transfer of electronic excitation energy between Pr^{3+} ions localized in different cation sites. The luminescence decay law of the Pr^{3+} optical centers is determined by the concentration of activator ions and has a complicated non-single-exponential character; the quenching of the luminescence of the Pr^{3+} ions is due to the formation of dimers of these ions. © *2002 American Institute of Physics.* [DOI: 10.1063/1.1449186]

1. INTRODUCTION

Intensive investigation of the optical and luminescent properties of oxyorthosilicate crystals activated by rare-earth (RE) ions is motivated by the search for new materials for laser, display, and scintillation devices.[1–7] In oxyorthosilicate crystals the RE impurity ions form nonequivalent optical centers. It is of topical interest to elucidate the possible mechanisms of interaction between them.

The unit cell of Y_2SiO_5 (YSO) contains two nonequivalent Y^{3+} cation sites with a different coordination environment.[3,8] Therefore, Pr^{3+} ions in the YSO crystal form two optical centers, which we shall call optical centers of type I and type II.[9–11] This raises two important questions having both applied and fundamental aspects. First, how do the Pr^{3+} ions occupy the nonequivalent cation sites of YSO? Second, is there an interaction between the Pr^{3+} impurity ions found in different cation sites?

Both the first and second questions have been partially discussed in Refs. 11 and 12. However, a more detailed experimental study of these questions by the technique of selective excitation of the nonequivalent Pr^{3+} optical centers is presented here for the first time. For example, in Ref. 11 it was concluded on the basis of an analysis of the variation of the integrated intensity of the spectral lines of the two optical centers that the occupation of the nonequivalent cation sites of YSO by Pr^{3+} ions is irregular. This conclusion requires further quantitative refinement: it is necessary to elucidate how the average distance between Pr^{3+} optical centers changes as the concentration of activator ions in the YSO crystal is increased.

In the YSO crystal under selective excitation of the Pr^{3+} optical centers of type I in the region of the resonance transition $^3H_4 \rightarrow {}^3P_0$ the luminescence spectrum corresponding to optical transitions $^1D_2 \rightarrow {}^3H_4$ from the metastable level of the $^1D_2$ term contains spectral lines belonging to Pr^{3+} optical center of type II.[12] The concentration of activator ions in that case was 0.1 at. %. The spectral features and the presence of an ascending part of the experimental luminescence decay curve of the type-II Pr^{3+} optical centers (see Fig. 3 in Ref. 12) attest to the transfer of electronic excitation energy between nonequivalent Pr^{3+} optical centers.[12] This observation has not been given the necessary explanation.

We note that the transfer of energy between nonequivalent RE-ion optical centers in crystals is intimately related to the important problem of creating intensely luminescing stoichiometric materials for microlasers.[13] In Ref. 13 an idea for obtaining intense luminescence of stoichiometric rare-earth ions, i.e., ions incorporated regularly in the crystal, was first set forth. The essence of this idea is that rare-earth ions incorporated regularly in a crystal lattice should be separated by extended isolating complexes in order to ensure a weak interaction between ions. Intense luminescence has been observed[13–17] in the crystals NdP_5O_{14}, $Nd_xLa_{1-x}P_5O_{14}$, $NdLiP_4O_{12}$, and $NdAl_3(BO_3)_4$. However, in some cases[18] the luminescence of stoichiometric RE ions is strongly quenched. This is due to the appearance of several optical centers in the crystal in spite of the fact that the RE ions are incorporated regularly in the crystal lattice. The exact microscopic nature of the multicenteredness in stoichiometric crystals is unclear and is probably due to the uncontrolled defect state of the crystal lattice. At the same time, in oxyorthosilicate crystals RE impurity ions form two distinct types of optical centers,[9–11] making it possible to study the basic regularities of the energy transfer in such systems.

To answer the above questions, in the present study we have for the first time used selective excitation of Pr^{3+} optical centers in the YSO crystal at the transition $^3H_4 \rightarrow {}^1D_2$ and measurement of the luminescence decay curves. In the analysis of the latter we have used the well-known relationships between the shape of the luminescence decay curves for impurity ions in the case of concentration quenching and migration of excitation energy.[19]

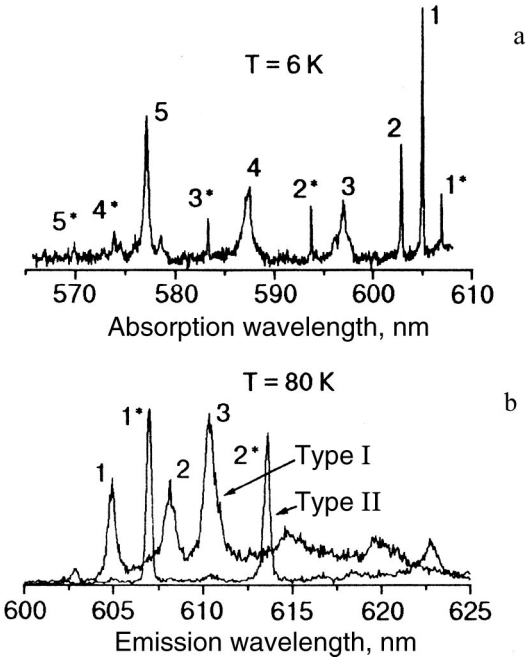

FIG. 1. Absorption spectra at the transition $^3H_4 \rightarrow {}^1D_2$(a) and luminescence spectra at the transition $^1D_2 \rightarrow {}^3H_4$ (b) for two types of Pr^{3+} optical centers in the YSO crystal. The spectral lines of the optical transitions of Pr^{3+} optical centers of type I are indicated by a number, and those for centers of type II by a number with an asterisk. The spectral lines 1 and 1* correspond to optical transitions between the lower Stark components of the terms $^3H_4$ and $^1D_2$ of the two Pr^{3+} optical centers.

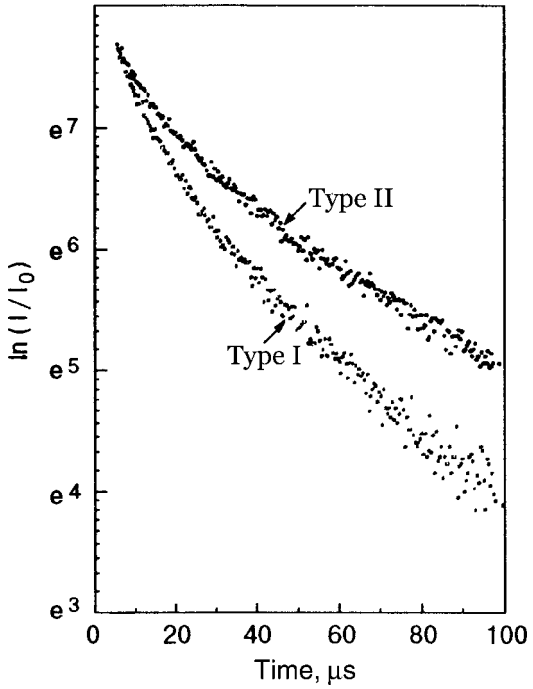

FIG. 2. Luminescence decay curves of two Pr^{3+} optical centers in the YSO crystal at $T = 80$ K. The luminescence decay curves were taken at the wavelengths of spectral lines 1 and 1* upon selective excitation of the nonequivalent Pr^{3+} optical centers.

EXPERIMENTAL RESULTS AND DISCUSSION

The experiments were done on the equipment described in detail in Refs. 9–11. For varying the temperature of the samples we used a temperature-regulated optical cryostat. The samples were in helium vapor. YSO:Pr^{3+} crystals with different concentrations of activator ions (0.3, 0.6, and 1.8 at. %) were grown by the Czochralski method.

The selective luminescence of nonequivalent Pr^{3+} optical centers in the YSO crystal was excited in the region of the optical transitions $^3H_4 \rightarrow {}^1D_2$(absorption lines of optical centers of type I are denoted by a number alone, and those for type II by a number with an asterisk) [Fig. 1a].[9–11] Using a frequency-tunable narrow-band laser ($\Delta\nu_{\mathrm{FWHM}} \sim 0.1$ cm^{-1}), we obtained the luminescence spectrum for each optical center (in the luminescence spectra of the optical centers of type I the spectral lines are denoted by a number alone, and those for type II by a number with an asterisk) [Fig. 1b]. The luminescence spectra did not change when the laser lines was tuned over the spectral lines of the $^1D_2$ multiplet for each optical center [Fig. 1a]. We note in particular that under selective excitation of one Pr^{3+} optical center in the YSO crystal at the transition $^3H_4 \rightarrow {}^1D_2$the luminescence spectrum of the second Pr^{3+} optical center was not observed at any concentration of activator ions nor at any temperature in the interval 6–80 K.

The luminescence decay of nonequivalent optical centers in a YSO:Pr^{3+} crystal with a minimum concentration of activator ions (0.3 at. %) was described by an exponential law.[11] In Fig. 2 we clearly see the deviation of the luminescence decay curves from an exponential law when the concentration of Pr^{3+} ions is raised above 0.3 at. %. The higher the concentration of impurity ions, the more strongly the luminescence decay curves of both optical centers deviate from an exponential law. For the crystal with the highest concentration of activator ions the luminescence decay of the two Pr^{3+} optical centers depends on temperature in the interval 6–80 K. In a crystal with an intermediate concentration of activator ions we observed a weak temperature dependence of the luminescence decay curves only for optical centers of the first type. As the temperature was varied in the interval 6–80 K the luminescence decay curves suffered a change at times longer than 40 μs, corresponding to long decay times. At higher temperatures the luminescence at long times was damped more rapidly. The initial parts of the luminescence decay curves (for times less than 40 μs after the excitation pulse) remained practically unchanged.

Within the range of available excitation densities we did not observe any changes in the shape of the luminescence decay curves of the two optical centers. Furthermore, the experimental geometry was such that the propagation path of the luminescence phonons in the samples was minimal (~ 0.1 mm), eliminating any influence of a reabsorption effect on the shape of the luminescence decay curves.

The progressive deviation of the luminescence decay curves of the Pr^{3+} optical centers from an exponential law in the initial stage (Fig. 2) with increasing concentration of activator ions means that a transfer of excitation energy to traps occurs.[19] The nature of these traps will be discussed below. In addition, on the basis of the temperature dependence of the luminescence decay parameters of the Pr^{3+} optical centers at long times we should take into consideration the migration of electronic excitation energy. The migration and transfer of energy of electronic excitation of Pr^{3+} ions to traps are due to the dipole–dipole interaction between the

corresponding pairs.[19] In this case the decay of the luminescence of the donors (Pr^{3+} ions) is described by the following dependence:[19]

$$I_d(t)=I_0\exp\left(-\frac{t}{\tau_0}-\alpha\sqrt{t/\tau_0}-\beta\frac{t}{\tau_0}\right), \quad (1)$$

$$\alpha=7.4\cdot R_0^3 c_{\rm tr}, \quad (2)$$

$$\beta=8.6\cdot R_0^{3/2}(D\tau_0)^{3/4}c_{\rm tr}, \quad (3)$$

where τ_0 is the decay constant for the luminescence of the donors in the absence of traps, R_0 is the critical radius for transfer of electronic excitation energy, D is the diffusion coefficient for the energy of electronic excitation, and $c_{\rm tr}$ is the concentration of traps.

In a YSO:Pr^{3+} crystal with a small (0.3 at. %) concentration of activator ions relation (1) describes a purely exponential decay of the luminescence under the condition $\alpha=0$ and $\beta=0$. By approximating the experimental curves in this case one can determine the exponential decay constants of the luminescence for the first ($\tau_0^1=108$ μs) and second ($\tau_0^2=145$ μs) types of luminescence. The time constants found did not vary with temperature in the interval 6–80 K.[11] In order to use relation (1) correctly for approximating the luminescence decay curves of the Pr^{3+} optical centers in the samples with the intermediate and highest concentrations of activator ions, it is necessary to assign a specific value and physical meaning to the parameters appearing in relations (2) and (3). In particular, the condition $\alpha>0$ and $\beta=0$ means that a transfer of excitation energy from the donors to the traps occurs in the system in the absence of migration, and the luminescence decay curve should deviate from a purely exponential law.[19] Under the condition $\alpha=0$ and $\beta>0$, migration of excitation energy occurs, and the luminescence decay curve remains exponential with a temperature-dependent decay constant.[19]

A reasonable value of R_0 can be obtained from experiment in the following way. In the sample with an intermediate concentration of activator ions (0.6 at. %) the luminescence decay of the second type is close to exponential and is described by relation (1) with $\alpha=0.14$ and $\beta=0$. This means that the transfer of electronic excitation energy to traps is only nascent, and migration of energy by a diffusion mechanism is absent. For this case we can estimate the average distance between Pr^{3+} optical centers of the second type. We take into account that the unit cell of the YSO crystal contains 8 formula units of Y_2SiO5 (Refs. 3 and 8). The accuracy of the estimate of the average distance between Pr^{3+} optical centers can be improved substantially by using the results of Ref. 20, according to which the square of the dipole moment (d_1) for the transition ${}^3H_4\leftrightarrow{}^1D_2$ for Pr^{3+} optical centers of the first type is larger by a factor of 1.36 than that for the second type (d_2). Interestingly, the ratio $\tau_0^1/\tau_0^2=1.34$ gives just such a value. The ratio of the integrated intensities of spectral lines 1 and 1* is approximately equal to three. However, when it is taken into account that $(d_2/d_1)^2=1.34$, one can state that the real occupation of cation sites of the first type in the YSO lattice by Pr^{3+} ions is 2.24 times larger than for the sites of the second type. Consequently, for a total concentration of activator ions of 0.6 at. % only 0.21 at. % of them go to the formation of optical centers of the second type. Their concentration is $\sim3.3\times10^{19}$ cm^{-3}, and the average distance between them is 31 Å. This distance can be taken as R_0.

If $R_0=31$ Å, then, using relation (2) for $\alpha=0.14$, we find the concentration of traps $c_{\rm tr}=6.3\times10^{17}$ cm^{-3}, which is almost two orders of magnitude different from the concen-

TABLE I. Parameters of the approximation of the luminescence damping curves for Pr^{3+} ions in the Y_2SiO5 crystal.

T, K	0.3 at. % Pr^{3+}		0.6 at. % Pr^{3+}		1.8 at. % Pr^{3+}	
	Type I	Type II	Type I	Type II	Type I	Type II
77	$\tau_0=108\times10^{-6}$ $\alpha=0$ $\beta=0$	$\tau_0=145\times10^{-6}$ $\alpha=0$ $\beta=0$	$\tau_0=108\times10^{-6}$ $\alpha=0.4$ $\beta=0.19$ $c_{\rm tr}=1.8\times10^{18}$ $D=2.7\times10^{-10}$	$\tau_0=145\times10^{-6}$ $\alpha=0.14$ $\beta=0$ $c_{\rm tr}=6.3\times10^{17}$	$\tau_0=108\times10^{-6}$ $\alpha=2.3$ $\beta=1.24$ $c_{\rm tr}=10^{19}$ $D=3.5\times10^{-10}$	$\tau_0=145\times10^{-6}$ $\alpha=1.98$ $\beta=0.99$ $c_{\rm tr}=8.9\times10^{18}$ $D=2.2\times10^{-10}$
1.5					$\tau_0=108\times10^{-6}$ $\alpha=2.3$ $\beta=0.73$ $c_{\rm tr}=10^{19}$ $D=1.7\times10^{-10}$	$\tau_0=145\times10^{-6}$ $\alpha=1.98$ $\beta=0.54$ $c_{\rm tr}=8.9\times10^{18}$ $D=0.97\times10^{-10}$

Note: The parameters have the following dimensions: τ_0 (s); $c_{\rm tr}$ (cm^{-3}), D (cm^2s^{-1}).

tration of donors (optical centers of the second type). The traps cannot be uncontrolled impurities, since their concentration in the stock used for activation of the YSO crystals was at least three orders of magnitude lower than that.

Apparently, the traps may be associates (most likely dimers) of Pr^{3+} ions. Their presence is confirmed by the appearance of additional concentration-dependent spectral lines in YSO:Pr^{3+} samples with high concentrations of activator ions.[11] When the topology of the YSO lattice is taken into account, at a concentration of Pr^{3+} ions equal to 0.6 at. %, about 1.7% of the optical centers of the second type will be ion pairs. Their concentration is $\sim 5.6\times 10^{17}\text{cm}^{-3}$, which is close in value to the calculated trap concentration ($c_{\text{tr}}\sim 6.3\times 10^{17}\ \text{cm}^{-3}$).

The numerical estimates given above for the parameters appearing in relations (2) and (3) permit a full analysis of the experimental luminescence decay curves in YSO:Pr^{3+} crystals with intermediate and high concentrations of activator ions. The results of an approximation of the experimental luminescence decay curves of the samples at temperatures of 1.5 and 77 K with the use of relation (1), in which the parameters α and β were varied, are presented in Table I. Using the numerical values of the parameters α and β and also $R_0 = 31$ Å, we calculated the trap concentration and the diffusion coefficient of the electronic excitation energy for each case. As expected, the value of the diffusion coefficient for electronic excitation energy decreases with decreasing temperature. That is, the diffusion of the electronic excitation energy of the Pr^{3+} impurity ions is of a thermally activated character.

The data in Table I indicate that when the concentration of activator ions in the YSO crystal increases from 0.3 to 0.6 at. %, migration of excitation energy occurs only for Pr^{3+} optical centers of the first type. Consequently, with increasing activator concentration the average distance between Pr^{3+} impurity ions actually decreases. Such a conclusion cannot be reached on the basis of the spectral data[11] alone. The point is that with increasing concentration of Pr^{3+} activator ions the formation and growth of clusters of these ions can occur. Then, starting with a certain concentration of Pr^{3+} ions, its further increase would lead to the growth of clusters, while the average distance between Pr^{3+} ions would not change.

The absence of spectral lines belonging to the luminescence of type II optical centers upon the selective excitation of type I optical centers at the transition $^3H_4 \rightarrow {}^2D_2$indicates the absence of transfer of excitation energy between nonequivalent Pr^{3+} optical centers. However, the selective excitation of Pr^{3+} optical centers of type I at the optical transition $^3H_4 \rightarrow {}^3P_0$ leads to the transfer of excitation energy toward type II Pr^{3+} centers.[12] Here the energy transfer occurs between metastable levels of the multiplet $^1D_2$ after completion of the radiationless relaxation $^3P_0 \rightarrow {}^1D_2$ with large Stokes losses.[12] As a result of radiationless relaxation $^3P_0 \rightarrow {}^1D_2$ an energy of $\sim 4000\ \text{cm}^{-1}$ is dissipated at each impurity center. One can therefore assume that the large number of phonons arising as a result of dissipation of this excess energy stimulates the transfer of energy between nonequivalent Pr^{3+} optical centers in the YSO crystal.

CONCLUSION

The complicated luminescence decay law of nonequivalent optical centers in the YSO:Pr^{3+} crystal at a concentration of activator ions 0.6 at. % and higher is due migration of the electronic excitation energy via Pr^{3+} ions of the same type and to the transfer of energy to quenching centers. The traps for the electronic excitation energy are dimers of the activator ions. Depending on the activator concentration, the luminescence decay of two nonequivalent optical centers can be substantially different. These last two facts can have a detrimental effect in the case when the activated oxyorthosilicates are used as scintillators. Even though the frequency shift between metastable levels of the $^1D_2$ term of the two Pr^{3+} optical centers is not large ($\sim 50\ \text{cm}^{-1}$), upon their selective excitation in the region of the transitions $^3H_4 \rightarrow {}^1D_2$ there is no transfer of electronic excitation energy between them. In contradistinction to this, upon the selective excitation of Pr^{3+} optical centers of the first type at a transition of $^3H_4$ the transfer of energy to the second type of optical centers can occur with the participation of phonons.

[1)]E-mail: malyukin@isc.kharkov.com

[1] A. A. Kaminskiĭ, Dokl. Akad. Nauk **319**, 1037 (1981).
[2] M. Malinowski, M. F. Jourbert, and B. Jacquier, J. Lumin. **60–61**, 179 (1994).
[3] C. L. Melcher, R. A. Manente, C. A. Peterson, and J. S. Schweitzer, J. Cryst. Growth **128**, 1001 (1993).
[4] C. L. Melcher and J. S. Schweitzer, IEEE Trans. Nucl. Sci. **NS-39**, 502 (1992).
[5] P. Dorenbos, C. W. E. van Eijk, A. J. J. Bos, and C. L. Melcher, J. Lumin. **60–61**, 979 (1994).
[6] H. Suzuki, T. A. Tombrello, C. L. Melcher, and J. S. Schweitzer, Nucl. Instrum. Methods Phys. Res. A **320**, 263 (1992).
[7] Yun Liu, Chao-Nan Xu, Hiroaki Matsui, Takeshi Imamura, and Tadahiko Watanabe, J. Lumin. **87–89**, 1297 (1994).
[8] J. Felsche, ''The crystal chemistry of rare-earth silicates,'' in *Structure and Bonding*, Vol. 13, Springer-Verlag (1973), p. 99.
[9] Yu. V. Malyukin, B. I. Minkov, R. S. Borisov, V. P. Seminozhenko, N. V. Znamenskii, E. A. Manykin, D. V. Marchenko, and E. A. Petrenko, Fiz. Nizk. Temp. **24**, 571 (1998) [Low Temp. Phys. **24**, 432 (1998)].
[10] R. S. Borisov, B. V. Grinev, N. V. Znamenskiĭ, Yu. V. Malyukin, É. A. Manykin, D. V. Marchenko, B. I. Minkov, and E. A. Petrenko, Zh. Éksp. Teor. Fiz. **115**, 704 (1999) [JETP **88**, 385 (1999)].
[11] Yu. V. Malyukin, R. S. Borisov, P. N. Zhmurin, A. N. Lebedenko, B. V. Grinev, N. V. Znamensky, É. A. Manykin, Yu. V. Orlov, E. A. Petrenko, and T. G.Yukina, Fiz. Nizk. Temp. **26**, 494 (2000) [Low Temp. Phys. **26**, 894 (2000)].
[12] Yu. V. Malyukin, R. S. Borisov, A. N. Lebedenko, N. I. Leonyuk, and M. Roth, Fiz. Nizk. Temp. **26**, 494 (2000) [Low Temp. Phys. **26**, 363 (2000)].
[13] H. G. Danielmeyer and H. P. Weber, IEEE J. Quantum Electron. **QE-8**, 805 (1972).
[14] H. G. Danielmeyer, J. Lumin. **12–13**, 179 (1976).
[15] J. M. Flaherty and R. C. Powell, Phys. Rev. B **19**, 32 (1978).
[16] K. Otsuka, T. Yamada, M. Saruwatarti, and T. Kimura, IEEE J. Quantum Electron. **QE-11**, 330 (1975).
[17] Y-P. Hong and K. Dwight, Mater. Res. Bull. **9**, 1661 (1974).
[18] F. Kellendonk and G. Blasse, J. Chem. Phys. **72**, 561 (1981).
[19] V. M. Agranovich and M. D. Galanin, *Electronic Excitation Energy Transfer in Condensed Matter*, North-Holland, Amsterdam (1982).
[20] Y. Sun, F. Konz, R. L. Cone, and R. W. Equall, *International Conference on Dynamical Processes in Excited States of Solids, Lyon, July 1–4, 2001*, Book of Abstracts, p. 79.

Translated by Steve Torstveit

PHYSICAL PROPERTIES OF CRYOCRYSTALS

Low-temperature unsteady creep of parahydrogen single crystals

L. A. Alekseeva,* A. V. Pustovalova, V. I. Khatuntsev, and Yu. V. Butenko

B. Verkin Institute for Low Temperature Physics and Engineering, National Academy of Sciences of Ukraine, pr. Lenina 47, 61103 Kharkov, Ukraine
(Submitted May 24, 2001; revised August 23, 2001)
Fiz. Nizk. Temp. **28**, 79–83 (January 2002)

The low-temperature plasticity of single crystals of solid parahydrogen (orthohydrogen concentration $\sim 0.2\%$, nonhydrogen impurities $\sim 1.5\times 10^{-4}\%$, and isotopic impurities of hydrogen — deuterium — $[D]/[H]\sim(5-6)\times 10^{-3}\%$) in the is investigated in the temperature range 1.8–4.2 K under conditions of sample creep under the influence of a static mechanical stress σ. A complicated dependence of the constant of the logarithmic creep of p-H_2 on the stress and temperature is observed, along with the anomalous features of the creep that indicate either the possible involvement of vacancies in the kinetics of the unsteady creep of parahydrogen single crystals at small σ or the coherent motion of kinks on dislocations. © *2002 American Institute of Physics.* [DOI: 10.1063/1.1449187]

1. INTRODUCTION

The physics of such phenomena as plasticity and strength is based on the concept of the existence of imperfections of the crystal lattice which are carriers of plastic deformation (see, e.g., Refs. 1 and 2). The kinetics of deformation in the case of solid H_2 is of great interest, since H_2 belongs to an unusual group of crystalline objects—quantum crystals.[3] At sufficiently low temperatures the low-dimensional defects in them take on substantially quantum properties and can tunnel through the potential barriers separating one equilibrium position from another in the lattice. For this reason the behavior of these crystals under load can exhibit quantum features, in particular, their quantum flow at a temperature of absolute zero under the influence of extremely small forces.[4] In view of the small mass of the H_2 molecules, the high amplitude of the zero-point lattice vibrations and the weak intermolecular interaction in the lattice, and also the fact that the Debye temperature of H_2 is almost an order of magnitude higher than the temperature of crystallization (see Ref. 3 and references therein), the manifestation of quantum effects (from the participation of quantum fluctuations to the coherent band motion of defects, including those of a dislocation character) can be observed in the kinetic properties of hydrogen practically throughout the entire existence region of the crystalline state. Quantum effects are manifested most clearly in a phenomenon such as creep, especially in its unsteady stage. The participation of quantum fluctuations due to the influence of the zero-point vibrations of dislocation strings[5] lends an athermal character to the low-temperature creep of metallic crystals, which thereby acquires traits of a quantum process. The latter is manifested in the deviation of the temperature dependence of the creep deformation from that which is characteristic for a thermally activated process as the temperature is lowered. The unsteady creep of hydrogen has been investigated previously on polycrystalline samples.[6,7] The single-crystal nature of the samples makes it easier to ascertain the characteristic deformation mechanisms and to observe and study subtle processes and phenomena of dislocation kinetics, which are masked in polycrystals by grain boundaries and structural defects in the interior of the grains. At the same time, there is no information about the characteristic of unsteady creep in single crystals of p-H_2. In this paper we present the results of a study of the kinetics of plastic flow of p-H_2 single crystals deformed in the creep regime under the influence of a static stress σ at temperatures of 1.8–4.2 K and of a variation of σ and T. It is found that the creep of p-H_2 single crystals in the unsteady stage has a logarithmic time dependence. Anomalous behavior of the constant of logarithmic creep is observed, and it is conjectured that it is due to the manifestation of quantum effects in the kinetics of low-temperature plasticity of p-H_2 single crystals.

2. EXPERIMENTAL TECHNIQUE

For preparation of the samples we used H_2 that had been purified by diffusion through Ni or generated by a calibrated source of the industrial type (SKhPV-500). The most highly purified fractions of H_2 were not used because it was impossible to obtain solid samples from them.[8] The samples were grown at a rate of 0.2–0.5 mm/min in a liquid-^{4}He-cooled glass ampoule of the cryostat described in Ref. 9 from the liquid phase of p-H_2 ($[D]/[H]\sim(5-6)\times 10^{-3}\%$) which had reached the equilibrium ortho–para composition ($\sim 0.2\%$ o-H_2) during a long hold in the presence of $Fe(OH)_3$. The loading of the annealed samples was done by means of the arm of a beam balance (sensitivity ± 200 mg). The change in length of the samples was measured by an inductive displacement sensor with an accuracy of $\pm 10^{-5}$ cm.

The temperature of the ends of the crystals was monitored by two semiconductor resistance thermometers with an accuracy of $\pm 2\times 10^{-2}$ K. The monocrystallinity of the

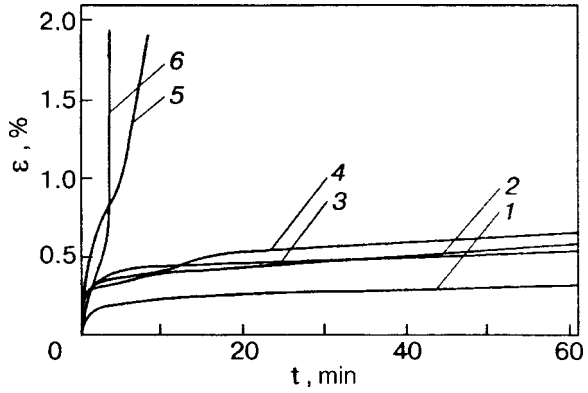

FIG. 1. Curves of the creep of p-H_2 single crystals at temperatures of 4.2 K (curves *1, 3, 5*) and 1.8 K (curves *2, 4, 6*) and at various values of the stress σ [gf/mm^2]: 1.0 (*1*), 0.9 (*2*), 0.8 (*3*), 0.7 (*4*), 2.1 (*5,6*).

samples was confirmed by their visual observation in crossed polarizers. The absence of planar defects was judged from the characteristic irreversibility of the change in the dimensions and shape of the deformed samples.

3. EXPERIMENTAL RESULTS AND DISCUSSION

The typical form curves of the time (t) dependence of the relative elongation ε of the p-H_2 single-crystal samples is shown in Fig. 1 for various values of the stress and at temperatures of 4.2 and 1.8 K. It was found that holding the p-H_2 single crystals under an applied static stress σ (even a low one) leads to a continuous increase of their original length with time, and creep is observed at all values of the temperature down to 1.8 K. Here there occurs both an instantaneous growth of the length, observed directly at the time of application of the load, and a subsequent growth in the transient (unsteady) state. As time goes on, the $\varepsilon(t)$ curves exhibit stages of steady creep with a constant rate of strain of the p-H_2. For large values of σ the stages of accelerated creep with extremely intense development of the deformation of the samples are rapidly reached.

To ascertain the character of the change in deformation of p-H_2 single crystals in time we used a logarithmic, $\varepsilon = \alpha \ln(\beta t+1)$, and a power-law, $\varepsilon = At^n$, dependence of the creep, with constants α, β, A, and n. In addition, the experimental curves of the creep $\varepsilon(t)$ were approximated by the sum function $\varepsilon = \alpha \ln(\beta t+1)+At^n$ by the Levenberg–Marquardt method.[10,11] A comparison of the rms deviation of the experimental curves from the theoretical showed that the trend of the observed functions $\varepsilon(t)$ at the investigated values of T and σ is described by a logarithmic function over a wide interval of their values. The role of the power-law term in this is insignificant and may be neglected completely.

To obtain the dependence of the constant α on temperature and stress, p-H_2 single crystals that had been subjected to a stress σ at $T=$ const were heated to a higher temperature or the applied stress was increased to a higher level. The experiments showed that changing T or σ leads to a change of the constant α. The sign of this change is determined by the temperature and the value of the stress. The anomalous directionality of the trend of $\alpha(\sigma)$ (in comparison with the conventional growth of the logarithmic creep constant with stress) is shown in Fig. 2.[1)] In a comparative analysis we

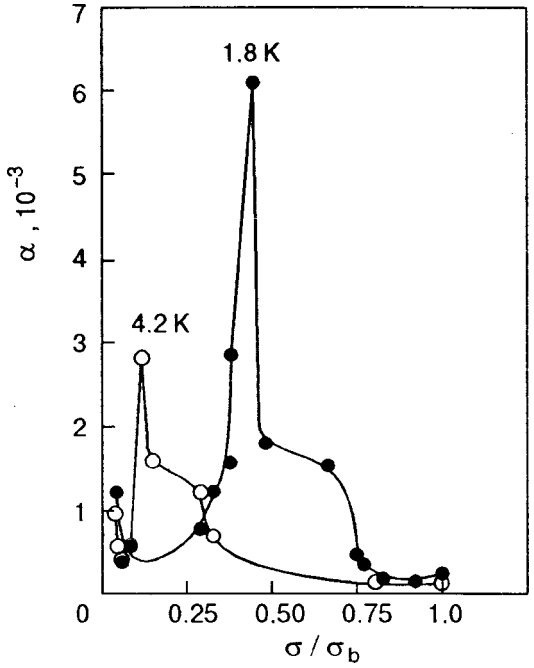

FIG. 2. Curves of the logarithmic creep constant α for p-H_2 single crystals versus the reduced stress in normalized coordinates at $T=4.2$ (○) and 1.8 K (●).

used a selection of identical single crystals with approximately the same orientation of the c axis relative to the axis of tension with allowance for the anisotropy of the mechanical properties of hcp p-H_2 (Ref. 8). We see the regions of loads which are characterized by satisfaction of the inequalities $\alpha^2_{\sigma_2} < \alpha_{\sigma_1}$ (under the condition $\sigma_2 > \sigma_1$) and $\alpha_{4.2\text{ K}} < \alpha_{1.8\text{ K}}$. The fact that the complicated shapes of these curves obtained at $T=1.8$ and 4.2 K are remarkably identical and are of a reproducible character attests to the reliability of the experimental results.

In view of the fact that the curves given in Fig. 2 were obtained at the edges of the investigated temperature interval, it can be assumed that the same features are also present inside the interval. The generality of the $\alpha(\sigma^{1)})$ curves obtained for different temperatures is indicative of a commonality of the mechanisms governing the development of the deformation of single-crystal p-H_2 with time under the conditions $T, \sigma =$ const for each of the three regions: region 1—fall-off of α with increasing σ at small σ; region 2—subsequent growth of α with increasing σ; region 3—decrease of the logarithmic creep constant α with increasing σ. In the first region the values of α do not depend on temperature. The second and third regions are characterized by an explicit temperature effect, and one observes a tendency for the critical values of the stress for succession of the different regions to shift with changing temperature. The "background" values of α (and certain fragments of the curves) are close to those observed in the case of polycrystalline H_2 (see Refs. 6 and 7 for details).

Thus it follows from the data obtained that: 1) with decreasing temperature the value of the deformation of equally loaded p-H_2 crystals increases, i.e., it behaves anomalously from the standpoint of the concepts of thermally activated plasticity; 2) when a certain threshold value of the load is

reached, an unstable state of enhanced plasticity arises in the deformed p-H_2 crystal; this state can be observed from the appearance of a sharp, narrow peak on the $\alpha(\sigma)$ curve.

A logarithmic law of creep is characteristic for low-temperature dislocation creep.[5,12] In that case a single crystal with the hcp lattice is the most easily analyzed system from the standpoint of the motion of dislocations and dislocation fluxes.[1,12] At comparatively high σ the decrease of α with increasing σ in p-H_2 is apparently due not only to a decrease of the mean free path of the dislocations but also a change of their density, as a rule,[12] as a result of the their accumulation in front of subboundaries in the single crystal. It follows from Fig. 2 that the critical stress for this process to come into play increases with decreasing temperature.

The mobility of dislocations in region 2 for p-H_2 single crystals is governed by the presence of isotopic impurity in the samples and a residual impurity of the ortho modification. In this case the effective mean free path of dislocations can be influenced both by isolated ortho molecules and by ortho pairs arising as a result of the electrostatic quadrupole–quadrupole interaction between o-H_2 molecules[13] (at an o-H_2 concentration of $\sim 0.2\%$ the probability of the appearance of larger clusters at the temperatures under study is negligible).[14] In the case of the interaction of edge dislocations with HD or D_2 molecules the interaction energy is 4.45 or 9.04 K, respectively.[15] The most difficult to overcome of the binary clusters also require the expenditure of an energy of the order of 3.2 K.[14] Like the isotopic molecules, these obstacles can be overcome by dislocations either by purely mechanical means under the applied stress or with the help of quantum fluctuations.[5,16]

At low stresses (region 1) the development of deformation is due either to the motion of vacancies[17] or by dislocation kinks in the Peierls relief,[18–20] which is distorted by ortho and isotopic impurities. In view of the anomalous decrease of α with increasing σ, the observed features of the deformation of p-H_2 can be described in terms of the quantum motion of defects. It may be assumed that the motion of the dislocation kinks is of a coherent character[20–22] and comes about mainly in the secondary Peierls relief under conditions of a slightly irregular crystal. It follows from Fig. 2 that the creation of ''quasi-kinks'' with increasing σ does not occur, and that the development of deformation of the p-H_2 is due solely to the existing dislocation configurations.

The narrow, sharp peak on the $\alpha(\sigma)$ curves may be evidence of growth of the effects of correlated motion of dislocations as a result of the evolution of the defect structure of the p-H_2 samples with increasing σ. The presence of a parallel organizing process which leads to fragmentation of the p-H_2 samples competes with the main processes responsible for its low-temperature plasticity.

In closing we note that the presence of impurities in p-H_2, as it turned out, facilitates the realization of irreversible changes in the dimensions and shape of the p-H_2 samples, and these changes were observed in the experiment. This is partly analogous to an effect observed in Ref. 19—a widening of the temperature interval in which macroscopic quantum effects are observed in the plastic deformation of β-Sn single crystals containing a small amount (0.01 at.%) of cadmium impurity.

The authors thank V. G. Manzhelii, M. A. Strzhemechny, K. A. Chishko, A. N. Aleksandrovskii, V. D. Natsik, and A. I. Prokhvatilov for a discussion of the results of this study and for helpful comments, and D. N. Kazakov (Moscow, Russia) and L. A. Vashchenko for practical assistance in obtaining high-purity hydrogen and for doing the precision mass spectrometric and chromatographic analyses of the samples.

*E-mail: alekseeva@ilt.kharkov.ua

[1)] As the reduction parameter along the abscissa we have used the quantity σ^*, which is normalized by the ultimate loads σ_b corresponding to the maximum deformation of p-H_2 reached in tensile testing. Analysis showed that σ_b is practically independent of temperature: $\sigma_{b(4.2\ \mathrm{K})} = 8.6$ gf/mm^2, $\sigma_{b(1.8\ \mathrm{K})} = 8.9$ gf/mm^2.

[1] A. M. Kosevich, *Physical Mechanics of Real Crystals* [in Russian], Naukova Dumka, Kiev (1981).
[2] H. G. van Beuren, *Imperfections in Crystals*, 2nd ed., North-Holland, Amsterdam (1961), Izd. Inostr. Lit., Moscow (1962).
[3] V. G. Manzhelii, M. A. Strzhemechnyĭ, ''Quantum molecular crystals,'' in *Cryocrystals* [in Russian], edited by B. I. Verkin and A. F. Prikhot'ko, Naukova Dumka, Kiev (1983).
[4] A. F. Andreev and I. M. Lifshits, Zh. Éksp. Teor. Fiz. **56**, 2057 (1969) [Sov. Phys. JETP **29**, 1107 (1969)].
[5] V. D. Natsik, A. I. Osetskii, V. P. Soldatov, and V. I. Startsev, Phys. Status Solidi B **54**, 99 (1972).
[6] D. N. Bol'shutkin, Yu. E. Stetsenko, L. A. Indan, and A. A. Khudoteplaya, in *Physical Processes of Plastic Deformation at Low Temperatures* [in Russian], Naukova Dumka, Kiev (1974), p. 345.
[7] L. A. Alekseeva, O. V. Litvin, and I. N. Krupskii, Fiz. Nizk. Temp. **8**, 211 (1982) [Sov. J. Low Temp. Phys. **8**, 105 (1982)].
[8] L. A. Alekseeva, L. A. Vashchenko, D. N. Kazakov, V. V. Karonik, and O. V. Nikolaeva, ''Use of the sorption–desorption cycle in research on the mechanical properties of solid p-H_2'' [in Russian], Preprint 30–89, Kharkov (1989).
[9] I. N. Krupskii, A. V. Leont'eva, L. A. Indan, and O. V. Evdokimova, Fiz. Nizk. Temp. **3**, 933 (1977) [Sov. J. Low Temp. Phys. **3**, 453 (1977)].
[10] P. E. Gill, W. Murray, and M. H. Wright, *Practical Optimization* [Academic Press, New York (1981); Mir, Nauka, Moscow (1987)].
[11] V. I. Belan, K. V. Maslov, A. A. Motornaya, and V. I. Khatuntsev, ''Dialog system of optimization for the ES computer,'' in *Applied Software Packages for Optimization Problems* [in Russian], Nauka, Moscow (1987), p. 108.
[12] J. Friedel, *Dislocations* [Pergamon Press, Oxford (1964); Mir, Moscow (1967)].
[13] A. B. Harris, L. I. Amstutz, H. Meyer, and S. M. Myers, Phys. Rev. **175**, 603 (1968).
[14] S. E. Kal'noi and M. A. Strzhemechnyi, Fiz. Nizk. Temp. **11**, 803 (1985) [Sov. J. Low Temp. Phys. **11**, 440 (1985)].
[15] L. A. Alekseeva, M. A. Strzhemechny, and Yu. V. Butenko, Fiz. Nizk. Temp. **23**, 448 (1997) [Low Temp. Phys. **23**, 329 (1997)].
[16] V. D. Natsik, Fiz. Nizk. Temp. **5**, 400 (1979) [Sov. J. Low Temp. Phys. **5**, 191 (1979)].
[17] L. A. Alekseeva and I. N. Krupskiĭ, Fiz. Nizk. Temp. **10**, 327 (1984) [Sov. J. Low Temp. Phys. **10**, 170 (1984)].
[18] B. V. Petukhov and V. L. Pokrovskiĭ, Zh. Éksp. Teor. Fiz. **63**, 634 (1972) [Sov. Phys. JETP **36**, 336 (1973)].
[19] V. D. Natsik, G. I. Kirichenko, V. V. Pustovalov, V. P. Soldatov, and S. É. Shumilin, Fiz. Nizk. Temp. **22**, 965 (1996) [Low Temp. Phys. **22**, 740 (1996)].
[20] M. A. Strzhemechnyi, Fiz. Nizk. Temp. **10**, 663 (1984) [Sov. J. Low Temp. Phys. **10**, 348 (1984)].
[21] A. F. Andreev, Usp. Fiz. Nauk **118**, 251 (1976) [Sov. Phys. Usp. **19**, 137 (1976)].
[22] Yu. Kagan and L. A. Maksimov, Zh. Éksp. Teor. Fiz. **84**, 792 (1983) [Sov. Phys. JETP **57**, 459 (1983)].

Translated by Steve Torstveit

Irreversible magnetostriction and magnetization of superconducting $2H$-$NbSe_2$ single crystals in a peak-effect regime

V. V. Eremenko, V. A. Sirenko,* and Yu. A. Shabakayeva

B. Verkin Institute for Low Temperature Physics and Engineering of the National Academy of Sciences of Ukraine, 47 Lenin Ave., 61103 Kharkov, Ukraine

R. Schleser

Grenoble High Magnetic Field Laboratory, MPI-FKF and CNRS BP-166, F 38042, Grenoble Cedex 09, France

P. L. Gammel

Bell Laboratories, Lucent Technologies, Murray Hill, New Jersey 07974, USA
(Submitted August 31, 2001)
Fiz. Nizk. Temp. **28**, 10–15 (January 2002)

Magnetostriction measurements in the mixed state of superconducting $2H$-$NbSe_2$ single crystals under in-plane magnetic fields 0–12 T have revealed a peak on the magnetostriction versus magnetic field dependences in the vicinity of the upper critical field H_{c2}. The peak value of the longitudinal magnetostriction is higher by more than an order of magnitude in comparison with that of the transverse magnetostriction when measured along the hexagonal axis. Analysis of the measured field dependences of the magnetostriction and magnetization of $2H$-$NbSe_2$ allows one to relate the observed peculiarities of magnetostriction with the loss of order in the lattice of Abrikosov vortices, which occurs by a first-order phase transition.
 [DOI: 10.1063/1.1449178]

1. INTRODUCTION

The observation of giant magnetostriction in high-temperature superconductors,[1–3] along with establishing its relation to the interactions between the crystal lattice inhomogeneities and the arrangement of Abrikosov vortices,[4] enables one to use magnetostriction measurements as a tool for examination of a variety of phenomena in the vortex assembly, which results from magnetic flux pinning. An important direction in this field of investigation is elucidation of the origin of the peak effect, which is the peak on the field dependences of the critical current near the upper critical field H_{c2}, manifested as the maximum on the field dependences of the irreversible magnetization,[5] and of its connection with the phase transitions in a flux-line lattice.[6] It should be mentioned that an advantage of magnetic studies of the peak effect is that they provide direct data on the thermodynamic parameters of the transition.

Many years of research on the field dependences of the critical currents and magnetization of type-II superconductors have shown that in general the peak effect is observed in different ranges of magnetic fields between the lower H_{c1} and upper H_{c2} critical fields, and the shape of the peak is described by an expression $(H_{c2})^n f(b)$, with $f(b)$ similar at all temperatures below T_{SN}, where b is the reduced magnetic induction in the sample, and $n=1$–3, depending on the type of pinning center and the pinning mechanism involved.[5] The peaks on the field dependences of the magnetostriction were observed in Refs. 2, 7, and 8 on single crystals of high-temperature superconductors (HTSCs) of the 1-2-3 type with rare-earth substitutions, polycrystals of Nb–Ti alloys, and single crystals of the layered compound $2H$-$NbSe_2$, respectively. For HTSCs it was shown[2] that the peaks in the intermediate field range correspond to the traditional mechanisms of pinning ($n=2.5$). For explanation of the observed value $n=4.5$ for the magnetostriction peak in Nb–Ti the field dependence of the Young's moduli of the crystal lattice was taken into account. The value $n=6.5\pm0.2$ for the magnetostriction in $2H$-$NbSe_2$ will be analyzed in the present work.

2. EXPERIMENTAL RESULTS

The measurements were performed on high-quality single crystals of the superconducting compound $2H$-$NbSe_2$ with a superconducting transition temperature $T_{SN}=7.2$ K.

2.1. Magnetostriction measurements

The magnetostriction measurements were performed in a cryogenic capacitance dilatometer.[8] The longitudinal $\lambda(a,a)$

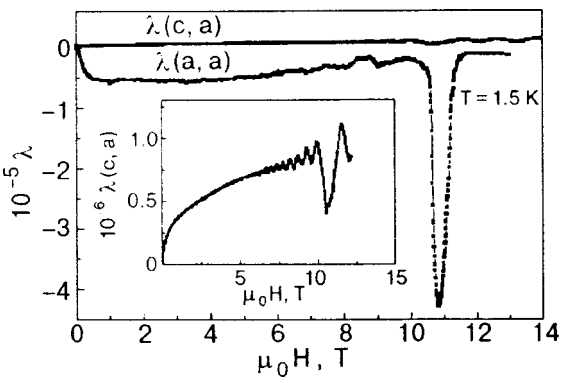

FIG. 1. Magnetostriction λ versus magnetic field measurements.

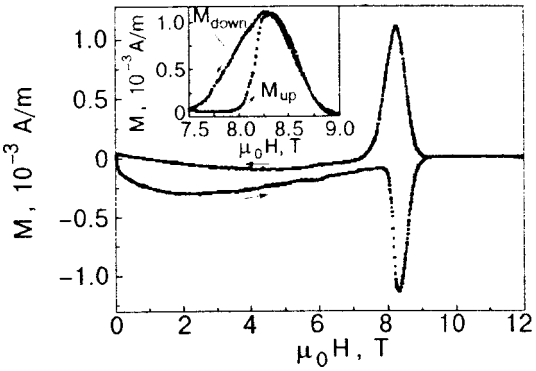

FIG. 2. Absolute magnetization measurements along the c direction for an in-plane direction of the magnetic field. The inset shows the enlarged region of the peak effect.

and transverse $\lambda(c,a)$ magnetostriction values were measured in a field applied in the basal plane of the sample along the a axis. The measurements of $\lambda(c,a)$ and $\lambda(a,a)$ in increased field at temperature $T=1.5$ K are presented in Fig. 1. It is clearly seen that at fields near H_{c2} a pronounced peak is observed, and the absolute values of $\lambda(c,a)$ are much lower than those for $\lambda(a,a)$.

2.2. Magnetization measurements

The magnetization measurements were performed along the crystallographic c direction by means of a magnetic capacitance torquemeter technique.[9] The absolute values of the magnetization were obtained using a calibration coil.[10]

The measurements at temperature $T=1.5$ K are shown in Fig. 2. Figure 3 presents the irreversible component of magnetization for different temperatures. Figure 4 demonstrates the irreversible magnetostriction and magnetization in reduced coordinates. For the magnetostriction and magnetization measurements the scaling law with $n=6.5\pm0.2$ is fulfilled.

3. DISCUSSION

The unit cell of this compound comprises two sandwiches. Each of them is a hexagonally packed plane of Nb between two hexagonally packed planes of Se. The planes are shifted with respect to each other, and atoms of Se form a trigonal environment of the Nb atoms. The Nb planes are responsible for the superconductivity of this compound. The distance between the nearest Nb planes is $d=c/2=6.27$ Å, where c is the lattice spacing along the hexagonal axis. The in-plane lattice parameters are $a=b=3.45$ Å. The ratio of the lattice parameters attests to pronounced crystallographic anisotropy. At the same time $2H$-$NbSe_2$ should not be considered as a quasi-two-dimensional superconductor, as its superconducting coherence length along the hexagonal axis is twice the interplane spacing $\xi_c > d$ ($\xi_c(0)=23$ Å). This is a typical highly anisotropic superconductor ($\xi_{ab}(0)=78$ Å), which is characterized by an anisotropy parameter $\gamma=(M/m)^{1/2}=\xi_{ab}/\xi_c=3$, or in alternative definitions, $\varepsilon^2=m/M\approx0.09$ ($m=m_1=m_2$ and $M=m_3$ are the effective electron masses along and normal to the crystallographic planes). Such high values of the anisotropy parameters of $2H$-$NbSe_2$ provide an adequate description of its supercon-

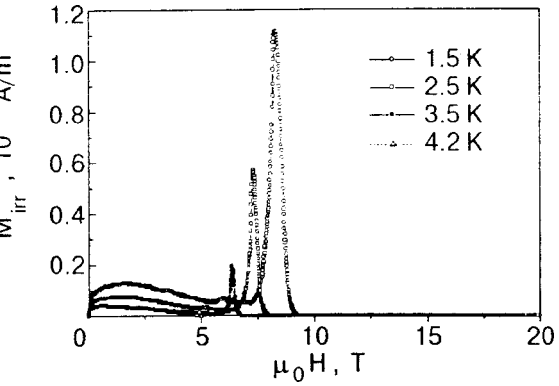

FIG. 3. Field dependence of the irreversible magnetization.

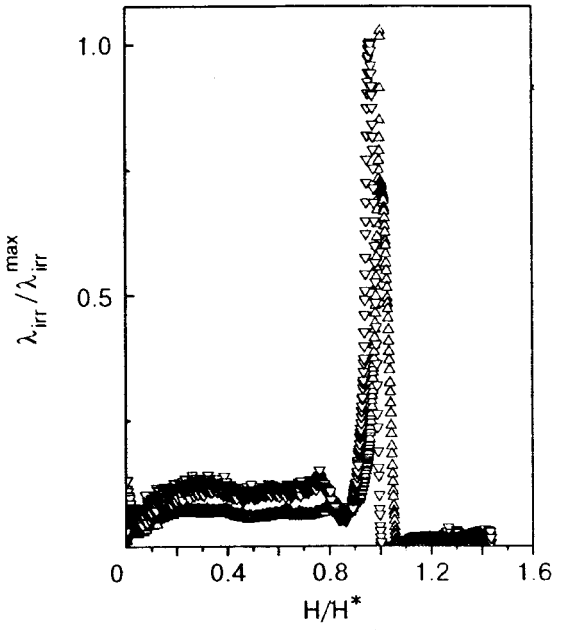

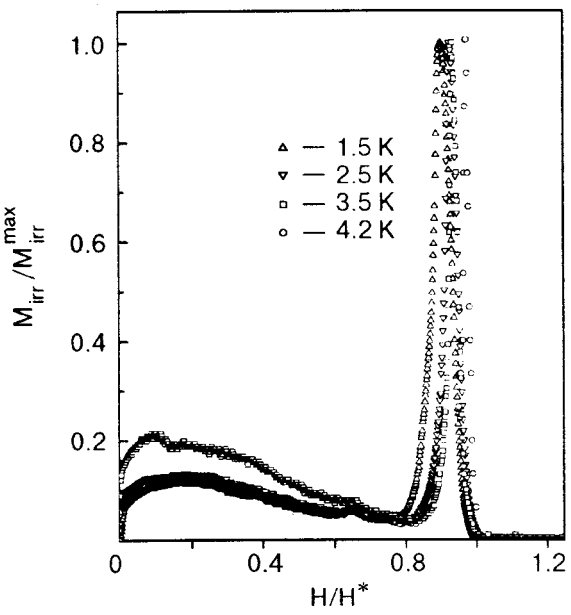

FIG. 4. Reduced field dependence of the irreversible magnetostriction[8] and magnetization, normalized to their values at the peak.

ducting properties by the Ginzburg–Landau equations[11] with the anisotropic mass tensor (Ref. 12 and references therein). For our case $m_1=m_2<m_3; m_1/m_3=[H_{c2}(\|c)/H_{c2}(\perp c)]^2$. We take into consideration the following expression

$$H_{c2}(\theta)=\Phi_0/[2\pi(\sin^2\theta+\varepsilon^2\cos^2\theta)^{1/2}\xi_{ab}^2] \quad (1)$$

(Φ_0 is the quantum of magnetic flux, and θ is the angle between the direction of the applied magnetic field and the c axis), which defines the coherence length values.

Validity of this approach significantly simplifies analysis of the angular dependences of the measured properties, which in part will be considered in this paper.

3.1. Anisotropy of magnetostriction at $H_{c1}<H\ll H_{c2}$

The observed differences of $\lambda(c,a)$ and $\lambda(a,a)$ in fields below the peak values may be explained in the following way. In fields applied along the extended surface of the sample in the a axis direction, magnetic flux penetrates the sample along the b axis. Under this condition the penetration is postponed by a surface barrier until the magnetic field H is increased to the value $H\approx 2.7H_c$ (Ref. 5), where H_c is the critical field, which is determined by the difference of free energy values in the normal and superconducting states, and which is much higher than H_{c1}. The low-temperature limit of H_c for the compound under investigation is $H_c\approx 0.14$ T.[13] In this range of magnetic fields the magnetostriction is determined by the pressure of the magnetic field and by the ratio of elastic constants in different crystallographic directions. From the theory of elasticity the relation between $\lambda(c,a)$ and $\lambda(a,a)$ may be derived:

$$\lambda(c,a)/\lambda(a,a)=-C_{13}(C_{11}-C_{12})/(C_{11}C_{33}-C_{13}^2).$$

The right side of this relation includes the components of the elastic-modulus tensor of the crystal lattice. Introducing their values from Ref. 13, one obtains the ratio $\lambda(a,a)/\lambda(c,a)=-0.76/0.12=-6.3$, which is in good agreement with the measurements in fields well below H_{c2}. When the magnetic flux penetrates the sample along the b axis, the values of $\lambda(c,a)$ are determined by the ratios of the volumes of the normal and superconducting parts of the sample[8] and are proportional to the size differences $\delta_T(\|c)$ in the normal and superconducting states along the distinguished crystallographic direction in the absence of magnetic field. This quantity is determined by the relation $\delta_T(\|c)\sim H_c[\partial H_c/\partial P(\|c)]$, or according to Ref. 13, $\delta_T(\|c)\sim H_c^2/T_{SN}[\partial T_{SN}/\partial P(\|c)]$. Substitution of the values $\partial T_{SN}/\partial P(\|c)\approx 1.8\times 10^{10}$ from Ref. 14 gives satisfactory agreement with the measurements[8] $\delta_T(\|c)\approx 2\times 10^{-7}$. It is known[14] that the in-plane pressure dependence of T_{SN} differs significantly from that in the c direction. Pressure along the c axis weakly increases the transition temperature, while in-plane pressure increases it significantly. In first approximation it should be assumed that below the peak values, $\lambda(a,a)$ is also defined by the volumetric ratio of the normal part of the sample due to weak pinning [the ratio of the depinning and depairing critical currents $j_c/j_0=10^{-6}$ (Ref. 15), is surprisingly small]. Therefore, the ratio of $\lambda(c,a)$ to $\lambda(a,a)$ in a field below the peak is defined by the relation $[\partial T_{SN}/\partial P(\|c)]/[\partial T_{SN}/\partial P(\perp c)]\approx 0.45$ (Ref. 15), which satisfies the experimental data for the reversible component of the magnetostriction.[8] It appears that for explanation of the irreversible magnetostriction we cannot neglect the pinning in the basal plane parallel to applied magnetic field.

3.2. Magnetostriction in the fields near H_{c2}

In Refs. 16 and 17 the peak effect in the field dependences of the critical currents near H_{c2} was attributed to the change of the elastic moduli of the flux-line lattice when the field approaches H_{c2}. In Ref. 16 it was the decrease of the shear modulus C_{66}, which occurs faster than the decrease of the pinning force. As a result, the vortices redistribute in accordance with the spatial distribution of pinning centers or the pinning potential relief. This situation corresponds to a loss of spatial order in the flux-line lattice and, in principle, resembles melting processes. It was described in Ref. 18 in terms of the correlation volume V_c of the flux-line lattice regions which can move independently of each other. The results of this work have been used successfully for examination of transformations in the vortex arrays of anisotropic superconductors. The possibility of transformations developing via a first-order phase transition was analyzed in Ref. 19. It was suggested that the transition is realized in the fluctuation regime when the Lindemann criterion[20] is fulfilled, i.e., when the mean-square amplitude to of the vortex fluctuation displacements amounts to about $0.2a_0$, where a_0 is the vortex lattice parameter. It is a result of the loss of order in the vortex lattice or the decrease of V_c when the magnetic field approaches H_{c2}. A comparative analysis of the magnetostriction and magnetization measurements allows us to check if this situation is characteristic for our case. It should be noted that a fluctuation contribution to the behavior of superconducting $2H$-$NbSe_2$ is probable, as the Ginzburg number,[21] which characterizes importance of the fluctuation contribution, is rather high: $\mathrm{Gi}=k_BT_{SN}/H_c^2\varepsilon\xi^3\approx 10^{-4}$. For HTSCs it is of the order of 10^{-2}, and for other conventional superconductors it is of the order 10^{-8} (Ref. 15). This is, in part, the reason for the noticeable difference between the fields H_{c2} and H^*, where H^* is the field above which all irreversible characteristics vanish ($H^*\approx H_{c2}$). The advantage of $2H$-$NbSe_2$ for analysis of the transition processes is that, in contrast to HTSCs, there is no flux creep in it, notwithstanding the high level of thermal fluctuations. In addition, the inset in Fig. 2 demonstrates that in the peak regime the magnetization run (the low-field arm of the peak) is irreversible. It may be proof of a first-order phase transition, on the one hand, and a manifestation of vortex lattice disordering and the consequent spread over pinning centers, on the other. So, the experimental data do not contradict the proposed description.

In comparing the data on the magnetostriction and magnetization we should keep in mind that in the latter case the torque was registered in a tilted field, which is a necessary condition for application of such a measuring technique. The chosen value $\theta=77°$ corresponds to the maximum signal.[22] Analysis of the angular dependences and comparison of the data obtained at different θ is possible due to applicability of Ginzburg–Landau theory with an anisotropic mass tensor to the compound under study (the relations are presented in Ref. 16).

3.3. Phase transition

In order to analyze the possibility that a first-order phase transition in the vortex array is manifestated in the peak effect, the relation derived for the flux-line lattice from the Lindemann criterion[19,20] will be used:

$$H_m(T)=\beta_{\rm m}(c_L/{\rm Gi})H_{c2}(0)(T/T_{\rm SN})^2 \times[1-(T/T_{\rm SN})-H_{\rm m}/H_{c2}(0)]^2, \quad (2)$$

where $\beta_{\rm m}\approx 5.6$, $c_L=0.23-0.15$ is the Lindemann criterion in systems with variable pinning, and $H_{\rm m}$ is the melting field of the flux-line lattice. The location of the measured high-field magnetostriction and magnetization peak-effect curves, namely H^*, suits well the value of $H_m(T)$ if the superconducting parameters of $2H$-$NbSe_2$ are substituted into Eq. (2). The experimentally observed jump in the equilibrium magnetization near H^* at $T=1.5$ K is $\Delta M\approx 5$ G, and the corresponding elongation is $\Delta L\approx 2\times 10^{-8}$ mm. Therefore, the pressure derivative of the transition field may be estimated using the Clapeyron–Clausius relation; $\Delta L(\|c)/\Delta M=\partial H^*/\partial P(\|c)$. Substitution of the magnitudes obtained gives a reasonable[14] estimate $\partial H^*/\partial P(\|c)\approx 0.6-0.8$ G/bar.

3.4. Scaling law for isothermal field dependences of the magnetostriction

Analysis of the magnetostriction measurements in the peak regime according to the scheme of Refs. 2 and 7 have shown that the field dependences of the irreversible component of the magnetostriction $\lambda_{\rm irr}(c,a)$ measured at different temperatures follow the scaling laws $M_{\rm irr}\sim(H^*)^n$ and $\lambda_{\rm irr}\sim(H^*)^n$ with the same power $n=6.5\pm 0.2$. Consequently, for analysis of the observed dependences the concepts developed for the trivial peak effect may be used, and the field dependences of the elastic moduli of the crystal lattice may in our case be excluded from consideration of the magnetostriction peak. In view of the softening of the flux-line lattice in a peak-effect regime and the independent displacements of its parts with the correlation volume V_c, the relation for collective pinning in the peak region[18] may be used for description of the irreversible magnetization:

$$M_{\rm irr}\sim(n_{\rm p}f_{\rm p}^2/V_c)^{1/2}, \quad (3)$$

where $n_{\rm p}$ is the density of pinning centers, $f_{\rm p}$ is the elementary pinning force, and $n_{\rm p}^{1/2}f_{\rm p}$ is the volume density of the pinning force. Usually, the latter is characterized by a power-law dependence on H_{c2} with a power of 1–3 for different types of pinning centers.[5] Its contribution to n may also be estimated from analysis of the broad maximum of the magnetization in fields of about $H=2.4$ T. The nearly same position of the maxima at different temperatures suggests a matching between the flux-line lattice spacing and the distance between the pinning centers involved.[5] The flux-line lattice spacing may be estimated from the well known relation $a_0\approx(\Phi_0/B)^{1/2}=178$ Å, which can easily correspond to the distance between the stacking faults in the Nb planes arising below the charge-density-wave transition ($T_{\rm CDW}=34$ K), with the appearance of an incommensurate structure of niobium atoms, characterized by a lattice spacing of about $3a_0$ (Ref. 23). Estimation of the corresponding pinning force from Ref. 24 gives the power $n_1\approx 2.5$.

Now the contribution of the correlation volume V_c will be estimated. It goes as the inverse square of the tilt and shear moduli of the vortex lattice, or $(H_{c2})^{-4}$, which means that expression (3) comprises a multiplicative factor with the power $n_2=2$.

And, finally, the thermofluctuational character of the transition near H^* means that expression (3) should be supplemented by a temperature-dependent factor.[25] It is determined by temperature dependence of the depinning energy for thermal fluctuations, which to a first approximation is linear in the temperature.[5] Using the temperature dependence of the critical fields, a factor with $n_3=2$ is obtained.

In this way a total power $n=6.5$ is obtained, which agress with that derived from magnetostriction and magnetization measurements in the peak-effect regime.

CONCLUSIONS

It was found that the maximum on the field dependences of the irreversible magnetostriction in superconducting $2H$-$NbSe_2$ corresponds to the field range of structural transformations in the vortex array, which is realized after a first-order phase transition scenario. The measured field dependence in the peak region is described by a scaling law $\lambda_{\rm irr}\sim(H^*)^{6.5\pm 0.2}$, similar to that for the irreversible magnetization $M_{\rm irr}\sim(H^*)^{6.5\pm 0.2}$. It is shown that the power $n=6.5\pm 0.2$ is determined by the field dependences of the elementary pinning force and correlation volume and by thermal fluctuations near the upper critical field. It should be noted that the analysis presented is the first one of this kind, but similar dependences may be expected for the irreversible magnetostriction in HTSCs in the high-field peak-effect regimes. According to the arguments proposed, in conventional superconductors with a low probability of thermal fluctuations the power of H_{c2} in the high-field-peak scaling law should be a few times lower.

*E-mail: sirenko@ilt.kharkov.ua

[1] H. Ikuta, N. Hirota, Y. Nakayama, K. Kishio, and K. Kitazawa, Phys. Rev. Lett. **70**, 2166 (1993).
[2] C. de la Fuente, A. Del Moral, J. I. Arnaudas, and J. S. Abell, Physica C **244**, 214 (1993).
[3] V. V. Eremenko, V. A. Sirenko, H. Szymczak, and A. Nabialek, Fiz. Nizk. Temp. **25**, 311 (1999) [Low Temp. Phys. **25**, 221 (1999)].
[4] A. A. Abrikosov Zh. Eksp. Teor. Fiz. **32**, 1442 (1957) [Sov. Phys. JETP **5**, 1174 (1957)].
[5] A. M. Campbell and J. E. Ivetts, Critical Currents in Superconductors, Taylor and Francis, London (1972).
[6] G. Blatter, M. V. Feigel'man, V. B. Geshkenbein, A. I. Larkin, and V. M. Vinokur, Rev. Mod. Phys. **66**, 1125 (1994).
[7] U. Wyder, P. J. E. M. van der Linden, H. P. van der Meulen, A. Gerber, V. H. M. Duyn, J. A. A. J. Perenboom, A. de Visser, and J. J. M. Franse, Physica B **211**, 265 (1995).
[8] V. V. Eremenko, V. A. Sirenko, R. Schleser, and P. L. Gammel, Fiz. Nizk. Temp. **27**, 412 (2001) [Low Temp. Phys. **27**, 305 (2001)].
[9] D. Shoenberg, *Magnetic Oscillations in Metals*, Cambridge University (1984).
[10] V. Eremenko, V. Sirenko, Yu. Shabakayeva, R. Schleser, and P. L. Gammel, Fiz. Nizk. Temp. **27**, 952 (2001) [Low Temp. Phys. **27**, 700 (2001)].
[11] V. L. Ginzburg, Zh. Eksp. Teor. Fiz. **23**, 236 (1952).
[12] V. G. Kogan and J. R. Clem, Phys. Rev. B **24**, 2497 (1981).
[13] V. G. Kogan, L. N. Bulaevskii, P. Miranovic, and L. Dobrosavljevic-Grujic, Phys. Rev. B **51**, 15344 (1995).
[14] T. Sambongi, J. Low Temp. Phys. **18**, 139 (1975); P. Molinie, D. Jerome,

and A. J. Grant, Adv. Phys. **23**, 1091 (1974); M. A. Obolenskii, Kh. B. Chashka, V. I. Beletskii, and V. M. Gvozdikov, Fiz. Nizk. Temp. **15**, 984 (1989) [Low Temp. Phys. **15**, 544 (1989)]; R. E. Jones, H. R. Shanks, and D. K. Finnemore, Phys. Rev. B **6**, 835 (1972); K. Yamaya and T. Sambongi, J. Phys. Soc. Jpn. **32**, 1150 (1972).
[15] M. J. Higgins and S. Bhattacharya, Physica C **257**, 232 (1996).
[16] A. B. Pippard, Philos. Mag. **19**, 217 (1969).
[17] R. Labush, Phys. Status Solidi **32**, 439 (1969).
[18] A. I. Larkin and Yu. N. Ovchinnikov, J. Low Temp. Phys. **34**, 409 (1979).
[19] D. R. Nelson and H. S. Seung, Phys. Rev. B **39**, 9153 (1989).
[20] F. Lindemann Phys. Z. (Leipzig) **11**, 69 (1910).
[21] V. L. Ginzburg, Fiz. Tved. Tela (Leningrad) [Sov. Phys. Solid State **2**, 1824 (1961)].
[22] V. G. Kogan, Phys. Rev. B **38**, 7049 (1988).
[23] B. Gianbattista, A. Johnson, R. V. Coleman, B. Drake, and P. K. Hansma, Phys. Rev. B **17**, 2741 (1988).
[24] H. C. Freyhardt, in *Proceedings of the International Discussion Meeting on Flux Pinning in Superconductors, Sonnenberg, Germany (1974)*, p. 98.
[25] L. Niel, Cryogenics **32**, 975 (1992).

This article was published in English in the original Russian journal. Reproduced here with stylistic changes by AIP.

Effect of nonmagnetic impurities on the spontaneous magnetostriction in β-O_2 crystals

A. I. Prokhvatilov,[a] Yu. A. Freiman, N. N. Galtsov, and Yu. E. Stetsenko

B. Verkin Institute for Low Temperature Physics and Engineering, National Academy of Sciences of Ukraine, pr. Lenina 47, 61103 Kharkov, Ukraine

(Submitted August 29, 2001)
Fiz. Nizk. Temp. **28**, 84–90 (January 2002)

X-ray investigations of weak solid solutions of oxygen with argon, krypton, and nitrogen are done at temperatures in the existence region of the rhombohedral β-O_2 phase. It is found that the spontaneous inhomogeneous magnetostriction effect previously studied in pure oxygen is enhanced by the introduction of the atomic impurities Ar and Kr and weakened by the dissolution of nitrogen molecules. The possible reasons for the different effect of atomic and molecular impurities on the inhomogeneous spontaneous magnetostriction in β-O_2 crystals are discussed. [DOI: 10.1063/1.1449188]

INTRODUCTION

Oxygen is unique among the simplest molecular substances in that it is a molecular magnet. Against the background of relatively weak van der Waals forces it has a rather strong intermolecular magnetic interaction. This circumstance is responsible for the majority of the features of the physical and structural properties of condensed phases of oxygen. In the solid state at equilibrium vapor pressure oxygen has three crystalline phases.[1,2] The low-temperature monoclinic α phase (space group $C2/m$, $T<23.88$ K) and the intermediate rhombohedral β phase (space group $R3m$, $23.88<T<43.8$ K) have the same orientational structure with a collinear stacking of molecules parallel to the principal axis of the lattice. The high-temperature γ phase (space group $Pm3n$, $T>43.8$ K) has a disordered sublattice (two molecules in $2a$ positions, symmetry point group $m3$) and a partially ordered sublattice (six molecules in $6d$ positions, symmetry point group $\bar{4}2m$). The molecules in the latter positions process at an angle of 90° to the [100] axes and as a result form chains of ''disks'' along these directions. The magnetic structure of these solid phases of oxygen changes first from quasi-two-dimensional antiferromagnetically ordered two-sublattice[3,4] (α phase) to quasi-two-dimensional three-sublattice in regions of short-range order[5–7] (β phase) and then to quasi-one-dimensional in a system of chains of ''disks''[8,9] (the γ phase). In liquid oxygen near the triple point the structure of the short-range orientational and magnetic order is similar to that observed in crystals of the high-temperature γ phase.[9,10] This accounts for the high values of its density and heat of vaporization, the low values of the vapor pressure, and also the jump in volume (density) on crystallization.[1]

In recent investigations of solid oxygen, particular attention has been paid to the magnetic structure of the rhombohedral β phase.[5–7,11–16] This is largely because, in spite of the absence of long-range order in the spin subsystem,[6,7,15,16] β-O_2 crystals have many properties inherent to magnets.[17,18] In particular, as was shown in Ref. 19, the β phase of pure oxygen has a characteristic spontaneous magnetostriction, which is indicative of a strong magnetoelastic interaction. Since the latter arises in crystals with relatively weak van der Waals forces, this leads to a rather large inhomogeneous microstrain of the lattice, $\Delta d/d \sim 5\times 10^{-3}$, and strong broadening of the x-ray reflections, growing on approach to the $\beta \rightarrow \alpha$ transition. The character of the significant anisotropy of the inhomogeneous local distortions, as established by x-ray studies,[19] and also the data on the inelastic scattering of polarized neutrons[7,16] are evidence in favor of a quasi-two-dimensional three-sublattice model of the structure of short-range magnetic order. This is the so-called Loktev structure,[5] in accordance with which the β-O_2 crystal can be treated as a set of weakly coupled close-packed basal planes with three magnetic sublattices.

To obtain additional information about the magnetostriction effect in oxygen, it is of interest to study how the magnetic structure and magnetoelastic interaction are affected by the change in the intermolecular forces in β-O_2 when nonmagnetic atomic and molecular impurities are dissolved in it. Some preliminary data on the effect of argon and krypton impurities on the spontaneous magnetostriction in β-O_2 crystals (the width of the x-ray diffraction reflections was investigated over the entire existence region of the intermediate phase) were given in Ref. 19 and presented at the International Conference on Low-Temperature Physics LT-21.[20] In the present paper we give the results of detailed studies of weak solutions of oxygen with argon and krypton and with a quadrupolar impurity—molecular nitrogen.

EXPERIMENTAL TECHNIQUE

The experiments were done on a DRON-3M x-ray diffractometer with personal computer automation. We used polycrystalline samples with a grain size of 10^{-4}–10^{-5} cm, obtained by condensation of gaseous mixtures of specified concentration (with a ~1%–3% argon, krypton, or nitrogen impurity) on a substrate with $T=40$ K, and annealed at 45 K for one hour. The high-temperature transition in oxygen is accompanied by an appreciable volume jump (~5.4%). To avoid creating appreciable elastic stresses in the samples at the transition from the high-temperature to the intermediate phase, they were cooled in the region of the γ–β transition at a rate of 0.2–0.3 deg/min. In preparing the solutions we

used oxygen and impurity gases with purities of 99.99% or better. We obtained powder diffraction patterns and analyzed the intensities of the x-ray reflections, their half-width, and angular position as functions of temperature and of the cycling in the existence region of the β phase and through the $\alpha-\beta$ transition. Analysis of the intensity and half-width of the reflections was done using the Origin multislit code with an error of $\pm 1\%$ and $\pm 1.5\%$, respectively.

RESULTS AND DISCUSSION

Before turning to a discussion of the results of studies of weak solutions of substitution of oxygen with inert elements and nitrogen, let us review some of the features of the phase diagrams of these systems. All three binary systems have extremely complex phase diagrams, with peritectic and eutectoid triple points, and a high probability of metastable phases.[21–25] The equilibrium solubility limit in oxygen of both the atomic (Ar, Kr)[21,22] and molecular (N_2)[23] impurities is extremely low in the low-temperature phases with a strong magnetic interaction and does not exceed 1%–2% in the α and 2%–3% in the β modification. Only in the region of the γ phase, where the magnetic interaction is considerably weaker, does the solubility increase to 23% for Ar, to 9% for Kr, and to 11% for N_2. Consequently, in respect to the impurity concentration the experiments in each system were limited by the existence of rather narrow single-phase regions for oxygen-based solutions. In all three systems the introduction of the impurity led to an appreciable decrease of the phase transition temperatures. For example, at the solubility limit of $\sim 2\%$ Ar in oxygen the temperature of the low-temperature $\alpha-\beta$ transformation decreases to 19 K, while that of the high-temperature $\beta-\gamma$ transformation decreases to 39 K.[21] In comparison with pure solid oxygen, the presence of atomic and molecular impurities also leads to enlargement of the coexistence regions of the two phases adjacent to the transition, and these regions grow wider with increasing concentration. This effect is very pronounced at the $\gamma-\beta$ transition.[21–25] We took these features into account in doing the experiments and in our analysis of the results.

ATOMIC IMPURITIES

The results of the measurements of the half-widths of the diffraction reflections from weak solid solutions of oxygen with argon and krypton together with the data for pure oxygen[19] are presented in Figs. 1 and 2. From an analysis of the results we note the following points.

First, the introduction of Ar or Kr atoms to the lattice leads to an increase in the positional disorder, most likely because of concentration-related nonuniform microstrains arising in the solid solutions on account of the difference of the molecular diameters of the components. For this reason, in the region $T>40$ K, where the magnetoelastic interaction in the oxygen lattice has become substantially weaker, a significant increase in the initial half-widths of the reflections is observed for samples containing impurities in comparison with pure oxygen (Figs. 1 and 2).

Second, in solutions with inert elements, as in pure oxygen, as the temperature approaches the low-temperature transition to the magnetically ordered α phase, the half-widths of the reflections from the planes inclined to the basal plane increases linearly, while those for reflections from the basal planes (001) remain practically uncharged with temperature.

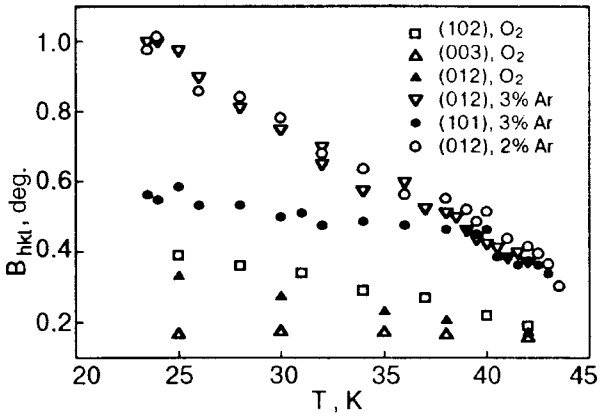

FIG. 1. Temperature dependence of the half-widths of x-ray reflections B_{hkl} from different planes of the rhombohedral phase of O_2-Ar solid solutions in comparison with the data for pure oxygen.[19]

Third, the half-widths of the reflections from planes inclined to the basal planes directly near the $\beta\rightarrow\alpha$ transition ($T=25$ K) in solutions with Ar and Kr are substantially larger than the typical values for pure oxygen[19] (Figs. 1 and 2). This means that the introduction of an atomic impurity in the β-O_2 crystal appreciably increases the value and anisotropy of the nonuniform magnetoelastic distortions of the lattice.

Impurities can serve as centers of crystallization, especially in the case of solidification from the liquid phase. Here, for the samples containing an impurity a ''fragmenting'' of the substructure of the samples can occur, as compared to that of the pure material obtained under the same conditions of crystallization. The significant influence of the atomic impurities on the diffraction pattern (the linewidths) of oxygen observed in the experiments, particularly on its change with temperature in β-O_2, can hardly be due to the dispersing effect of the impurities on the microstructure of the samples. This conclusion follows from the fact that no substantial difference is observed between the half-widths of the reflections in the high-temperature and intermediate

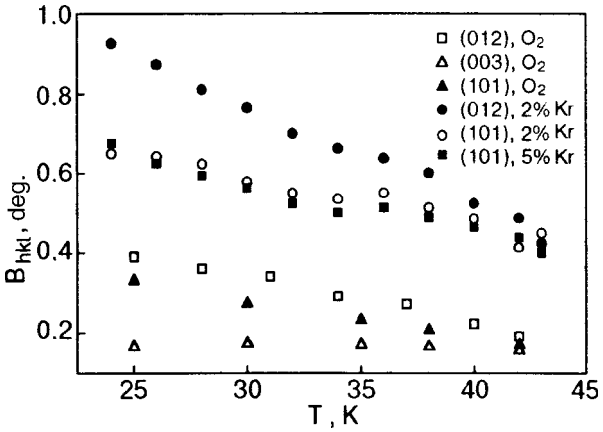

FIG. 2. Temperature dependence of the half-widths of the x-ray reflections B_{hkl} from different planes of the rhombohedral phase of O_2-Kr solutions in comparison with the data for pure oxygen.[19]

phases near the $\beta-\gamma$ transition, at least at concentrations up to 3%. The total impurity effect (a nonuniform local dilatation of the lattice because of the difference of the diameters of the impurity and host components and also the possible dispersion of the samples by the impurity during crystallization) is in fact expressed in the higher background of distortions of the structure observed at 43 K in the high-temperature existence region of the β-O_2 phase (Figs. 1 and 2).

The features described above are most likely a consequence of the weakening effect of the impurities on the intermolecular interaction in the ordered intermediate phase of oxygen, ultimately leading to enhancement of the magnetostriction effect. In view of this, the following arguments seem reasonable. Ar and Kr atoms have diameters of 3.405 Å and 3.624 Å,[25] noticeably larger than the minor axis of the oxygen molecule, 3.174 Å.[27–29] Because of this, when the oxygen molecules are substituted by spherically symmetric impurities, these inert elements locally weaken the central van der Waals forces and the noncentral orientational quadrupole coupling forces in the β-O_2 crystals (especially in the close-packed basal planes). As a result, the magnetoelastic interaction takes place in a ''softer'' lattice, and this promotes the formation of larger nonuniform microstrains than in the case of pure oxygen. Naturally, this effect becomes stronger with decreasing temperature. In addition, in β-O_2 the three-sublattice magnetic structure is disrupted at the sites of the Ar or Kr atoms. Here it could be the case that a pseudomonoclinic symmetry, similar to that of α-O_2, arises in the orientation of the spins of the molecules surrounding the impurity,[13] and the magnetic interaction becomes stronger.

According to Ref. 30, the random strain fields caused by substitutional impurities have a strong effect on the magnetic subsystem of a crystal and cause a local change of symmetry. For example, in superconducting (lanthanum, yttrium, etc.) ceramics, which are quasi-two-dimensional antiferromagnets with a weak interlayer exchange (between magnetically ordered CuO_2 planes), the introduction of superstoichiometric oxygen ions in the lattice leads to local rhombic deformations.[30] These ideas are confirmed by the experimentally established facts reflected in Figs. 1 and 2. In solid solutions of oxygen with inert elements, as in pure β-O_2, an increase in the nonuniform microstrains predominantly in the basal planes occurs with decreasing temperature on account of the enhancement of the magnetoelastic interaction for the reasons indicated above. It turned out that the value of these strains and their change with temperature are possibly independent of the impurity concentration in the samples over the range of concentrations studied. This fact in itself attests to the high stability of the magnetic structure of the β phase. The steeper dependence of the half-widths of the reflections on temperature $B_{hkl}(T)$ in the case of solutions (Figs. 1 and 2) is due not only to a ''softening'' of the oxygen lattice on doping by atomic impurities but possibly also to an enhancement of the spin–spin interaction of the O_2 molecules with decreasing temperature in local regions with a pseudomonoclinic magnetic structure.

MOLECULAR IMPURITIES

An impurity of molecular nitrogen has a completely different effect on the structure and properties of orientationally ordered phases of oxygen. O_2-N_2 solid mixtures were first studied by Prikhot'ko.[31] Later the authors of Ref. 32 in a study of the optical absorption spectra established that a ni-

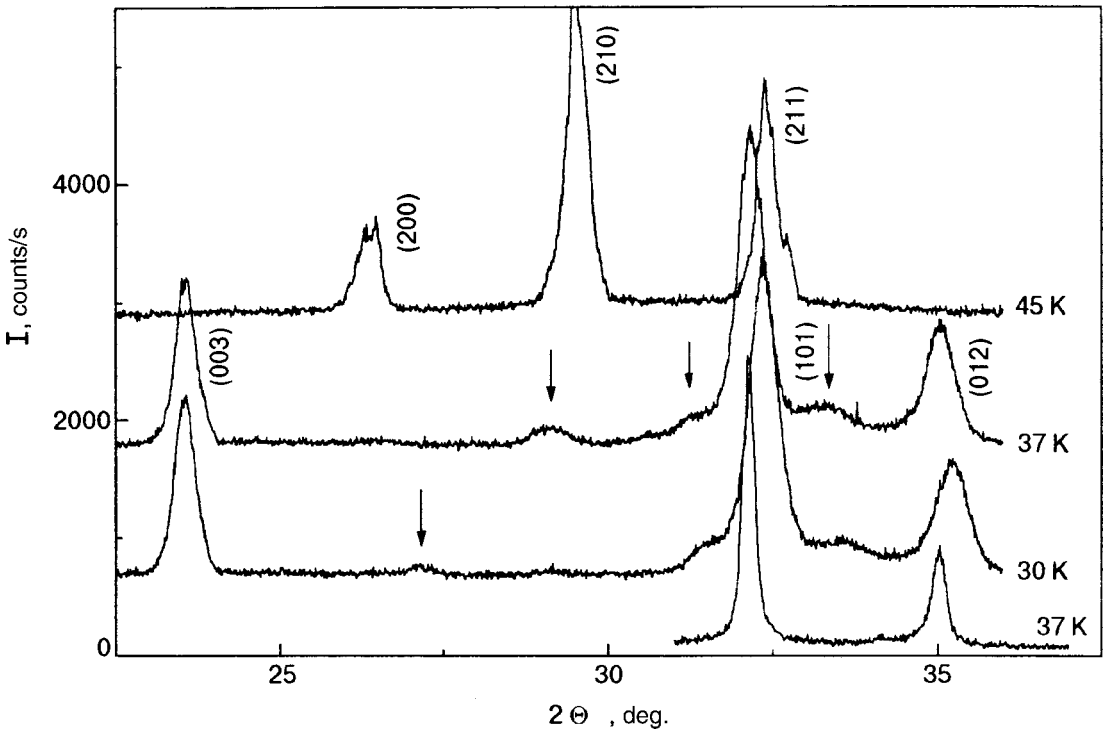

FIG. 3. Typical x-ray diffraction patterns from $O_2+1\%N_2$ solutions and pure oxygen in the existence region of the rhombohedral phase of oxygen. The arrows indicate reflections not characteristic for β-O_2.

trogen impurity had a strong weakening effect on the exchange interaction in α-O_2, ultimately destroying the long-range magnetic order.

In the present study we have established the following features. First, when samples of a solid solution containing 1% nitrogen are cooled through the $\beta-\gamma$ transition, one observes not only reflections from the rhombohedral phase β-O_2 but also some additional relatively weak lines (Fig. 3). The intensity of these reflections is practically independent of the nitrogen concentration in the interval 1%–3% but decreases noticeably as the temperature is lowered. This last fact suggests that they belong to some regions of supercooled γ-O_2. However, a comparison of the corresponding diffraction patterns (Fig. 3) shows that only two lines at small angles of reflection can be assigned to γ-O_2, and then only in a forced way, while the remaining lines have no relation to it whatsoever. According to their angular position, the additional reflections most likely correspond to the diffraction pattern from the previously observed α' phase,[33,34] the appearance of which has also been attributed to an impurity effect. However, as follows from the data of Ref. 26, in a nonequilibrium pass through the high-temperature transition the diffraction patterns in the β-O_2 region also contain x-ray reflections that can be assigned to α'-O_2. In this case the formation of the additional phase is apparently due to the presence of a high level of nonuniform elastic stresses arising in the crystal as a result of the large volume jump at the $\beta-\gamma$ transition.

A comparison of the diffraction patterns of pure and nitrogen-doped oxygen at 37 K clearly demonstrates the substantial influence of even small impurities of N_2 molecules on the width of the x-ray reflections (Fig. 3). For crystals containing a nitrogen impurity we investigated the influence on the width of the reflections not only of temperature but also of heating and cooling cycles in the existence region of β-O_2.

We found that, unlike the cases of the pure β-O_2 phase and solutions of oxygen with inert elements, for solutions of N_2 in oxygen there is almost no change of the half-width and integrated intensities of the reflections with temperature in the entire existence region of the rhombohedral phase. As a example, Fig. 4 shows data for two lines, which in β-O_2 have indices of (101) and (012). It should be noted that the observed diffraction pattern is reproduced qualitatively and quantitatively when the samples are heated from the existence region of the low-temperature α phase. In addition, the level of the nonuniform concentration shifts that occur when a nitrogen impurity is introduced into the oxygen is approximately the same as in the case of impurities of atomic impurities of inert elements. This is evidenced by the fact that for $T>40$ K for all three forms of solutions, O_2–Ar, O_2–Kr, and O_2–N_2, close values are obtained for the increase in the half-widths of the x-ray reflections over the typical values for pure oxygen (Figs. 1, 2, and 4).

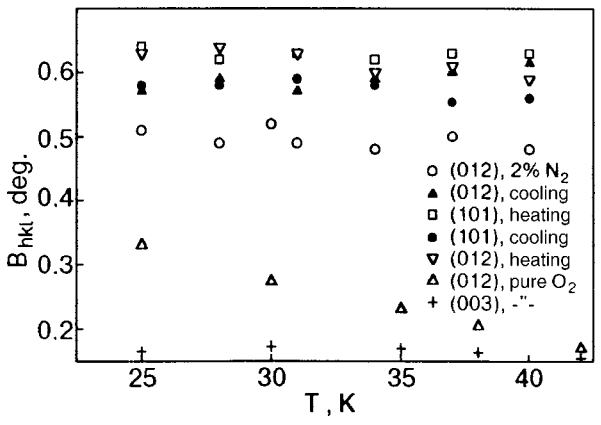

FIG. 4. Temperature dependence of the half-widths of the x-ray reflections B_{hkl} from different planes of the rhombohedral phase of O_2–N_2solutions. The various symbols represent data obtained in regimes of heating and cooling at temperatures within the existence region of β-O_2.

The fact that the influence of N_2 molecules on the structural characteristics of the oxygen matrix was found to be of a qualitatively different character was to be expected, since the N_2 impurity molecules, having molecular parameters very close to those of the host molecules (the transverse and longitudinal electronic diameters of the N_2 molecule are 3.386 Å and 4.339 Å, respectively, while those for the O_2 molecule are 3.175 and 4.180 Å),[27,28] are incorporated in the β-O_2 lattice without substantial deformational disruptions in the orientational subsystem, while in the translational subsystem they are of approximately the same order as when the oxygen is substituted by Ar or Kr.

The absence (within the error limits) of temperature dependence of the half-widths of the x-ray reflections B_{hkl} from the lattice of oxygen crystals containing a nitrogen impurity may be due to two compensating factors. The N_2 molecules, on the one hand, like atoms of inert elements, weaken the van der Waals interaction and act on the magnetic subsystem, locally disrupting the three-sublattice spin structure. On the other hand, the nitrogen molecules present in the β-O_2 lattice enhance the noncentral nonmagnetic intermolecular interaction, since the impurity molecules introduced in the crystals have a quadrupole moment considerably larger than that of O_2 (Refs. 2 and 25). This, in turn, should act to decrease the magnetostriction because of an increase in the ''stiffness'' of the lattice. These effects cause microstrains of different sign in the lattice, and the net effect in the given system is close to zero. In contrast, the influence of nitrogen impurity molecules on the magnetic subsystem of oxygen is actually so large that even small amounts ($\sim 1\%$ or less) will lead not only to a significant decrease of the magnetoelastic interaction but also possibly to a partial destruction of the three-sublattice quasi-two-dimensional structure of β-O_2, which is accompanied, as we have said, by a lowering of the symmetry in part of the crystal and the formation of a new phase there. The presence of additional weak lines of a second phase in the diffraction pattern from such weak solutions (Fig. 3) is apparently evidence of this. In had been conjectured previously[33] on the basis of the experimental results that this additional phase, which is called[34] the α' phase, is paramagnetic and is formed in oxygen that contains impurities—molecules of nitrogen in particular.

It follows from the data presented in Fig. 4 that thermocycling of the samples between temperatures within the existence region of β-O_2 increases B_{hkl} somewhat. However, this effect is absent in pure oxygen.[19] The growth of nonuniform local deformations during thermocycling in the weak solutions studied here is most likely due to the long relax-

ation time of concentration-related stresses in the impurity-doped crystals.

[a)]E-mail: prokhvatilov@ilt.kharkov.ua

[1] B. I. Verkin (ed.), *Handbook of Properties of Condensed Phases of Hydrogen and Oxygen*, Hemisphere Publ. Corp., New York (1990).
[2] V. G. Manzhelii, A. I. Prokhvatilov, V. G. Gav-rilko, and A. P. Isakina, *Structure and Thermodynamic Properties of Cryocrystals*, Begell House, New York (1998).
[3] I. A. Burakhovich, I. N. Krupskiĭ, A. I. Prokhvatilov, Yu. A. Freĭman, and A. I. Érenburg, JETP Lett. **25**, 32 (1977).
[4] I. N. Krupskiĭ, A. I. Prokhvatilov, Yu. A. Freĭman, and A. I. Érenburg, Fiz. Nizk. Temp. **5**, 271 (1979) [Sov. J. Low Temp. Phys. **5**, 130 (1979)].
[5] V. M. Loktev, Fiz. Nizk. Temp. **5**, 295 (1979) [Sov. J. Low Temp. Phys. **5**, 142 (1979)].
[6] P. W. Stephens, R. J. Bergeneau, C. F. Majkrzak, and C. Shirane, Phys. Rev. B **28**, 452 (1983).
[7] P. W. Stephens and C. F. Majkrzak, Phys. Rev. B **33**, 1 (1986).
[8] A. P. Brodyanskii and Yu. A. Freiman, Fiz. Nizk. Temp. **11**, 1292 (1985) [Sov. J. Low Temp. Phys. **11**, 714 (1985)].
[9] A. P. Brodyanskii, Yu. A. Freiman, and A. Jezowski, J. Phys.: Condens. Matter **1**, 999 (1989).
[10] A. P. Brodyanskiĭ and Yu. A. Freĭman, Fiz. Nizk. Temp. **12**, 1212 (1986) [Sov. J. Low Temp. Phys. **12**, 684 (1986)].
[11] V. A. Slyusarev, Yu. A. Freiman, and R. P. Yankelevich, Fiz. Nizk. Temp. **7**, 536 (1981) [Sov. J. Low Temp. Phys. **7**, 265 (1981)].
[12] I. M. Vitebskii, V. M. Loktev, and A. A. Chabanov, Fiz. Nizk. Temp. **18**, 862 (1992) [Low Temp. Phys. **18**, 607 (1992)].
[13] I. M. Vitebskii, V. L. Sobolev, A. A. Chabanov, and V. M. Loktev, Fiz. Nizk. Temp. **19**, 151 (1993) [Low Temp. Phys. **19**, 107 (1993)].
[14] I. M. Vitebskii, A. I. Knigavko, and A. A. Chabanov, Fiz. Nizk. Temp. **19**, 542 (1993) [Low Temp. Phys. **19**, 385 (1993)].
[15] M. F. Collins, Proc. Phys. Soc. **89**, 415 (1966).
[16] F. Danstetter, V. P. Plakhti, and J. Schweizer, J. Magn. Magn. Mater. **72**, 258 (1988).
[17] A. S. Borovik-Romanov, M. P. Orlova, and P. G. Strelkov, Dokl. Akad. Nauk **99**, 699 (1954).
[18] C. G. Defotis, Phys. Rev. B **23**, 4714 (1981).
[19] A. S. Baryl'nik and A. I. Prokhvatilov, Fiz. Nizk. Temp. **20**, 912 (1994) [Low Temp. Phys. **20**, 716 (1994)].
[20] A. I. Prokhvatilov, A. Jezowski, J. Mucha, P. Stachowiak, Yu. A. Freiman, V. V. Sumarokov, and A. S. Barylnik, Czech. J. Phys. **46**, 525 (1996).
[21] A. I. Prokhvatilov and A. S. Baryl'nik, Fiz. Nizk. Temp. **11**, 1280 (1985) [Sov. J. Low Temp. Phys. **11**, 707 (1985)].
[22] A. S. Baryl'nik and A. I. Prokhvatilov, Fiz. Nizk. Temp. **14**, 1204 (1988) [Sov. J. Low Temp. Phys. **14**, 665 (1988)].
[23] A. S. Baryl'nik, A. I. Prokhvatilov, and L. D. Yantsevich, Fiz. Nizk. Temp. **15**, 501 (1989) [Sov. J. Low Temp. Phys. **15**, 282 (1989)].
[24] L. Meyer, Adv. Chem. Phys. **16**, 343 (1969).
[25] V. G. Manzhelii, A. I. Prokhvatilov, I. Ya. Minchina, and L. D. Yantsevich, *Handbook of Binary Solutions of Cryocrystals*, Begell House, New York (1996).
[26] A. I. Prokhvatilov, N. N. Galtsov, and A. V. Raenko, Fiz. Nizk. Temp. **27**, 532 (2001) [Low Temp. Phys. **27**, 391 (2001)].
[27] T. Kihara and K. Sakai, Acta Crystallogr., Sect. A: Cryst. Phys., Diffr., Theor. Gen. Crystallogr. **34**, 326 (1978).
[28] R. F. Bader, W. H. Henneker, and P. E. Cade, J. Chem. Phys. **46**, 3341 (1967).
[29] A. C. Wahl, Science **151**, 961 (1966).
[30] M. A. Ivanov, V. M. Loktev, and Yu. G. Pogorelov, Zh. Éksp. Teor. Fiz. **101**, 596 (1992) [JETP **74**, 317 (1992)].
[31] A. F. Prikhot'ko, Zh. Éksp. Teor. Fiz. **8**, 671 (1939).
[32] Yu. G. Litvinenko, V. V. Eremenko, and T. I. Garber, Phys. Status Solidi **30**, 49 (1968).
[33] I. N. Krupskii, A. I. Prokhvatilov, Yu. A. Freiman, and A. I. Erenburg, ''Structure, low-energy elementary excitation spectrum and thermodynamic properties of solid oxygen'' [in English], Preprint ITF 79-4E, Kiev (1979), p. 45.
[34] E. M. Hörl, Acta Crystallogr., Sect. B: Struct. Crystallogr. Cryst. Chem. **25**, 2515 (1969).

Translated by Steve Torstveit

SHORT NOTES

On the non-Heisenberg contribution to the spin–spin interaction of an antiferromagnet with $S=3/2$

V. M. Kalita and A. F. Lozenko*

Institute of Physics of the National Academy of Sciences of Ukraine, pr. Nauki 46, 03650 Kiev, Ukraine
(Submitted March 5, 2001)
Fiz. Nizk. Temp. **28**, 91–94 (January 2002)

It is shown that the spin Hamiltonian of the spin–spin interactions, written with the use of effective spinons defined on the two lowest doublets of magnetic ions with a partially frozen orbital moment, has a non-Heisenberg form. The Heisenberg contribution is represented by spin–spin terms containing three powers of ion spin projections and is anisotropic and comparable to the bilinear spin–spin interaction. © *2002 American Institute of Physics.*
[DOI: 10.1063/1.1449189]

The inter-ion spin–spin interactions in spin Hamiltonians are specified using effective spins defined on the ground state functions of the atoms. Such Hamiltonians are used to calculate spin excitations, the temperature dependence of the magnetization and magnetic susceptibility, the values of the sublattice collapse fields, etc. Most often the spin Hamiltonian is written phenomenologically in such a way as to conform to the symmetry of the crystal. As a rule, the spin Hamiltonian of an antiferromagnet contains several phenomenological parameters which are determined using the data of various experiments. In their analysis it must be taken into account that the magnetization of the sublattice and the value of its average spin, defined as the average of the sum of the effective spins, are not equal to each other. Agreement between the magnetization and the average spin is achieved by introducing a g factor. It can happen that the values of the g factor determined from electron magnetic resonance, antiferromagnetic resonance, and the magnetization data in a field are noticeably different.

For systems with a frozen orbital moment the spin Hamiltonian has the form of a sum of scalar products of spins. For the two-sublattice antiferromagnet $CoCl_2$ the spin Hamiltonian[1] calculated on the functions of the ground-state doublets of the Co^{++} ions, because of their partially frozen orbital moments, is bilinear in the spins and highly anisotropic, with binary spin–spin anisotropy.

In this paper we construct the spin Hamiltonian of a two-sublattice antiferromagnet whose ion spins are defined on their two lowest doublets, when the ions have an effective spin $s=3/2$. As an example we consider the $CoCl_2$ crystal. For $CoCl_2$ the use of a spin Hamiltonian with effective ion spins $s=1/2$ (Ref. 1) does not give a satisfactory description of the temperature dependence of the antiferromagnetic resonance frequencies[2,3] and collapse field.[2,4] The temperature dependence of the collapse field in $CoCl_2$ is similar to the temperature dependence of the square of the average spin of the sublattice. Such a dependence of the collapse field on spin was explained in Ref. 2 using the approximation of an appreciable (comparable to the bilinear) biquadratic contribution to the spin–spin interaction.

The temperature dependence of the spontaneous magnetostriction anisotropic in the basal plane in $CoCl_2$ (Ref. 4) is similar to the temperature dependence of the fourth power of the average spin of the sublattice. A phenomenological description of such a temperature dependence of the magnetostriction was given in Ref. 4 under the assumption that the non-Heisenberg interactions of fourth power in the spin give the predominant contribution to the magnetoelasticity of $CoCl_2$.

The magnetostriction anisotropic in the basal plane in $CoCl_2$ at $T=4.2$ K has a value of 6×10^{-4} (Refs. 5 and 6). The authors of Ref. 7 attribute the formation of this large magnetostriction to a single-ion mechanism. Using an effective spin Hamiltonian with $s=1/2$, one cannot adopt a single-ion mechanism[7] for the magnetostriction of $CoCl_2$, since in that case one cannot introduce quadratic (or higher) single-particle spin operators.

According to Hund's rules, the free Co^{++} ion has an orbital moment $L=3$ and a spin moment $S=3/2$. The predominance of the cubic contribution of the crystalline field over the trigonal allows one to carry out a single-particle treatment of the ionic states of Co^{++} in $CoCl_2$ with the aid of a Hamiltonian[1] written in the form

$$H=\lambda\mathbf{I}\cdot\mathbf{S}+\delta(l_z^2-2/3), \tag{1}$$

where λ is the spin–orbit interaction constant, δ is the parameter of the trigonal component of the crystalline field, and $\mathbf{l}$ is the effective orbital moment operator written with allowance for the effect of a higher-than-cubic component of the crystalline field[8] ($l=1$). The ratio of the parameters of Hamiltonian (1) in $CoCl_2$ is $\delta/\lambda\approx1.6$.[1] The quantization axis in (1) is directed along the trigonal axis.

The wave functions of the ground-state doublet and the next doublet for the Co^{++} ion are[1]

$$|\psi_{1\pm}\rangle=c_1|\mp1,\ \pm3/2\rangle+c_2|0,\ \pm1/2\rangle+c_3|\pm1,\ \mp1/2\rangle, \tag{2}$$

$$|\psi_{2\pm}\rangle = b_1|0,\ \pm 3/2\rangle + b_2|\pm 1,\ \pm 1/2\rangle. \quad (3)$$

The matrices of the components of the spin moment, calculated only for the ground-state doublet (2), are proportional to the Pauli matrices,[1] and the effective spin is $s=1/2$. In such a treatment spin–spin interaction Hamiltonian in $CoCl_2$ is bilinear in the spins of neighboring ions and is anisotropic.

In accordance with the level diagram of the Co^{++} ion in the $CoCl_2$ crystal[9] the energy difference of the two lowest ionic doublets is 699 GHz or of the order of 35 K. The paramagnetic temperature, proportional to the exchange, is equal to 38 K in $CoCl_2$ (Ref. 10). We see that these values are comparable. In $CoCl_2$ a situation is realized in which the exchange is much smaller than the parameters of Hamiltonian (1), while the energy difference of the two lowest levels of Hamiltonian (1) is comparable to the exchange. Therefore the definition of the spin–spin interaction Hamiltonian in $CoCl_2$ must be made with allowance for the two lowest doublets of the magnetic ion.

Using the wave functions (2) and (3), we write the matrix elements of the S_z projections of the ion spin:

	$\|\psi_{2+}\rangle$	$\|\psi_{1+}\rangle$	$\|\psi_{1-}\rangle$	$\|\psi_{2-}\rangle$
$\|\psi_{2+}\rangle$	$\frac{3}{2}b_1^2+\frac{1}{2}b_2^2$	0	0	0
$\|\psi_{1+}\rangle$	0	$\frac{3}{2}c_1^2+\frac{1}{2}c_2^2-\frac{1}{2}c_3^2$	0	0
$\|\psi_{1-}\rangle$	0	0	$-\frac{3}{2}c_1^2-\frac{1}{2}c_2^2+\frac{1}{2}c_3^2$	0
$\|\psi_{2-}\rangle$	0	0	0	$-\frac{3}{2}b_1^2-\frac{1}{2}b_2^2$

In exactly the same way we calculate the matrix elements of the S_x projections of the ion spin:

	$\|\psi_{2+}\rangle$	$\|\psi_{1+}\rangle$	$\|\psi_{1-}\rangle$	$\|\psi_{2-}\rangle$
$\|\psi_{2+}\rangle$	0	$\frac{\sqrt{3}}{2}b_1c_2+b_2c_3$	0	0
$\|\psi_{1+}\rangle$	$\frac{\sqrt{3}}{2}b_1c_2+b_2c_3$	0	$\sqrt{3}c_1c_3+c_2^2$	0
$\|\psi_{1-}\rangle$	0	$\sqrt{3}c_1c_3+c_2^2$	0	$\frac{\sqrt{3}}{2}b_1c_2+b_2c_3$
$\|\psi_{2-}\rangle$	0	0	$\frac{\sqrt{3}}{2}b_1c_2+b_2c_3$	0

The matrix for the S_y projections is analogous in form to that for S_x.

Introducing the effective spin $s=3/2$, we can write these matrices in the form

$$S_z=\gamma_1 s_z+\gamma_2 s_z^3, \quad S_{x,y}=\eta_1 s_{x,y}+\eta_2(s_{x,y}s_z^2+s_z^2 s_{x,y}), \quad (4)$$

where s_i $(i=x,y,z)$ are the projections of the effective spin with $s=3/2$. The parameters γ and η in (4) are expressed in terms of the parameters of the wave functions (2) and (3):

$$\gamma_1=\frac{1}{24}[27(3c_1^2+c_2^2-c_3^2)-(3b_1^2+b_2^2)],$$

$$\gamma_2=\frac{1}{6}[3b_1^2+b_2^2-3(3c_1^2+c_2^2-c_3^2)], \quad (5)$$

$$\eta_1=\frac{1}{4\sqrt{3}}[5\sqrt{3}(\sqrt{3}c_1c_3+c_2^2)-\sqrt{3}b_1c_2-2b_2c_3],$$

$$\eta_2=\frac{1}{2}\left[b_1c_2+\frac{2}{\sqrt{3}}b_2c_3-\sqrt{3}c_1c_3-c_2^2\right].$$

The exchange interaction of a pair of neighboring ions is written as

$$H_{ij}=J\mathbf{S}_i\cdot\mathbf{S}_j, \quad (6)$$

where i,j specify the position of the neighboring ions, and J is the exchange parameter.

Using Eq. (4) and the results of Ref. 1, we find that the spin–spin interaction Hamiltonian implemented on the two lowest doublets of the Co^{++} ions has the form

$$\begin{aligned}H_{ij}=J\{&\gamma_1^2 s_{iz}s_{jz}+\gamma_1\gamma_2(s_{iz}s_{jz}^3+s_{iz}^3s_{jz})+\gamma_2^2 s_{iz}^3 s_{jz}^3\\&+\eta_1^2 s_{ix}s_{jx}+\eta_1\eta_2[s_{ix}(s_{jx}s_{jz}^2+s_{jz}^2s_{jx})+s_{jx}(s_{ix}s_{iz}^2\\&+s_{iz}^2s_{ix})]+\eta_2^2(s_{ix}s_{iz}^2+s_{iz}^2)(s_{jx}s_{jz}^2+s_{jz}^2s_{jx})\\&+\eta_1^2 s_{iy}s_{jy}+\eta_1\eta_2[s_{iy}(s_{jy}s_{jz}^2+s_{jz}^2s_{jy})+s_{jy}(s_{iy}(s_{iz}^2\\&+s_{iz}^2s_{iy})]+\eta_2^2(s_{iy}s_{iz}^2+s_{iz}^2s_{iy})(s_{jy}s_{jz}^2+s_{jz}^2s_{jy})\}. \quad (7)\end{aligned}$$

Hamiltonian (7) with the effective spins (4) contains bilinear spin–spin terms and spin–spin terms which are cubic in the projections of the effective spin of the ions.

The spin representation of the two lowest doublets of the single-particle Hamiltonian (1) can be written in the form[8]

$$D\left[s_z^2-\frac{1}{3}s(s+1)\right], \tag{8}$$

where the constant D is equal to the energy difference of the lowest doublets E_1 and E_2 and is comparable to J:

$$D=\frac{E_2-E_1}{2}. \tag{9}$$

Denoting the intrasublattice and intersublattice (interlayer) exchange parameters as J_{11} and J_{12}, we write the spin Hamiltonian for $CoCl_2$, with allowance for (4) and (5), as

$$\begin{aligned}H=&\frac{1}{2}\sum_{\alpha\beta ij}J_{\alpha\beta}\{\gamma_1^2 s_{\alpha iz}s_{\beta jz}+2\gamma_1\gamma_2 s_{\alpha iz}s_{\beta jz}^3+\gamma_2^2 s_{\alpha iz}^3 s_{\beta jz}^3\\&+\eta_1^2(s_{\alpha ix}s_{\beta jx}+s_{\alpha iy}s_{\beta jy})+2\eta_1\eta_2[s_{\alpha ix}(s_{\beta jx}s_{\beta jz}^2\\&+s_{\beta jz}^2 s_{\beta jx})+s_{\alpha iy}(s_{\beta iy}s_{\beta jz}^2+s_{\beta jz}^2 s_{\beta jy})]\\&+\eta_2^2[(s_{\alpha ix}s_{\alpha iz}^2+s_{\alpha iz}^2 s_{\alpha ix})(s_{\beta jx}s_{\beta jz}^2+s_{\beta jz}^2 s_{\beta jx})\\&+(s_{\alpha iy}s_{\alpha iz}^2+s_{\alpha iz}^2 s_{\alpha iy})(s_{\beta jy}s_{\beta jz}^2+s_{\beta jz}^2 s_{\beta jy})]\}\\&+\sum_{\alpha i}D\left(s_{\alpha iz}^2-\frac{1}{3}s(s+1)\right),\end{aligned} \tag{10}$$

where $\alpha,\beta=1,2$ is the number of the sublattice.

In writing Eq. (10) we have assumed that J_{11} and J_{12} are much smaller than the parameters δ and λ. The level structure calculated for the Co^{++} ion in Ref. 1 is determined by the value of the ratio δ/λ. It is similar to the structure given in Ref. 9. Accepting the value of the ratio δ/λ used in Ref. 1 and substituting into (5) the values calculated in Ref. 1 for the parameters of the wave functions (2) and (3), viz., $c_1=0.59$, $c_2=-0.70$, $c_3=0.40$, $b_1=0.88$, $b_2=-0.47$, we obtain an estimate of the numerical values of the parameters of Hamiltonian (10): $\gamma_1=1.440$, $\gamma_2=-0.263$, $\eta_1=1.333$, $\eta_2=-0.649$.

The anisotropy of the bilinear terms in Ref. 10, judging from the numerical values of γ_1 and η_1, which are almost equal to each other, is insignificant and is of the easy-axis type rather than the easy-plane type as in $CoCl_2$. The products of the parameters $\gamma_1\gamma_2$ and $\eta_1\eta_2$ are negative, with $\eta_1\eta_2<\gamma_1\gamma_2$, and therefore the anisotropy of the terms containing the first and third powers of the operators of the neighboring spins will be of the easy-axis type, provided that the average of the cubic components of the spin operators has the same sign as the average of the linear spin operators. When their signs are different, then this spin–spin anisotropy will be of the easy-plane type. The terms containing the third powers of the spin operators of a pair of ions has anisotropy of the easy-plane type.

The spin Hamiltonian (10) contains single-ion anisotropy terms. It follows from the given numerical values of the parameters of Hamiltonian (1) that the single-ion anisotropy described by the parameter D in (1) is predominant and results in anisotropy of the easy-plane type in $CoCl_2$.

It follows from Eqs. (4) and (10) that the true spin of the ion and, hence, the mean field in which the ion in the ordered state is found are nonlinear in the value of the effective spin of the ion. The problems discussed at the beginning of this paper regarding the magnetism of the $CoCl_2$ crystal may result from this nonlinearity. A study of the properties of Hamiltonian (10) will be the subject of future papers.

In closing we note that the non-Heisenberg contribution to the spin Hamiltonian is ordinarily obtained using perturbation theory, and in general it cannot be very large. Here we are mainly talking about a biquadratic contribution[11] to the spin–spin interaction, of the type $(\mathbf{s}_1\cdot\mathbf{s}_2)^2$. The non-Heisenberg contribution to the spin Hamiltonian obtained in this study is due to the partial freezing of the orbital moment. Such a non-Heisenberg effective spin Hamiltonian is described by terms of the third power in projections of the spin operators of the ions and is highly anisotropic. The contribution of such a non-Heisenberg admixture is comparable to the contribution of the bilinear terms.

The authors thank Professor S. M. Ryabchenko for a discussion in the course of this study.

*E-mail: lozenko@iop.kiev.ua

[1] M. E. Lines, Phys. Rev. **131**, 546 (1963).
[2] A. F. Lozenko and S. M. Ryabchenko, Zh. Éksp. Teor. Fiz. **65**, 1085 (1973) [Sov. Phys. JETP **38**, 538 (1974)].
[3] I. S. Jacobs, S. Roberts, and S. D. Silverstein, J. Appl. Phys. **39**, 816 (1968).
[4] V. M. Kalita, A. F. Lozenko, and S. M. Ryabchenko, Fiz. Nizk. Temp. **26**, 671 (2000) [Low Temp. Phys. **26**, 489 (2000)].
[5] A. F. Lozenko, P. E. Parkhomchuk, S. M. Ryabchenko, and P. A. Trotsenko, Fiz. Nizk. Temp. **14**, 941 (1988) [Sov. J. Low Temp. Phys. **14**, 517 (1988)].
[6] V. M. Kalita, A. F. Lozenko, S. M. Ryabchenko, and P. A. Trotsenko, Ukr. Fiz. Zh. (Russ. Ed.) **43**, 1469 (1998).
[7] E. Callen and H. Callen, Phys. Rev. **139**, 455 (1965).
[8] S. A. Al'tshuler, B. M. Kozyrev, *Electron Paramagnetic Resonance* [in Russian], Nauka, Moscow (1972)
[9] K. R. A. Ziebeck and C. Escribe, Solid State Commun. **23**, 867 (1977).
[10] C. Starr, F. Bitter, and A. R. Kaufman, Phys. Rev. **58**, 977 (1940).
[11] K. Yosida, J. Appl. Phys. **39**, 511 (1968).

Translated by Steve Torstveit

LETTER TO THE EDITOR

On the magnetic anisotropy of La_2CuO_4 above the Néel temperature

V. M. Loktev*

N. N. Bogolyubov Institute of Theoretical Physics, National Academy of Sciences of Ukraine, ul. Metrologicheskaya 14-b, 03143 Kiev, Ukraine

(Submitted August 20, 2001)
Fiz. Nizk. Temp. **28**, 95–98 (January 2002)

It is conjectured that, because of the orthorhombicity of the lattice, which is preserved above the Néel temperature T_N, and the quasi-two-dimensional character of the magnetic interactions, the destruction of the long-range antiferromagnetic order in La_2CuO_4 is brought about by the thermal generation of kink–antikink pairs. An attempt is made to interpret qualitatively the experiments of A. N. Lavrov *et al.*, Phys. Rev. Lett. **87**, 017007 (2001), on the observation of anisotropy of the magnetic susceptibility in the paraphase of this antiferromagnet. © *2002 American Institute of Physics.* [DOI: 10.1063/1.1449190]

1. The question of the direct relation of the magnetic and superconducting properties of copper oxides was raised immediately after the discovery of the first high-T_c superconductor (HTSC), La–Ba–Cu–O, the parent (undoped) compound of which, La_2CuO_4, is an antiferromagnetic (AFM) insulator. In his now-famous paper,[1] Anderson called attention to two important physical features of HTSCs: the presence of strong electronic correlations in the Cu^{2+} ion, which are described by the Hubbard model Hamiltonian, and the layered structure of the lattices, which often allows one, when calculating some characteristic or other of the HTSCs, to limit consideration to a single cuprate (CuO_2) layer. The first feature is due to the localized character of the charges (or, equivalently, in AFM phases, the spins) and the applicability of the Hubbard model for describing the magnetism of undoped HTSCs; the second feature has become the basis of attempts to transfer to the two-dimensional (2D) case the scenarios involving topological excitations—spinons and holons—which are inherent to one-dimensional (1D) AFMs. Later, the spin–holon and many other magnetic mechanisms of pairing that can lead to a high T_c have become the subject of intensive and never-ending studies, the results of which have been set forth in numerous review articles (see, e.g., Refs. 2–7).

2. In spite of the fact that long-range magnetic order is absent in conducting HTSC compounds, understanding the physical, including superconducting, properties of cuprates is impossible without an understanding of the evolution of their magnetism at the transition from the insulating (including the lightly doped) state to the metallic state. Therefore, it is not surprising that the study of HTSCs specifically as magnetic materials is actively continuing. In particular, the recent paper by Lavrov *et al.*[8] reported the direct observation of magnetic anisotropy (which had previously been less clearly manifested in neutron scattering[9,10]) of the insulating compounds $La_{2-x}Sr_xCuO_4$ ($x \lesssim 3\%$) and $La_2CuO_{4+\delta}$ ($\delta \lesssim 1\%$) over a wide range of temperature (from 0 to ≈ 400 K). The static magnetic susceptibility $\chi_{jj}(T)$ was measured, and its anisotropy was found to be clearly preserved even at temperatures above the Néel point $T_N(x)$, although it is usually assumed (see Ref. 11) that after loss of the long-range magnetic order the spin subsystem of the CuO_2 layers will become isotropic and can be described consistently by a 2D Heisenberg model (or by the nonlinear σ model, which is to a certain degree analogous to it). It is also important that the experiments of Ref. 8 used single crystals containing practically no twins, a fact which makes the results more reliable.

For an analysis of the results let us turn to the Hamiltonian of the spin subsystem of La_2CuO_4. Of course, its main term is the exchange interaction $J\Sigma_{\mathbf{n},\boldsymbol{\rho}}\mathbf{S}_\mathbf{n}\cdot\mathbf{S}_{\mathbf{n}+\boldsymbol{\rho}}$ ($\mathbf{S}_\mathbf{n}$ are the spins of the sites) with a large interaction constant ($\sim 10^3$ cm^{-1}; Ref. 11) between nearest neighbors $\mathbf{n}$ and $\mathbf{n}+\boldsymbol{\rho}$.[1)] However, it is not the isotropic exchange interaction, which is common to all compounds, but the comparatively weak anisotropic terms of relativistic and exchange–relativistic origin that determine the specifics of the magnetic subsystem in each HTSC. We note here that because of the fact that the Cu^{2+} spin $S=1/2$, the magnetic anisotropy, like the exchange interaction, in cuprates has an inter-ionic character, i.e., is defined by an operator of the form $\Sigma_{j,k}\Sigma_{\mathbf{n},\boldsymbol{\rho}}\Delta J_{jk}\mathbf{S}^j_\mathbf{n}\cdot\mathbf{S}^k_{\mathbf{n}+\boldsymbol{\rho}}$. Its specific form requires knowledge of the crystal structure. Then it is necessary to take into account that at $T_{T-O}(x=0)\approx 530$ K (Ref. 11) La_2CuO_4 undergoes a structural transition from the high-temperature tetragonal $I4mmm(D^{17}_{4h})$ phase, where $|\mathbf{a}|=|\mathbf{b}|\neq\mathbf{c}$, to the orthorhombic $B_{mab}(D^{18}_{2h})$ phase with $|\mathbf{a}|<|\mathbf{b}|<|\mathbf{c}|$, accompanied by the rotation ($\approx 4°$) of the stretched octahedra, which extend along the axis $\mathbf{c}\|Y$. As a result, on the one hand, there arises a Dzyaloshinskii interaction $\Delta J_{YZ}\equiv D$, with $\mathbf{D}\|\mathbf{a}\|X$ (Refs. 14–16), and, on the other hand, the symmetry of the local crystalline field acting on the Cu^{2+} ion on the part of the ligands is lowered to monoclinic, so that the magnetic anisotropy of this crystal on the whole becomes biaxial;[16] this is usually ignored.

The Dzyaloshinskii interaction ''lays'' the vectors $\mathbf{S}_\mathbf{n}$ into bc plane; as to the other constants ΔJ_{jj}, it is impossible

from general considerations to establish their values or even their signs. It follows from the measurements, however, that predominantly $\mathbf{S_n}\|\mathbf{b}\|Z$, from which we conclude that La_2CuO_4 has a magnetic anisotropy of the easy-plane (i.e., uniaxial) type.[2)] Indeed, a quantum-mechanical calculation confirms this and gives for the correction to the exchange interaction of the Y components of the spin a value $\Delta J_{YY} \equiv \Delta J_{ab} \approx 4.2\times 10^{-3}$ cm^{-1} (Ref. 19). Here, however, in accordance with the biaxiality there is another, somewhat larger quantity $\Delta J_{XX} \equiv \Delta J_{bc} \approx 2.3\times 10^{-2}$ cm^{-1}. Then, proceeding from the condition $\Delta J_{ab} > \Delta J_{bc}$, at least, we find that the effect of these two anisotropic exchange interactions in La_2CuO_4 gives an easy axis **b**, as was pointed out by Bar'yakhtar *et al.*[16] from purely phenomenological considerations, and a hard axis **a**, which follows unambiguously from the measurements.[8] Thus it can be regarded as established that the magnetic anisotropy of La_2CuO_4 in the low-temperature phase has an ''Ising-like'' character, in the parlance of the day.

Now it is not hard to understand why the components $\chi_{yy}(T)$ and $\chi_{zz}(T)$ have a descending, ''longitudinal,'' temperature dependence. While $\chi_{zz}(T)$ is actually the longitudinal component of the static magnetic susceptibility tensor, since the magnetic field $\mathbf{H}\|\mathbf{S_n}$, the component $\chi_{yy}(T)$ acquires this quality only by virtue of the Dzyaloshinskii interaction $\mathbf{D}\neq 0$. Here its ''longitudinal'' character is due to the AFM sequence of weak moments of the CuO_2 planes along **c**. It should be pointed out that the Dzyaloshinskii interaction has been mentioned[8] as one of the possible reasons for the ''longitudinal'' behavior of the transverse component of the static susceptibility; we note only that this is one of the results that cannot be interpreted in the ''one-plane'' approximation.

3. It is more complicated to describe (and, to a certain extent, understand) the anisotropy of the static magnetic susceptibility observed above $T_N(x)$, where, as we have said, there is no long-range magnetic order. Here, however, it should be kept in mind that, because of the anomalously large value of J ($J \gg T_N(x)$) and the quasi-2D character of all the exchange interactions, the average (in the proper reference frame) value of the site spin is nonzero even above $T_N(x)$, and the AFM order is preserved at all distances r within the correlation length $\xi_{AFM}(x,T) \equiv \xi_{AFM}$ (Refs. 5 and 11). The low symmetry of the lattice due to $T_N(x) < T_{T-O}(x)$ also remains unchanged; consequently, despite the rather high temperature (but, of course, for $T < T_{T-O}$) the directions **b** and **a** remain ''easy'' and ''hard,'' respectively, for the spins in the crystal. Under these conditions a natural source of suppression of the long-range magnetic order can be the thermal generation of kink–antikink pairs or domain walls of width $d_{DW} \sim J/\sqrt{\Delta J_{bc} J + D^2}$, which separate regions with opposite directions of the AFM vectors[3)] and in which rotations of the latter occur in the easy planes bc. The dynamic structure that arises should have a characteristic 1D modulation along **a** (with walls of the Bloch type) or **b** (Néel type). On the whole, for $r \gg \xi_{AFM}$ this system is similar to a paramagnet, while for $r \lesssim \xi_{AFM}$ it manifests many signs (including magnetic anisotropy) of antiferromagnetism with long-range magnetic order; this is most likely what was observed in Ref. 8. For example, excitations with $|\mathbf{k}| > \xi_{AFM}^{-1}$ are weakly damped in a fluctuating system of this kind. Here it should also be mentioned that the 1D modulation, which was ascribed in Ref. 8 to the formation of spin-density waves, was observed in the experiments of Refs. 9 and 10, which can also have a different interpretation, as set forth above, not involving the use of the σ model or the presence of stripes.

4. Our stated goal was a qualitative analysis of the temperature dependence of the static magnetic susceptibility of pure La_2CuO_4. It can be achieved by invoking the features of the magnetocrystalline structure of this cuprate in the entire volume. However, even here a consistent quantitative description of the static susceptibility cannot be given without information about the spectra of magnetic (linear and nonlinear) excitations. In particular, there are essentially no experimental data on the antiferromagnetic resonance, the investigation of which for different x would be extremely desirable.

Do the arguments about the role of magnetic anisotropy extend to doped systems? This apparently depends on what controls ξ_{AFM}—temperature or doping[5]—and the contribution of the latter (like that of the carriers) to the formation of the domain structure is unclear at the present time. Twinned crystals are on average isotropic, and the magnetic anisotropy of metallic phases should be measured in the absence of stripes; this requires specially grown samples. All of these aspects of the problem are also interesting and important to study both experimentally and theoretically.

This report was supported by the grant SCOPEC (Project 7UKPJ 062150.00/1) of the Swiss Science Foundation and was prepared during a stay at the Institute of Physics of the University of Neuchâtel, Switzerland. I would like to thank the Director of the Institute, Prof. H. Beck, for his hospitality, attention, and care.

*E-mail: vloktev@bitp.kiev.ua

1) Recently evidence has appeared which indicates that it is necessary to take into account the observability of the exchange interaction between next-nearest neighbors and also the four-spin cyclic exchange interaction.[12,13] They are much less than J, but most importantly, are isotropic, i.e., they cannot affect the investigated anisotropic magnetic properties of the lanthanum system.

2) The fact that the corresponding value $\Delta J_{YY} \equiv \Delta J_{ab} > 0$ is, generally speaking, nonstandard, since the anisotropy of the g factor of the Cu^{2+} ion in a stretched octahedron is such[17] that $g_\| > g_\perp$ (in La_2CuO_4, $g_\| = 2.3$ and $g_\perp \simeq 2.06$).[18] This type of inequality is usually accompanied by magnetic anisotropy of the easy-axis type.

3) In essence these are identical AFM domains, differing only by a permutation of the magnetic sublattices. This permutation ''occurs'' in the walls, and as long as $d_{DW} \ll \xi_{AFM}$, the domains are well defined. One can also assume that it is ξ_{AFM} that specifies their average size, and the spins of the walls contribute to the ''longitudinal'' character of the static magnetic susceptibility for $\mathbf{H}\|Y$.

[1] P. W. Anderson, Science **235**, 1196 (1987).
[2] A. P. Kamf, Phys. Rep. **249**, 219 (1994).
[3] E. Dagotto, Rev. Mod. Phys. **66**, 763 (1994).
[4] D. Scalapino, Phys. Rep. **250**, 329 (1995).
[5] V. M. Loktev, Fiz. Nizk. Temp. **22**, 3 (1996) [Low Temp. Phys. **22**, 1 (1996)].
[6] Yu. A. Izyumov, Usp. Fiz. Nauk **165**, 403 (1995).
[7] M. L. Kulic, Phys. Rep. **338**, 1 (2000).
[8] A. N. Lavrov, Y. Ando, S. Komiya, and I. Tsukada, Phys. Rev. Lett. **87**, 017001 (2001).

[9] S. Wakimoto, R. J. Birgeneau, M. A. Kastner, Y. S. Lee, R. Erwin, P. M. Gehring, S. H. Lee, M. Fujita, K. Yamada, Y. Endoh, K. Hirota, and G. Shirane, Phys. Rev. B **61**, 3699 (2000).
[10] M. Matsuda, M. Fujita, K. Yamada, R. J. Birgeneau, M. A. Kastner, H. Hiraka, Y. Endoh, S. Wakimoto, and G. Shirane, Phys. Rev. B **62**, 9148 (2000).
[11] M. A. Kastner, R. J. Birgeneau, G. Shirane, and Y. Endoh, Rev. Mod. Phys. **70**, 897 (1998).
[12] R. Coldea, S. M. Hyden, G. Aeppli, T. G. Perring, C. D. Frost, T. E. Mason, S.-W. Cheong, and Z. Fisk, Phys. Rev. Lett. **86**, 5377 (2001).
[13] C. J. Calzado and J.-P. Malrieu, Eur. Phys. J. B **21**, 375 (2001).
[14] A. S. Borovik-Romanov, A. S. Buzdin, N. M. Kreĭnes, and S. S. Krotov, JETP Lett. **47**, 697 (1988).
[15] T. Thio, T. R. Thurston, N. W. Preyer, P. J. Picone, M. A. Kastner, H. P. Jensen, D. R. Gabbe, C. Y. Chen, R. J. Birgeneau, and A. Aharony, Phys. Rev. B **38**, 905 (1988).
[16] V. G. Bar'yaktar, V. M. Loktev, and D. A. Yablonskii, Physica C **156**, 667 (1988).
[17] S. A. Al'tshuller and B. M. Kozyrev, *Electron Paramagnetic Resonance of Compounds of Elements of the Intermediate Groups* [in Russian], Nauka, Moscow (1972).
[18] Y.-C. Zhang, J.-H. Liu, K. Dwight, P. H. Rieger, and A. Wold, Solid State Commun. **63**, 765 (1987).
[19] M. D. Kuz'min, A. I. Popov, and A. K. Zvezdin, Phys. Lett. A **139**, 419 (1989).

Translated by Steve Torstveit